PREDICCIÓN DE FENÓMENOS METEOROLÓGICOS ADVERSOS MEDIANTE MODELOS DE ALTA RESOLUCIÓN Y SISTEMAS DE ALERTA TEMPRANA

David Suárez Molina

Directores:

Gustavo Montero García

Albert Oliver Serra

Las Palmas de Gran Canaria

5 de Junio de 2024

Universidad de Las Palmas de Gran Canaria. Programa de Doctorado en Tecnologías de Telecomunicación e Ingeniería Computacional

Universidad de Las Palmas de Gran Canaria

Programa de Doctorado en Tecnologías de Telecomunicación e Ingeniería Computacional

SIANI. Instituto Universitario de Sistemas Inteligentes y aplicaciones Numéricas en Ingeniería

PREDICCIÓN DE FENÓMENOS METEOROLÓGICOS ADVERSOS MEDIANTE MODELOS DE ALTA RESOLUCIÓN Y SISTEMAS DE ALERTA TEMPRANA

Doctorando: David Suárez Molina

Directores: Gustavo Montero García y Albert Oliver Serra

Las Palmas de Gran Canaria, a 5 de junio de 2024

ULPGC Universidad de Las Palmas de Gran Canaria | Escuela de Doctorado

ACTA DE AUTORIZACIÓN PARA PRESENTAR LA TESIS DOCTORAL

Código:00038/2024

Reunida a24/07/2024 la Comisión Académica del **Programa de Doctorado en Tecnologías de Telecomunicación e Ingeniería Computacional por la Universidad de Las Palmas de Gran Canaria** ha evaluado la solicitud de autorización para presentar la tesis doctoral de:

Apellidos: **SUÁREZ MOLINA**	Nombre: **DAVID**
DNI/NIE/Pasaporte: **78511093H**	Email: **david.suarez105@alu.ulpgc.es**
Tutor: **MONTERO GARCÍA,GUSTAVO**	
Directores: **MONTERO GARCÍA,GUSTAVO** **OLIVER SERRA,ALBERT**	
Programa de Doctorado: **Programa de Doctorado en Tecnologías de Telecomunicación e Ingeniería Computacional por la Universidad de Las Palmas de Gran Canaria**	
Línea de Investigación: **Sistemas inteligentes y aplicaciones numéricas en ingeniería**	
Título definitivo de la tesis: **PREDICCIÓN DE FENÓMENOS METEOROLÓGICOS ADVERSOS MEDIANTE MODELOS DE ALTA RESOLUCIÓN Y SISTEMAS DE ALERTA TEMPRANA.**	

Códigos de la UNESCO:

Campo	Disciplina	Subdisciplina
25 -CIENCIAS DE LA TIERRA Y DEL ESPACIO	**2509 -METEOROLOGÍA (VER 2501 Y 2502)**	**2509.09 -PREDICCIÓN NUMÉRICA METEOROLÓGICA**

La Comisión Académica ha tomado el siguiente acuerdo:

PRESENTACIÓN DE LA TESIS DOCTORAL
Solicitud de autorización de presentación de tesis **favorable**

COMPENDIO DE PUBLICACIONES
Solicitud de autorización de presentación de tesis **favorable**

En Las Palmas de Gran Canaria a fecha de la firma digital

Agradecimientos

Quiero agradecer en primer lugar a mi madre por enseñarme a levantar después de cada derrota y motivarme para volver a intentarlo con más fuerza y ganas, gracias de corazón por tu perseverancia e insistencia en indicarme el camino.

Gracias a mi padre que sufre y disfruta conmigo en la grada Curva, mis hermanas, mi sobrino y ahijado, mis primos "los Suárez" por escucharme siempre y hacerme sentir que les importo demasiado.

Gracias a mis suegros y cuñados por cuidarme como un hijo y un hermano.

Gracias a mis amigos y amigas por darme su tiempo y dejarme ser parte de sus vidas siempre que lo necesito y ese tiempo es fundamental para mí.

Gracias a mis compañeros y compañeras de AEMET por todos estos años (que en estos momentos ya son 15, en lo que considero mi casa) y por todo el apoyo que me brindan, en especial a los de la delegación de AEMET en Canarias.

Gracias a José Antonio Fernández Monistrol por confiar en mi trabajo y darme el apoyo necesario para llevar a cabo el paper del WRF.

Gracias a Carlos Marrero por ayudarme y aguantar mis charlas sobre el WRF en mis visitas a Tenerife.

Gracias a Javi de Luis por su compromiso y proactividad en generar herramientas operativas basadas en el conocimiento. Gracias por poner de forma operativa el conocimiento generado en el paper de "análisis de sondeos".

Gracias a todos los coautores de las publicaciones que forman el núcleo de esta tesis, sin su trabajo en cada una de ellas hubiese sido imposible publicarlas.

Gracias de corazón a mi compañero y gran amigo Emilio Cuevas. Sin su apoyo, sin su insistencia, sin sus consejos, sin su tenacidad, esta tesis no hubiese sido posible. Ha sido una persona fundamental en estos últimos años en mi carrera profesional y seguirá siéndolo ahora en esta nueva etapa de su vida. Gracias Emilio por tantos sabios consejos.

Gracias a mis directores Gustavo y Albert por abrirme las puertas de par en par y confiar en mi para desarrollar esta tesis.

Gracias a mis hijos Inés y David porque son el motor de mi vida, mi motivación, gracias por aportarme la luz necesaria cuando se hace de noche.

Quiero agradecer especialmente a mi mujer, por todo, por quererme como soy, por apoyarme en todos los ámbitos de mi vida, por cuidarme... Isabel eres los cimientos sobre los que emerge esto tan bonito llamado familia… nuestra familia.

Contenido

0. Motivación y justificación de la unidad temática

La presente tesis se ha llevado a cabo en el marco del programa de Doctorado en Tecnologías de Telecomunicación e Ingeniería Computacional. Dentro del programa se ha elegido la línea de investigación de Ingeniería Computacional. La división de Álgebra Numérica Avanzada y la división de Discretización y Aplicaciones del Instituto Universitario de Sistemas Inteligentes y Aplicaciones Numéricas en Ingeniería (SIANI) desarrollan simulaciones numéricas principalmente de cuatro problemas medioambientales: La predicción realista de campos de vientos, de radiación solar, de contaminación atmosférica y de incendios forestales. Por ello, la tesis que aquí se presenta encaja perfectamente con la unidad temática antes referida. Como se comprobará en los próximos apartados, así como en las publicaciones que forman el núcleo, la motivación y la justificación de la tesis es mejorar el conocimiento en la predicción de importantes problemas medioambientales y optimizar los sistemas de alerta temprana.

1. Introducción general

El cambio climático y los fenómenos meteorológicos adversos asociados son una realidad que enfrenta la humanidad en el siglo XXI. En efecto, fenómenos tales como tormentas, inundaciones, olas de calor y huracanes tienen un impacto profundo y multifacético en las sociedades contemporáneas. Estos eventos no solo generan significativas pérdidas económicas, sino que también resultan en la pérdida de vidas humanas, alterando profundamente el tejido social y económico de las comunidades afectadas. En este contexto, comprender y cuantificar estos impactos se torna crucial para el desarrollo de estrategias de mitigación y adaptación efectivas.

El Panel Intergubernamental sobre Cambio Climático (IPCC, por sus siglas en inglés) ha documentado de manera exhaustiva cómo el cambio climático amplifica la frecuencia y severidad de los fenómenos meteorológicos extremos (figura 1). En su informe más reciente, el IPCC destaca que eventos extremos como las olas de calor, las intensas precipitaciones y las tormentas tropicales se han vuelto más comunes y severas debido al calentamiento global. Se espera que la frecuencia de las olas de calor aumente en un factor de 5 a 10 en algunas regiones para el final de este siglo y la intensidad de las precipitaciones extremas puede incrementarse hasta en un 30% en regiones propensas a inundaciones [1]. Estos episodios no solo interrumpen las actividades económicas, sino que también causan daños significativos a la infraestructura, agricultura y propiedad, sumando costos enormes a las economías locales y nacionales.

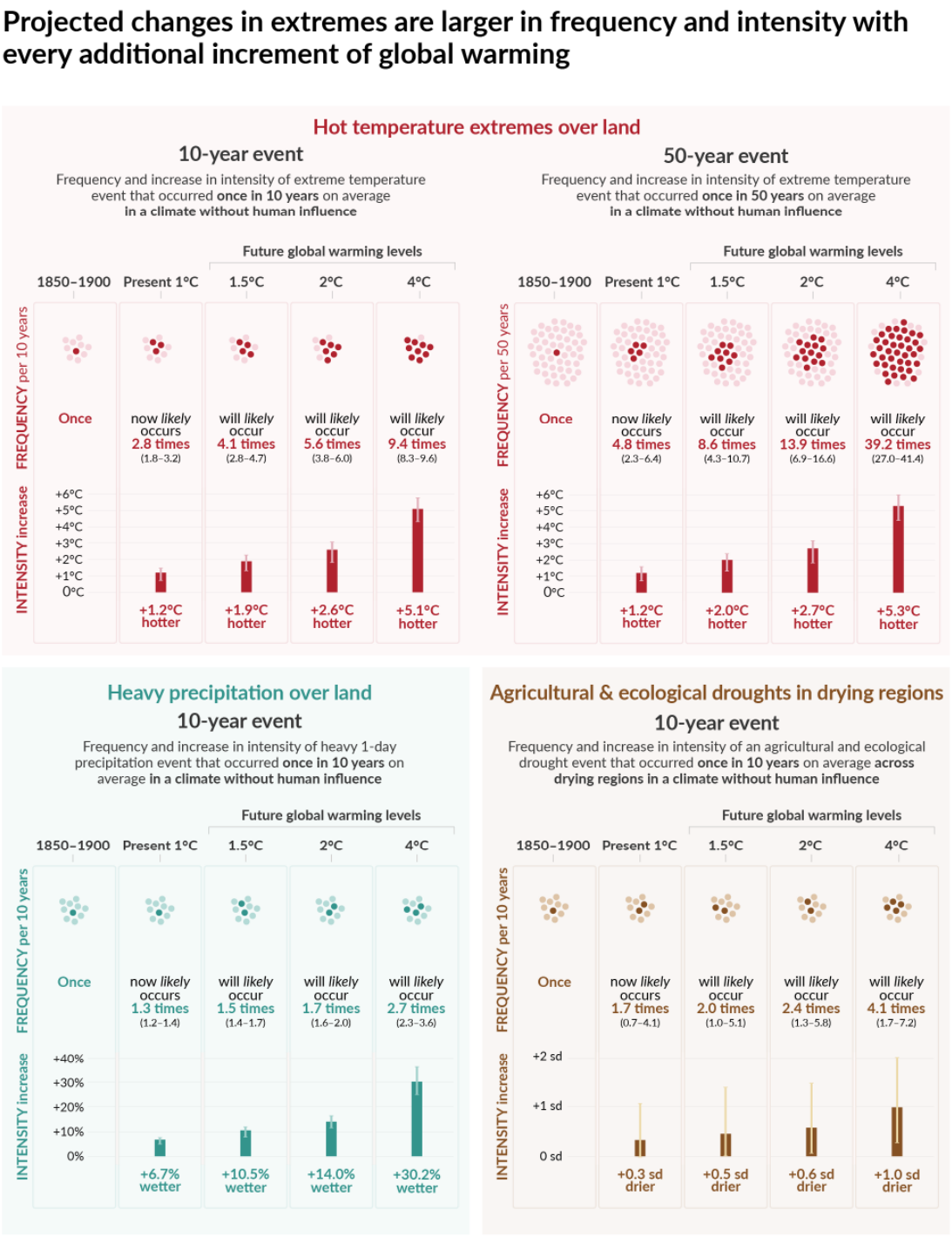

Figura 1: Proyecciones futuras en los cambios de los extremos que son más intensos y frecuentes por cada incremento del calentamiento adicional. (Figure SPM.6 in IPCC, 2021: Summary for Policymakers. In: Climate Change 2021: The Physical Science Basis. Contribution of Working Group I to the Sixth Assessment Report of the Intergovernmental Panel on Climate Change [Masson-Delmotte, V., P. Zhai, A. Pirani, S.L. Connors, C. Péan, S. Berger, N. Caud, Y. Chen, L. Goldfarb, M.I. Gomis, M. Huang, K. Leitzell, E. Lonnoy, J.B.R. Matthews, T.K. Maycock, T. Waterfield, O. Yelekçi, R. Yu, and B. Zhou (eds.)]. Cambridge University Press, Cambridge, UK and New York, NY, USA, pp. 3–32, doi: 10.1017/9781009157896.001.])

Por otro lado, el "Atlas sobre la mortalidad y pérdidas económicas por fenómenos meteorológicos, climáticos e hídricos (1970-2019)" de la Organización Meteorológica Mundial

(WMO, por sus siglas en inglés) proporciona un análisis detallado de los costos humanos y económicos de estos eventos a lo largo de cinco décadas. Según este informe, más de 2 millones de personas han perdido la vida debido a desastres naturales en este período (figura 2), con pérdidas económicas estimadas en 3.64 billones de dólares [2]. Además, el informe revela que el 91% de estas muertes ocurrieron en países en desarrollo, lo que subraya la vulnerabilidad de las naciones menos preparadas y con menores recursos para enfrentar estos desastres. En términos económicos, Estados Unidos, China y Japón se encuentran entre los países que han sufrido las mayores pérdidas absolutas, mientras que países pequeños y en desarrollo soportan una carga desproporcionada cuando se considera el impacto relativo sobre su PIB.

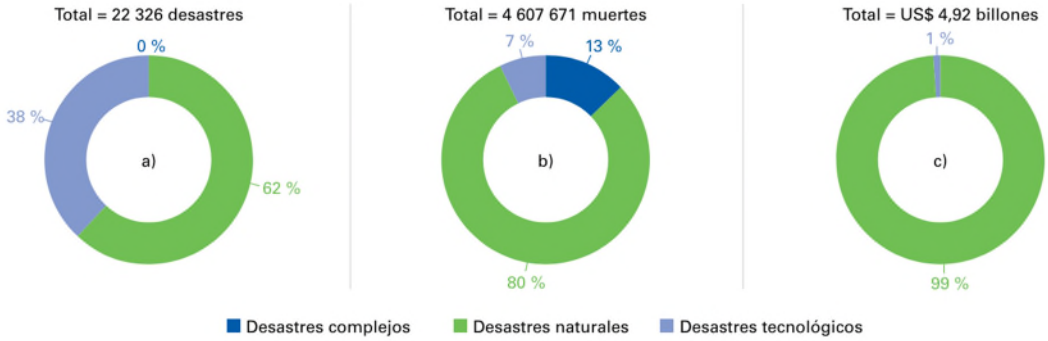

Figura 2: Distribución de a) el número de desastres, b) el número de muertes, y c) las pérdidas económicas que se produjeron durante el período comprendido entre 1970 y 2019 como consecuencia de todos los peligros registrados en la Base de Datos Internacional de Desastres (EM-DAT). Las categorías no representadas en las gráficas indican que su porcentaje se redondea o es igual a cero. (Extraída de [2]).

La precisión y efectividad de los modelos de predicción numérica son esenciales para anticipar los fenómenos meteorológicos adversos y mitigar sus impactos. Estos modelos, basados en complejos cálculos matemáticos y simulaciones computacionales, permiten prever con mayor exactitud la trayectoria, intensidad y efectos potenciales de eventos meteorológicos extremos. Según un estudio publicado en Nature [3], los avances en la predicción numérica del tiempo han mejorado significativamente la capacidad de los meteorólogos para emitir alertas tempranas, lo cual es crucial para la planificación y respuesta ante desastres.

Otro estudio [4] destaca que la integración de datos de satélites y sensores terrestres en estos modelos ha permitido una mejora continua en las previsiones, reduciendo los errores en la predicción y permitiendo respuestas más rápidas y precisas por parte de las autoridades y comunidades afectadas. Estas mejoras en la predicción no solo ayudan a salvar vidas mediante evacuaciones más efectivas, sino que también reducen las pérdidas económicas al permitir una mejor preparación y mitigación de daños.

La importancia de los sistemas de alerta temprana en la mitigación de estos impactos es cada vez más reconocida. Un informe de la Oficina de las Naciones Unidas para la Reducción del Riesgo de Desastres (UNDRR) destaca que los sistemas de alerta temprana son esenciales para salvar vidas y reducir pérdidas económicas. El informe menciona que la implementación de estos sistemas ha contribuido a una notable disminución en la mortalidad por desastres naturales. Por ejemplo, los ciclones en el sur de Asia han mostrado una reducción significativa en las tasas de

mortalidad gracias a sistemas de alerta temprana mejorados y procedimientos de evacuación más efectivos [5].

Estudios científicos recientes refuerzan la relación entre cambio climático y eventos meteorológicos adversos, destacando que la adaptación y mitigación son esenciales para reducir estos impactos. Un estudio publicado en "Nature Communications"[6] encontró que el aumento en la temperatura global ha incrementado la probabilidad de eventos climáticos extremos en más del 90% en muchas regiones, lo que ha llevado a pérdidas económicas significativas. El estudio estima que, sin medidas de adaptación adecuadas, las pérdidas económicas globales podrían alcanzar los 23 billones de dólares anuales para el año 2100, afectando particularmente a los países en desarrollo que tienen menor capacidad de recuperación.

Un estudio publicado en la revista "Nature Climate Change" [7] enfatiza que, sin medidas significativas de reducción de emisiones y adaptación, el costo económico global de los fenómenos meteorológicos extremos podría alcanzar cifras insostenibles. Los investigadores encontraron que el aumento en la frecuencia y severidad de eventos como huracanes y ciclones podría incrementar los costos de reconstrucción y adaptación en un 25% para 2050, lo que representa un desafío significativo para las economías globales, especialmente las más vulnerables .

Los fenómenos meteorológicos adversos representan una amenaza significativa tanto en términos económicos como de vidas humanas. La creciente frecuencia e intensidad de estos eventos, exacerbada por el cambio climático, demanda una acción urgente y coordinada a nivel global. La presente tesis se propone con el objetivo de mejorar el conocimiento de un amplio espectro de fenómenos meteorológicos adversos y sobre la importancia de mejorar la investigación en modelos numéricos de alta resolución, así como conocer sus limitaciones. Los estudios han sido realizados a escala regional, pero los resultados obtenidos pueden ser exportados a otras regiones de interés. Es necesario conocer, caracterizar y analizar los fenómenos y así ofrecer un marco para comprender mejor los desafíos y oportunidades en la gestión de riesgos climáticos y la implementación de políticas resilientes, destacando la importancia de los sistemas de alerta temprana como una herramienta crucial para salvar vidas y reducir las pérdidas económicas.

1.1. Fenómenos Meteorológicos Adversos (FMA)

Los fenómenos meteorológicos adversos son eventos climáticos extremos que pueden tener graves consecuencias tanto económicas como en vidas humanas. Para gestionar y mitigar los riesgos asociados con estos fenómenos, se han desarrollado diversos planes y sistemas de alerta en diferentes regiones. En Europa, el plan Meteoalarm proporciona una plataforma integrada para la emisión de alertas meteorológicas en tiempo real (figura 3), abarcando toda la región europea y facilitando la cooperación y coordinación entre los servicios meteorológicos nacionales. En España, la Agencia Estatal de Meteorología (AEMET) ha implementado el Plan Nacional de Predicción y Vigilancia de Fenómenos Meteorológicos Adversos, conocido como Meteoalerta, que opera con un enfoque similar, adaptado a las particularidades climáticas del territorio español (figura 4).

Los fenómenos meteorológicos adversos incluyen una variedad de eventos extremos que pueden clasificarse según sus características específicas. Entre los más comunes se encuentran:

1. Tormentas: Comprenden lluvias intensas, granizo, vientos fuertes y, en algunos casos, tornados. Estas pueden causar inundaciones, daños a infraestructuras y pérdida de vidas humanas.

2. Olas de calor: Periodos prolongados de temperaturas extremadamente altas, que pueden provocar golpes de calor y aumentar la mortalidad, especialmente entre las poblaciones vulnerables.

3. Olas de frío: Periodos de temperaturas muy bajas que pueden causar hipotermia y otros problemas de salud, así como interrupciones en el suministro de servicios esenciales.

4. Inundaciones: Generalmente causadas por lluvias torrenciales, desbordamientos de ríos o mareas ciclónicas, las inundaciones pueden devastar áreas residenciales y agrícolas.

5. Nevadas y heladas: Pueden causar problemas significativos en el transporte y la infraestructura, además de riesgos directos para la salud humana.

6. Vientos fuertes: Asociados a borrascas o tormentas tropicales, los vientos fuertes pueden causar daños estructurales, derribar árboles y provocar cortes de energía.

7. Tormentas de polvo y calima: Fenómenos que implican el transporte de grandes cantidades de polvo y arena a través del viento, reduciendo la visibilidad y afectando la calidad del aire. Estas tormentas pueden tener impactos significativos en la salud respiratoria y en la agricultura, además de causar interrupciones en el transporte y actividades económicas [8].

8. Fenómenos costeros: Incluyen marejadas ciclónicas, olas gigantes y erosión costera. Estos eventos pueden causar inundaciones costeras, daños a infraestructuras portuarias y costeras, y poner en peligro la vida de las personas que viven en áreas costeras. Las marejadas ciclónicas, en particular, pueden ser extremadamente destructivas durante huracanes y tormentas tropicales [9].

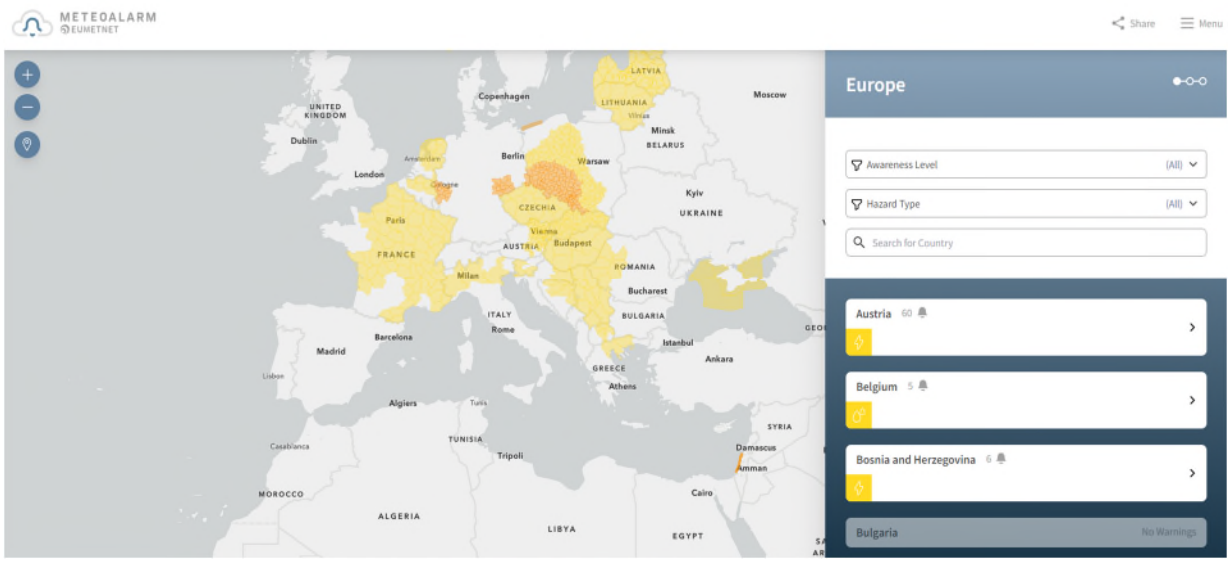

Figura 3: Captura de la web https://www.meteoalarm.org/en/live/ en la que se muestra el estado de los avisos meteorológicos en vigor del día 24-05-24.

Figura 4: Captura de la web https://www.aemet.es en la que se muestra el estado de los avisos meteorológicos (sin avisos en el territorio mostrado) en vigor del día 24-05-24.

1.2. FMA en Canarias y sus impactos

Las Islas Canarias, situadas en el Atlántico frente a la costa noroeste de África, están expuestas a diversos fenómenos meteorológicos adversos, incluidas tormentas, lluvias intensas, olas de calor y tormentas de polvo o "calima", e incluso ciclones tropicales. Estos eventos tienen impactos significativos en la economía local y en la salud y seguridad de sus habitantes.

Lluvias Intensas e Inundaciones

Las lluvias torrenciales pueden provocar inundaciones y deslizamientos de tierra que dañan infraestructuras, viviendas y cultivos. Un estudio realizado por Hernández et al. [10] documentó que las inundaciones en Tenerife en 2010 causaron pérdidas económicas superiores a 15 millones de euros. Estos eventos no solo destruyen propiedades, sino que también interrumpen el comercio y la vida diaria. Las inundaciones pueden arruinar cosechas, afectar el suministro de alimentos y aumentar los precios, lo que supone un impacto negativo en la economía local. Las lluvias intensas e inundaciones pueden propiciar brotes de enfermedades transmitidas por el agua y vectores, como el dengue y la leptospirosis. Las aguas estancadas después de una inundación crean un ambiente ideal para la reproducción de mosquitos, aumentando el riesgo de transmisión de enfermedades. Un informe de la OMS [11] destaca que las condiciones

climáticas extremas y las malas infraestructuras de saneamiento pueden contribuir a la propagación de estas enfermedades.

Olas de Calor

Las olas de calor tienen un impacto directo en el turismo, uno de los pilares económicos de las Canarias. Durante estos eventos, la afluencia turística puede disminuir considerablemente debido a las condiciones climáticas extremas, lo que resulta en pérdidas económicas significativas para la industria hotelera y otros sectores relacionados. Según el Instituto Nacional de Estadística (INE), las olas de calor pueden reducir la ocupación hotelera en hasta un 20%, lo que representa millones de euros en ingresos perdidos para el sector turístico. Las olas de calor están aumentando en frecuencia debido al cambio climático y pueden tener graves consecuencias para la salud. Un estudio [12] mostró una correlación directa entre las olas de calor y el aumento de hospitalizaciones y muertes en las islas, especialmente entre los ancianos y las personas con enfermedades crónicas. Las olas de calor pueden exacerbar condiciones como la deshidratación, los golpes de calor y las enfermedades cardiovasculares, y, por tanto, aumentar la mortalidad y la morbilidad.

Tormentas de Polvo (Calima)

Las tormentas de polvo, conocidas localmente como "calima", transportan polvo del desierto del Sahara hacia las islas, afectando la calidad del aire y reduciendo la visibilidad. Estos eventos pueden interrumpir el tráfico aéreo, afectando el turismo y el comercio. Según el estudio [13], las tormentas de polvo pueden causar la cancelación de vuelos y generar pérdidas económicas significativas para las aerolíneas y los aeropuertos, además de afectar negativamente a los negocios locales que dependen del flujo constante de turistas.

Durante el episodio severo de calima en febrero de 2020, más de 800 vuelos fueron cancelados o desviados, lo que resultó en pérdidas económicas estimadas en varios millones de euros para el sector turístico y comercial de las islas [14][15]. Además, estos eventos pueden afectar las actividades portuarias y pesqueras, e interrumpir el suministro de mercancías y productos frescos.

Las tormentas de polvo tienen graves consecuencias para la salud respiratoria. Durante estos eventos, la concentración de partículas finas y otros contaminantes en el aire aumenta significativamente, lo que puede provocar o agravar problemas respiratorios y cardiovasculares. Un estudio [16] encontró que, durante los episodios de calima, las hospitalizaciones por problemas respiratorios aumentan considerablemente, especialmente en niños y ancianos. La exposición prolongada a partículas de polvo puede provocar enfermedades crónicas y aumentar los costos de atención médica.

1.3. Sistemas de alerta temprana

Los sistemas de alerta temprana (SAT) son mecanismos diseñados para detectar, prever y alertar sobre fenómenos naturales peligrosos y permiten tomar medidas preventivas para reducir el impacto sobre las vidas humanas y bienes materiales. Estos sistemas se componen de cuatro elementos interconectados: conocimiento del riesgo, monitoreo y pronóstico, comunicación de alertas y capacidad de respuesta. Según la Organización de las Naciones Unidas (ONU), los SAT han demostrado ser extremadamente efectivos en la reducción de la mortalidad durante

desastres naturales. Un estudio de la Oficina de las Naciones Unidas para la Reducción del Riesgo de Desastres (UNDRR) indica que, entre 1970 y 2019, las alertas tempranas y la gestión del riesgo han contribuido a reducir la mortalidad por desastres naturales en más del 50 % [17]. Además de salvar vidas, los SAT también ofrecen beneficios económicos significativos. La Organización Meteorológica Mundial (OMM) estima que cada dólar invertido en SAT puede ahorrar hasta 10 dólares en daños evitados [18], lo que refleja una importante reducción en costos de emergencia y reconstrucción [19].

1.3.1. Sistemas de alerta temprana específicos para riesgos meteorológicos

Entre los sistemas de alerta temprana, específicamente para riesgos por fenómenos meteorológicos adversos, podemos citar Meteoalarm [9], que es un sistema de alerta europeo que proporciona información sobre fenómenos meteorológicos adversos a través de un sitio web accesible al público. Este sistema cubre 38 países y emite avisos en varios idiomas, clasificando los peligros por colores (verde, amarillo, naranja y rojo) según su severidad. Meteoalarm permite a los ciudadanos y autoridades locales prepararse y responder adecuadamente a eventos meteorológicos extremos. Por otro lado, Meteoalerta [8], gestionado por la Agencia Estatal de Meteorología (AEMET) en España, opera de manera similar a Meteoalarm. Este sistema emite avisos meteorológicos utilizando un código de colores para indicar la gravedad de los fenómenos: amarillo (riesgo), naranja (riesgo importante) y rojo (riesgo extremo). Meteoalerta establece unos umbrales específicos para cada zona de avisos (figura 5) y la superación de esos umbrales conllevaría a la emisión de avisos en una zona determinada, con un plazo de vigencia y también con un grado de certeza expresado en términos de probabilidad.

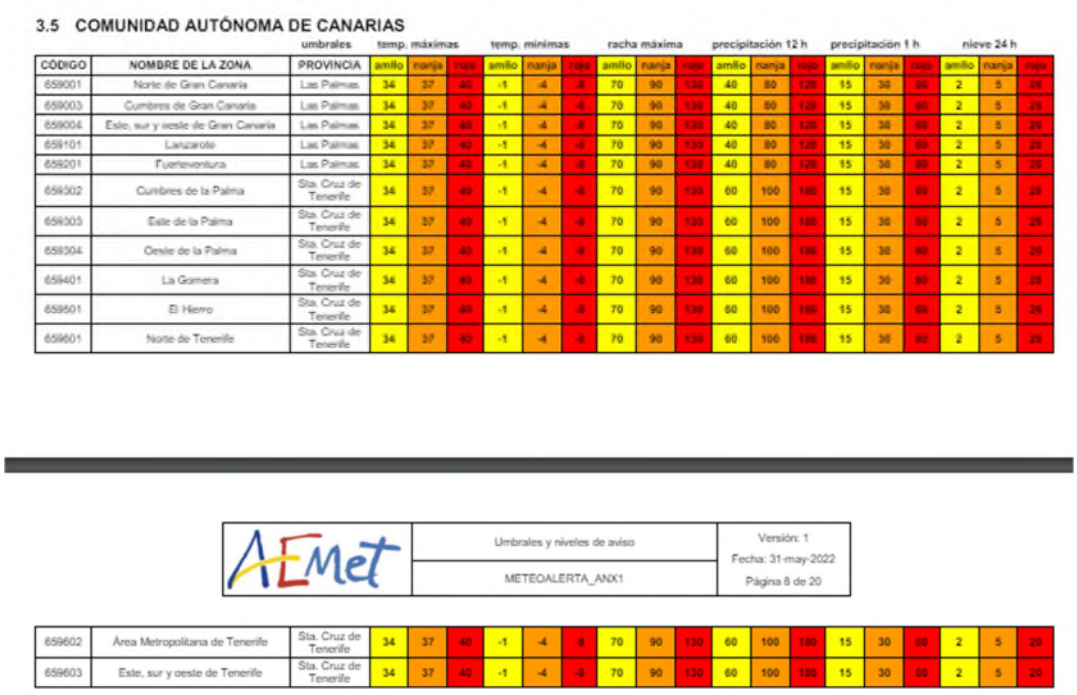

3.5 COMUNIDAD AUTÓNOMA DE CANARIAS

			umbrales	temp. máximas			temp. mínimas			racha máxima			precipitación 12 h			precipitación 1 h			nieve 24 h		
CÓDIGO	NOMBRE DE LA ZONA	PROVINCIA	amllo	naranja	rojo	amllo	naranja	rojo	amllo	naranja	rojo	amllo	naranja	rojo	amllo	naranja	rojo	amllo	naranja	rojo
659001	Norte de Gran Canaria	Las Palmas	34	37	40	-1	-4	-8	70	90	130	40	80	120	15	30	60	2	5	20
659003	Cumbres de Gran Canaria	Las Palmas	34	37	40	-1	-4	-8	70	90	130	40	80	120	15	30	60	2	5	20
659004	Este, sur y oeste de Gran Canaria	Las Palmas	34	37	40	-1	-4	-8	70	90	130	40	80	120	15	30	60	2	5	20
659101	Lanzarote	Las Palmas	34	37	40	-1	-4	-8	70	90	130	40	80	120	15	30	60	2	5	20
659201	Fuerteventura	Las Palmas	34	37	40	-1	-4	-8	70	90	130	40	80	120	15	30	60	2	5	20
659302	Cumbres de la Palma	Sta. Cruz de Tenerife	34	37	40	-1	-4	-8	70	90	130	60	100	180	15	30	60	2	5	20
659303	Este de la Palma	Sta. Cruz de Tenerife	34	37	40	-1	-4	-8	70	90	130	60	100	180	15	30	60	2	5	20
659304	Oeste de la Palma	Sta. Cruz de Tenerife	34	37	40	-1	-4	-8	70	90	130	60	100	180	15	30	60	2	5	20
659401	La Gomera	Sta. Cruz de Tenerife	34	37	40	-1	-4	-8	70	90	130	60	100	180	15	30	60	2	5	20
659501	El Hierro	Sta. Cruz de Tenerife	34	37	40	-1	-4	-8	70	90	130	60	100	180	15	30	60	2	5	20
659601	Norte de Tenerife	Sta. Cruz de Tenerife	34	37	40	-1	-4	-8	70	90	130	60	100	180	15	30	60	2	5	20

AEMet | Umbrales y niveles de aviso | Versión: 1
METEOALERTA_ANX1 | Fecha: 31-may-2022
Página 8 de 20

659602	Área Metropolitana de Tenerife	Sta. Cruz de Tenerife	34	37	40	-1	-4	-8	70	90	130	60	100	180	15	30	60	2	5	20
659603	Este, sur y oeste de Tenerife	Sta. Cruz de Tenerife	34	37	40	-1	-4	-8	70	90	130	60	100	180	15	30	60	2	5	20

Figura 5: Extracto del plan Meteoalerta que muestra los umbrales de los avisos para distintas variables meteorológicas para la Comunidad Autónoma de Canarias.

A continuación, se enumeran otros ejemplos de Sistemas de Alerta Temprana de relevancia:

1. *Sistema de Alerta Temprana para Tsunamis del Pacífico (PTWS)*: Gestionado por la OMM y la Comisión Oceanográfica Intergubernamental de la UNESCO, este sistema monitorea y alerta sobre tsunamis en el Pacífico [20].

2. *Sistema de Alerta Temprana del Programa Mundial de Alimentos (WFP)*: Utiliza datos meteorológicos y de seguridad alimentaria para alertar sobre sequías y crisis alimentarias inminentes en África [21].

3. *Red de Alerta de Inundaciones del Centro Nacional de Huracanes de EE.UU. (NHC)*: Proporciona pronósticos y alertas sobre huracanes y tormentas tropicales en el Atlántico y el Pacífico.

1.3.2. Protección Civil

En España, el sistema de protección civil se organiza bajo un marco normativo que establece la colaboración entre el gobierno central y las comunidades autónomas. El Estado español, a través de la Dirección General de Protección Civil y Emergencias, coordina y gestiona las políticas y planes nacionales de protección civil. Sin embargo, las comunidades autónomas tienen competencias propias en esta materia. Estas desarrollan y ejecutan sus propios planes específicos que están adaptados a las particularidades de su territorio. Un ejemplo destacado es el Plan Especial de Protección Civil de Fenómenos Meteorológicos Adversos (PEFMA) de Canarias, que aborda de manera detallada los riesgos meteorológicos específicos de la región.

El PEFMA del Gobierno de Canarias (GOBCAN) es un marco estratégico para gestionar y responder a fenómenos meteorológicos extremos. El PEFMA [22] establece procedimientos y protocolos para la coordinación entre diferentes agencias y autoridades, y garantiza una respuesta rápida y efectiva para proteger a la población y mitigar daños.

Entre las principales características del PEFMA se incluyen:

- *Monitoreo constante*: Utiliza datos de AEMET y otras fuentes para la vigilancia meteorológica continua.

- *Comunicación eficiente*: Emite alertas y recomendaciones a la población a través de múltiples canales, incluyendo medios de comunicación, redes sociales y aplicaciones móviles.

- *Capacitación y simulacros*: Realiza entrenamientos regulares y simulacros para preparar a las autoridades y a la población ante posibles emergencias.

- *Evaluación y mejora*: Incluye mecanismos de evaluación post-evento para mejorar continuamente las estrategias y procedimientos de respuesta.

Los sistemas de alerta temprana son herramientas esenciales para la protección de vidas y bienes. Su efectividad en la reducción de la mortalidad y los beneficios económicos asociados demuestran la importancia de su implementación y mantenimiento. Ejemplos como Meteoalarm y Meteoalerta, junto con planes específicos como el PEFMA, subrayan el papel crucial de estos sistemas en la gestión de riesgos meteorológicos (figura 6).

Figura 6: Relación entre los avisos y las alertas, es decir relación entre los servicios meteorológicos nacionales y los servicios de protección civil. (Extraída de https://aemetblog.es/2016/01/29/avisos-vs-alertas/)

1.4. Modelos Numéricos de Predicción

Los modelos numéricos de predicción del tiempo son herramientas matemáticas y computacionales que simulan la atmósfera y los océanos para prever las condiciones meteorológicas futuras. Estos modelos se basan en ecuaciones que describen el comportamiento de fluidos y gases en la atmósfera. En general, resuelven sistemas de ecuaciones diferenciales que representan la dinámica atmosférica, la termodinámica y los procesos físicos como la radiación, la convección y la formación de nubes. La resolución de los modelos numéricos de predicción del tiempo es crucial para obtener previsiones meteorológicas precisas y fiables. Un modelo de alta resolución es capaz de capturar estructuras meteorológicas con un mayor detalle y las variaciones locales en la atmósfera, lo que permite una mejor representación de fenómenos meteorológicos como tormentas, frentes fríos, y precipitaciones intensas. Estos modelos son especialmente importantes en áreas geográficas complejas, como regiones montañosas o costeras, donde las condiciones meteorológicas pueden variar significativamente en distancias cortas. Al mejorar la resolución, se puede proporcionar información más detallada y específica para comunidades locales, lo cual es vital para la planificación y respuesta ante eventos meteorológicos extremos.

Modelos Globales:

Los modelos globales de predicción del tiempo (GCM, por sus siglas en inglés) cubren toda la superficie del planeta (figura 7) y proporcionan pronósticos a largo plazo y escalas espaciales amplias. Las características principales de los modelos globales incluyen:

- *Cobertura Total*: Simulan la atmósfera a nivel mundial.

- *Resolución Espacial*: Utilizan una malla tridimensional que abarca la superficie terrestre y varios niveles de la atmósfera. La resolución típica varía entre 10 y 50 km.

- *Pronósticos a Largo Plazo*: Proveen predicciones de hasta 10 días o más.

Ejemplos de Modelos Globales:

- *GFS (Global Forecast System*): Desarrollado por el Centro Nacional de Predicción Ambiental de EE.UU., el GFS proporciona pronósticos cada tres horas con alcance de hasta 10 o 15 días en función del dominio, y es ampliamente utilizado para prever condiciones meteorológicas a escala global [23].

- *IFS (Integrated Forecast System):* Operado por el Centro Europeo de Predicciones Meteorológicas a Medio Plazo (ECMWF), el IFS es conocido por su alta precisión y se utiliza para pronósticos de hasta 15 días [24].

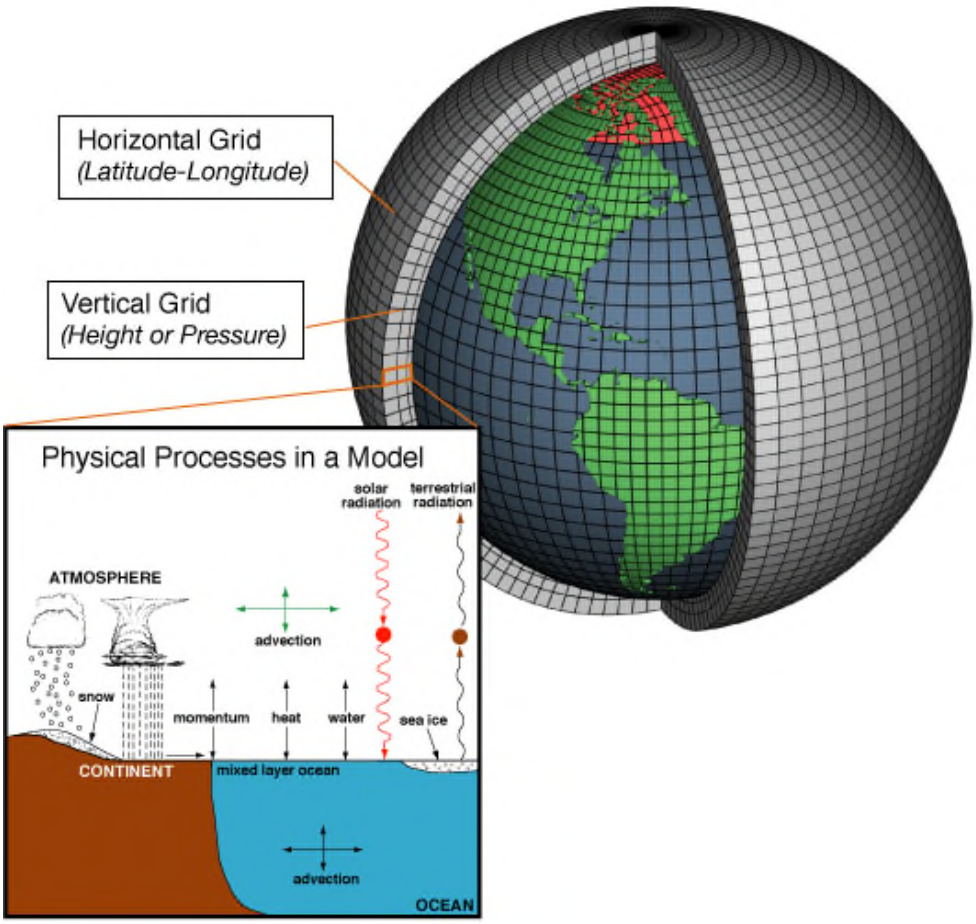

Figura 7: Representación esquemática de un modelo global y los procesos físicos implicados. (Fuente: http://celebrating200years.noaa.gov/breakthroughs/climate_model/AtmosphericModelSchematic.png)

Modelos de Área Local:

Los modelos de área local (LAM, por sus siglas en inglés) se centran en regiones específicas (figura 8) y proporcionan pronósticos de alta resolución que son cruciales para la predicción de fenómenos meteorológicos severos y locales. Características clave de los modelos de área local incluyen:

- *Alta Resolución Espacial*: Resoluciones típicas de 1 a 5 km, lo que permite una mayor precisión en la predicción de fenómenos locales.

- *Pronósticos a Corto Plazo*: Generalmente hasta 3 días.

- *Mayor Detalle*: Capaces de captar detalles finos de la topografía y los efectos locales.

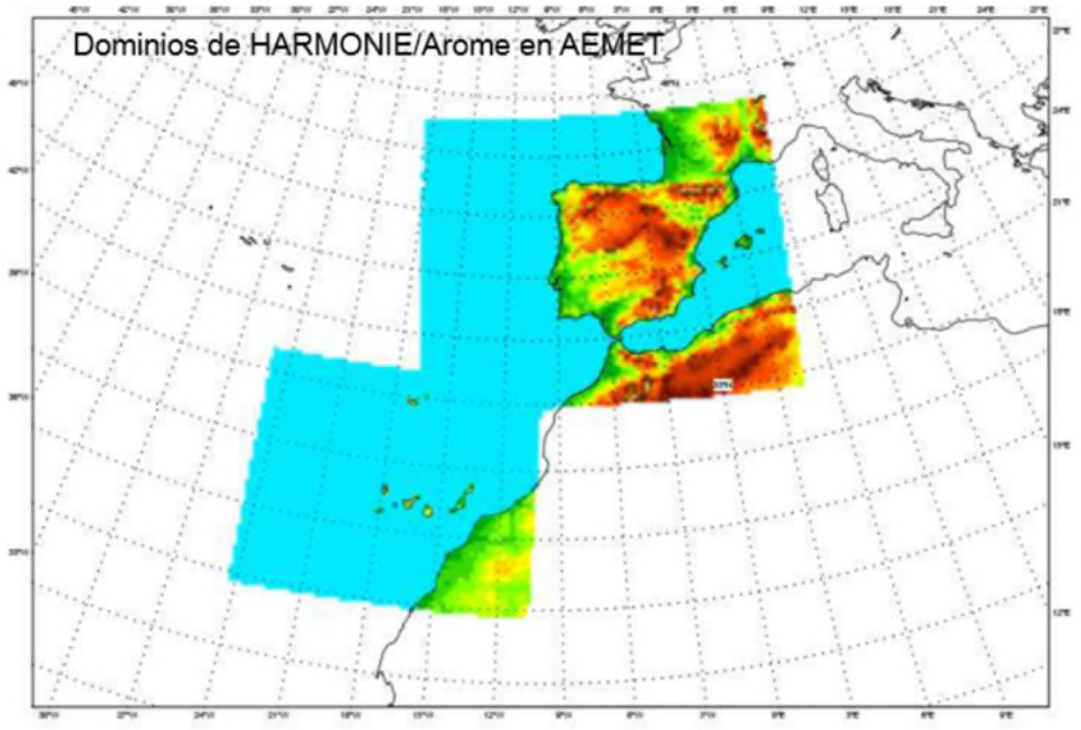

Figura 8: Dominios de integración de un modelo de área local (Harmonie-Arome). (Fuente: AEMET)

Ejemplos de Modelos de Área Local:

- *WRF (Weather Research and Forecasting Model):* Desarrollado por un consorcio de instituciones estadounidenses, el WRF es ampliamente utilizado para aplicaciones de investigación y operaciones meteorológicas regionales.

- *HIRLAM (High Resolution Limited Area Model):* Utilizado por varios servicios meteorológicos europeos, HIRLAM se enfoca en la predicción precisa a corto plazo para áreas específicas de Europa [25].

- *Harmonie-Arome:* Modelo operativo de AEMET que cuenta con dos dominios de integración (Península Ibérica y Baleares y el dominio de Canarias). Se describirá con más detalle en el siguiente punto.

En las últimas décadas, los avances en los modelos numéricos de predicción han sido notables y han reducido significativamente la incertidumbre en las previsiones meteorológicas. Estos avances incluyen:

- *Mejora en la Resolución*: Aumento de la resolución espacial y temporal, lo que supone una mejor captura de fenómenos meteorológicos pequeños y rápidos.

- *Supercomputadores*: Uso de supercomputadores más potentes que permiten la ejecución de modelos más complejos y precisos.

- *Mejores Datos Iniciales*: Avances en la recolección de datos a través de satélites, radares y estaciones meteorológicas que mejoran la precisión de las condiciones iniciales de los modelos.

- *Asimilación de Datos*: Desarrollo de técnicas avanzadas de asimilación de datos que integran mejor las observaciones en los modelos.

- *Modelos Integrados*: Uso de modelos acoplados que simulan la interacción entre la atmósfera, los océanos, el hielo marino y la tierra, y proporcionan una visión más completa del sistema climático [26].

Estos avances han permitido que las previsiones meteorológicas sean más precisas y fiables, lo que ha reducido la incertidumbre y mejorado la capacidad de respuesta ante fenómenos meteorológicos adversos.

1.4.1. Modelos Numéricos de Alta Resolución

Dentro de los modelos de área local hay que destacar los modelos de alta resolución. La predicción meteorológica ha avanzado considerablemente en las últimas décadas gracias al desarrollo de modelos numéricos de alta resolución. Estos modelos permiten una mayor precisión en la simulación de fenómenos meteorológicos a escalas espaciales y temporales finas, lo cual es esencial para mejorar las predicciones y las respuestas a eventos extremos. Dos de los modelos más destacados en esta área son el Harmonie-Arome y el Weather Research and Forecasting (WRF).

Los modelos numéricos de alta resolución son herramientas computacionales que simulan la dinámica de la atmósfera a una resolución espacial detallada, generalmente inferior a 5 km. Estos modelos utilizan ecuaciones matemáticas para describir procesos físicos como la convección, la turbulencia, y la formación de nubes y precipitación. La alta resolución permite capturar fenómenos meteorológicos locales, como tormentas convectivas, brisas costeras y efectos orográficos, que los modelos de resolución más baja no pueden representar adecuadamente [27]. Los modelos de alta resolución requieren una gran capacidad de cálculo y recursos computacionales, ya que deben procesar grandes volúmenes de datos en intervalos de tiempo cortos. Sin embargo, los beneficios en términos de precisión y detalle de las predicciones justifican estos costos. La implementación de estos modelos ha mejorado significativamente la capacidad de predicción de eventos meteorológicos severos, lo que ha permitido respuestas más rápidas y eficaces.

Modelo Harmonie-Arome

El modelo Harmonie-Arome es un sistema de predicción numérica de alta resolución desarrollado por el consorcio HIRLAM (High Resolution Limited Area Model) y el consorcio ALADIN (Aire Limitée Adaptation dynamique Développement InterNational). Este modelo combina la física avanzada de Arome (Application of Research to Operations at Mesoscale) con las técnicas de asimilación de datos y las configuraciones de Harmonie (Hirlam Aladin Research on Mesoscale Operational NWP in Europe) [28]. El modelo Harmonie-Arome se utiliza ampliamente en Europa para la predicción de fenómenos meteorológicos extremos. Ha demostrado ser eficaz en la mejora de las predicciones de precipitaciones intensas, vientos fuertes y otros eventos severos. Estudios han mostrado que Harmonie-Arome proporciona una

mejora significativa en la precisión de las predicciones a corto plazo en comparación con modelos de resolución más baja [28].

Características del Harmonie-Arome:

- *Resolución Espacial y Temporal:* Harmonie-Arome opera típicamente a resoluciones espaciales de 2.5 km o menores, lo que permite una simulación detallada de fenómenos locales. La resolución temporal puede ser tan baja como un minuto, lo que facilita el seguimiento preciso de eventos dinámicos.

- *Asimilación de Datos:* Utiliza avanzadas técnicas de asimilación de datos, como la incorporación de observaciones de satélites, radares y estaciones meteorológicas en ciclos cortos de asimilación para actualizar el estado inicial del modelo y mejorar las predicciones.

- *Física de la Atmósfera:* Incluye parametrizaciones detalladas de distintos procesos físicos como la microfísica de nubes, la radiación y la convección, lo que mejora la precisión en la representación de precipitaciones y otros fenómenos meteorológicos [29].

Modelo Weather Research and Forecasting (WRF)

El modelo WRF es otro sistema de predicción numérica de alta resolución ampliamente utilizado, desarrollado por el National Center for Atmospheric Research (NCAR) y otros colaboradores. WRF es conocido por su flexibilidad y capacidad para operar en diferentes escalas, desde globales hasta locales, con resoluciones espaciales que pueden ajustarse según las necesidades específicas [30]. WRF se utiliza globalmente en investigación y operaciones meteorológicas. Es particularmente útil en estudios de fenómenos severos como huracanes, tormentas convectivas y frentes fríos. La capacidad de WRF para realizar simulaciones detalladas a nivel local ha mejorado significativamente las predicciones meteorológicas y en la planificación de respuestas a desastres [30].

Características del WRF:

- *Resolución Espacial y Temporal:* WRF puede operar a resoluciones espaciales tan finas como 1 km o escalas sub-km, lo que permite la simulación de detalles finos en la atmósfera. La resolución temporal también es altamente configurable.

- *Configuraciones y Física Modular:* WRF ofrece múltiples opciones de configuración y esquemas de física. Así, permite a los usuarios personalizar el modelo según los requerimientos específicos de su estudio. Incluye avanzados esquemas de microfísica, convección, radiación y turbulencia.

- *Capacidad de AnidamientoAnidación:* Permite el uso de mallas anidadas, donde áreas de interés particular pueden ser simuladas a resoluciones más altas dentro de un dominio de resolución más baja y así optimizar los recursos computacionales [27].

Comparación y Desafíos

Ambos modelos, Harmonie-Arome y WRF, tienen sus fortalezas y desafíos. Harmonie-Arome es particularmente eficaz en la predicción de fenómenos meteorológicos en Europa, gracias a su integración con las redes de observación europeas y su configuración optimizada para esta región. Por otro lado, WRF destaca por su flexibilidad y amplia aplicabilidad a diversas regiones y condiciones meteorológicas.

Desafíos Comunes

-*Requerimientos Computacionales:* Ambos modelos requieren grandes recursos computacionales para ejecutar simulaciones de alta resolución. Esto puede ser una limitación en regiones con menos acceso a infraestructura de computación avanzada.

- *Asimilación de Datos:* La precisión de los modelos depende en gran medida de la calidad y cantidad de datos de observación disponibles. En áreas con menos estaciones de monitoreo y menor cobertura satelital, la asimilación de datos puede ser un desafío.

- *Modelización de Procesos Físicos:* Aunque los modelos incluyen avanzadas parametrizaciones físicas, aún existen incertidumbres en la representación de ciertos procesos, como la formación de nubes y la microfísica de precipitaciones, que pueden afectar la precisión de las predicciones [27] [28].

1.5. Estado del arte sobre los fenómenos convectivos en Canarias

La convección es un fenómeno meteorológico fundamental que implica el movimiento vertical del aire en la atmósfera, asociado frecuentemente con la formación de nubes y precipitación intensa. Las Islas Canarias experimentan una variedad de fenómenos meteorológicos convectivos influenciados por factores como la corriente en chorro subtropical, la topografía montañosa y la afección de un gran espectro de fenómenos originados por su localización en la región subtropical. La convección en Canarias puede manifestarse en forma de tormentas convectivas, chubascos intensos y fenómenos extremos como tormentas eléctricas y granizadas. Este apartado examina el estado actual del conocimiento sobre los fenómenos convectivos en Canarias, apoyado en estudios científicos recientes.

El uso de modelos numéricos de predicción y técnicas avanzadas de asimilación de datos ha mejorado significativamente la capacidad de prever fenómenos convectivos en Canarias. Modelos como el HARMONIE-AROME, utilizado por AEMET, ofrecen alta resolución espacial que permite capturar con mayor precisión los procesos convectivos locales. Además, la integración de datos de radar meteorológico y satélites facilita la monitorización en tiempo real y la validación de predicciones. Los avances en la modelización y la observación han mejorado nuestra comprensión y capacidad para prever estos eventos, aunque el cambio climático presenta nuevos desafíos. Continuar investigando y desarrollando tecnologías avanzadas es crucial para mitigar los impactos de los fenómenos convectivos en las Islas Canarias.

A continuación, se enumeran estudios científicos relevantes sobre la convección en Canarias:

El estudio detallado [31] analiza la climatología de las tormentas convectivas en Canarias utilizando datos de radar y estaciones meteorológicas. Se observa que la convección es más frecuente durante los meses de otoño e invierno, con un notable incremento durante episodios de bajas presiones atlánticas y la interacción de estas con la orografía local.

La investigación [32] destaca cómo la compleja topografía de las islas afecta la formación y desarrollo de células convectivas. Las montañas actúan como focos de elevación forzada del aire, intensifican la convección y promueven la formación de nubes de desarrollo vertical.

Por otro lado, el estudio [33] investiga el impacto del cambio climático en los patrones de convección en Canarias. Los resultados indican un aumento en la frecuencia e intensidad de

eventos convectivos extremos, atribuido a las temperaturas más cálidas y cambios en los patrones de circulación atmosférica.

Otros estudios han analizado la combinación de polvo sahariano (calima) y condiciones convectivas debido a sus efectos en la calidad del aire y la visibilidad. El estudio [34] examina cómo estas condiciones pueden intensificar la convección y afectar la salud pública.

Algunos ejemplos recientes de eventos extremos en Canarias son:

- La tormenta tropical Hermine [35], que azotó las Islas Canarias del 24 al 26 de septiembre de 2022 como un ciclón tropical extremadamente anómalo. Hermine se formó a partir de una onda del este que viajó desde Sudán hasta el Atlántico y dejó registros de precipitación sorprendentes para un mes de septiembre en Canarias.

- La Tormenta de Gran Canaria de 2015. Este evento convectivo extremo provocó lluvias torrenciales y granizo, causando inundaciones y daños significativos. Un análisis detallado de este evento [36] utilizó datos de radar y modelos numéricos para entender la dinámica de la tormenta y sus impactos.

- La tormenta tropical "Delta" [37], que los días 28 y 29 de noviembre del 2005 afectó a las islas Canarias con vientos que llegaron a alcanzar los 150 km por hora en las costas y cercanos a los 250 en zonas altas de la isla de Tenerife.

- La situación de precipitaciones torrenciales del 31 de marzo de 2002 en Santa Cruz de Tenerife [38]. Durante la tarde del 31 de marzo de 2002 se produjeron lluvias torrenciales en la ciudad de Santa Cruz de Tenerife, que ocasionaron 8 muertos y cuantiosos daños materiales. Las precipitaciones, que llegaron a acumular cantidades superiores a los 200 mm en menos de 3 horas, estuvieron asociadas con estructuras convectivas.

1.6. Estado del arte de la modelización numérica del tiempo en Canarias

Existen pocos estudios realizados en el entorno de Canarias sobre modelización numérica del tiempo. Los pocos estudios que se han realizado sobre análisis de sensibilidad en Canarias se han realizado para episodios de relevancia concretos como por ejemplo en el estudio [39] en el que se realizó un análisis de sensibilidad para el evento del ciclón tropical Delta.

A continuación, se enumeran algunos de los estudios científicos más relevantes sobre modelización en Canarias:

Un estudio realizado por Domínguez et al [40] evaluó el desempeño del modelo HARMONIE-AROME en la predicción de eventos meteorológicos extremos en Canarias. Los resultados indicaron que el modelo proporciona pronósticos precisos, especialmente en la predicción de lluvias intensas y vientos fuertes.

En otro estudio [41], los autores investigaron cómo la topografía compleja de Canarias afecta la precisión de los modelos numéricos. Los resultados destacaron la importancia de la alta resolución para capturar los efectos orográficos en la formación de nubes y precipitación.

Por otro lado, el estudio [42] analizó el impacto del cambio climático en la modelización numérica del tiempo en Canarias. El trabajo concluyó que se espera un aumento en la frecuencia

e intensidad de eventos extremos, lo que subraya la necesidad de mejorar continuamente los modelos numéricos.

1.7. Estado del arte de las intrusiones de aerosol desértico en Canarias

Las Islas Canarias, debido a la proximidad a África (la mayor región fuente de aerosol desértico), son frecuentemente afectadas por intrusiones de aerosol desértico, comúnmente conocido como polvo sahariano o calima. Estos eventos tienen significativas implicaciones meteorológicas, climáticas y de salud pública. Este apartado revisa el estado actual del conocimiento sobre las intrusiones de aerosol desértico en Canarias según estudios científicos recientes.

Las intrusiones de aerosol desértico en Canarias se caracterizan por la presencia de partículas finas y gruesas de polvo en la atmósfera, originadas principalmente en el desierto del Sahara. Estas partículas pueden ser transportadas a largas distancias por vientos alisios y corrientes en chorro que afectan a la calidad del aire y a la visibilidad en las islas.

El transporte de polvo sahariano hacia Canarias se produce principalmente a través de la capa de aire sahariana (SAL por sus siglas en inglés), una masa de aire seco y cargado de polvo que se desplaza desde el Sahara hacia el oeste sobre el Atlántico.

El estudio de Querol et al [43] examinó los efectos del polvo sahariano en la calidad del aire en Canarias. Los resultados mostraron que, durante los episodios de calima, las concentraciones de partículas PM10 y PM2.5 aumentan significativamente y llegan a superar los límites establecidos por la OMS para preservar la salud respiratoria de la población.

Los autores del estudio [44] investigaron la influencia del polvo sahariano en la meteorología y el clima de Canarias. El trabajo encontró que las intrusiones de polvo pueden alterar la radiación solar, modificar las temperaturas superficiales y afectar los patrones de precipitación. Además, el aerosol desértico actúa como núcleo de condensación, y estos núcleos de condensación influyen en la formación de nubes y tormentas.

En el estudio de Basart et al [45], se utilizaron modelos numéricos para predecir las intrusiones de polvo sahariano en Canarias. La investigación destacó la importancia de los modelos de transporte de aerosoles y su integración con modelos meteorológicos para mejorar la precisión de las predicciones. Estos modelos ayudan a emitir alertas tempranas y mitigar los efectos adversos de las intrusiones de polvo.

En la investigación de Rodríguez et al [46], se analizó el impacto del polvo sahariano en la agricultura y los ecosistemas de Canarias. El estudio encontró que, aunque el polvo puede tener efectos negativos en la salud de las plantas, también puede aportar nutrientes esenciales a los suelos empobrecidos.

En las últimas décadas, se han desarrollado tecnologías avanzadas para monitorear y predecir las intrusiones de aerosol desértico. Los satélites y las redes de observación terrestre, como el programa AERONET [47], proporcionan datos valiosos sobre la concentración y distribución de aerosoles. Estas herramientas permiten una mejor comprensión y gestión de los episodios de calima en Canarias.

- Como evento significativo y reciente destaca el *episodio de Febrero 2020*. Durante este evento, una intensa tormenta de polvo sahariano afectó a Canarias, redujo la visibilidad y elevó las concentraciones de partículas en el aire a niveles peligrosos. Este evento fue ampliamente estudiado por su severidad y duración [15] [48].

1.8. Objetivos de la tesis

En los apartados anteriores (1.5. a 1.7.) se ha expuesto el estado del conocimiento actual sobre los tópicos que cubre la presente tesis. Los objetivos se han planteado para cubrir, a partir de las publicaciones que se presentarán en el siguiente apartado, el déficit en cada uno de los temas señalados anteriormente. Para ello, los principales objetivos de la tesis son los siguientes:

1. Mejora en el conocimiento de los fenómenos meteorológicos adversos que afectan a Canarias.
2. Proponer umbrales relacionados con índices convectivos, de estabilidad y otros relacionados con el estado de la troposfera específicos para Canarias.
3. Mejora en el conocimiento en relación con las limitaciones que presentan los modelos numéricos de predicción en Canarias.
4. Realizar, por primera vez en Canarias, un análisis de sensibilidad en cuanto a modelización numérica se refiere, para conocer el impacto en la predicción de distintas configuraciones del modelo en un periodo extenso con el modelo WRF utilizando como condiciones iniciales las condiciones del modelo HRES-IFS de Centro Europeo de Predicción para Medio Plazo.
5. Desarrollo de herramientas de alerta temprana enfocados a fenómenos convectivos que tienen lugar en el área de interés en base al conocimiento adquirido (figura 9).
6. Mejorar el conocimiento en cuanto a la caracterización de intrusiones de polvo en Canarias mediante series temporales más extensas a las analizadas en la bibliografía actual. Hay que tener en cuenta que las series de espesor óptico de aerosol (OAD por sus siglas en inglés) y de material particulado de hasta 10 micras (PM10) comienzan en el año 2000. La aproximación utilizada en esta tesis a través de datos de visibilidad ha permitido realizar un análisis desde los años 80 del pasado siglo.
7. Desarrollo de un índice de severidad para el análisis objetivo de tormentas de polvo.

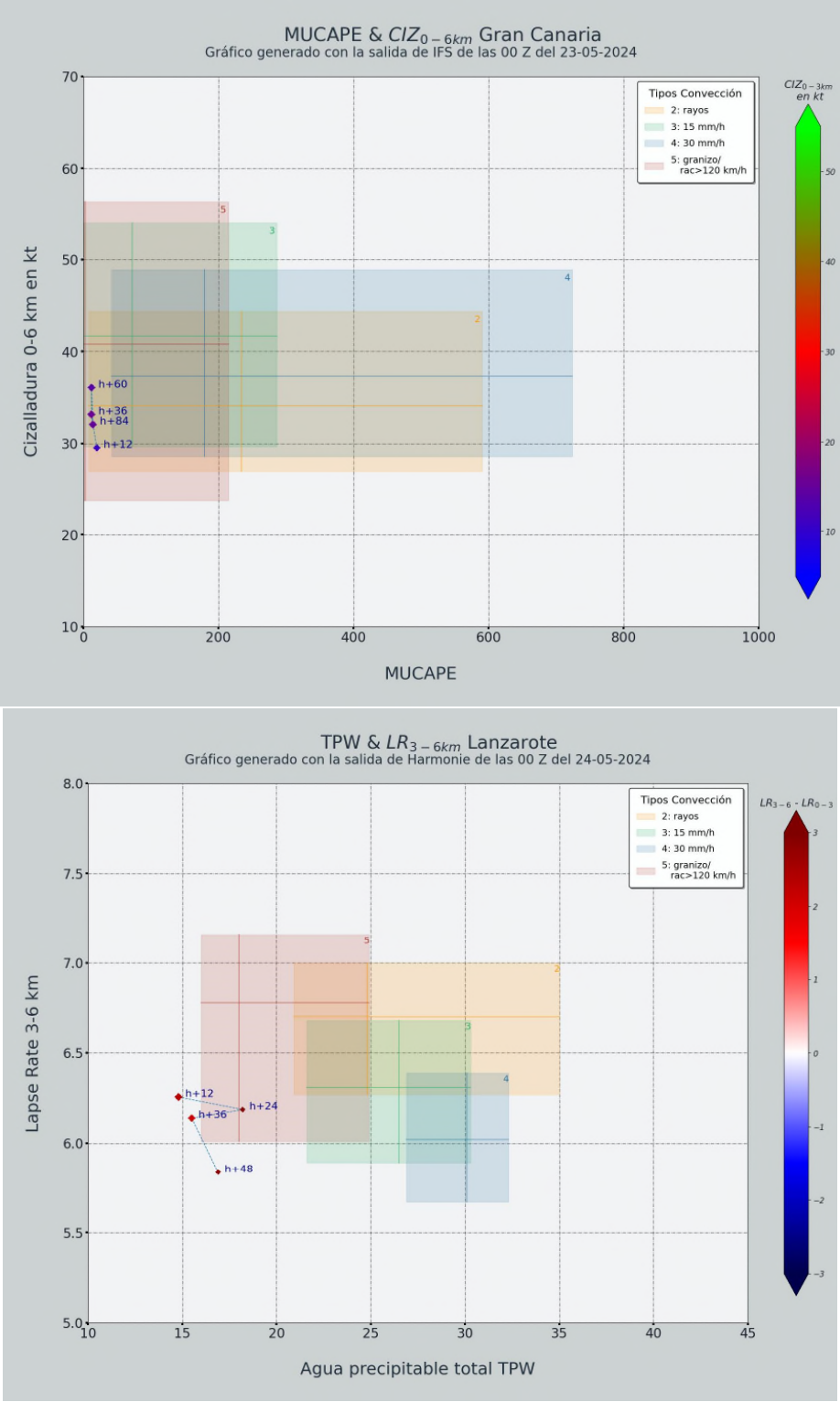

Figura 9: Gráficos que representan índices y variables extraídos de sondeos previsto del modelo Harmonie-Arome. En sombreado en colores aparecen las áreas de los tipos de situaciones en función de los valores que toman las variables. Estos umbrales están adaptados en base al estudio [49] que forma parte de esta tesis. (Figuras cortesía de Javier de Luis, Analista-predictor del Grupo de Vigilancia de AEMET en Canarias).

1.9. Presentación de los trabajos publicados

Esta tesis se propone como compendio de artículos. Para ello, se han publicado, en el marco de la tesis, tres artículos que se adjuntan en orden cronológico de publicación en el apartado 2 del presente documento.

Los artículos son los siguientes:

Molina, D. S., Fernández-González, S., González, J. C. S., & Oliver, A. (2020). Analysis of sounding derived parameters and application to severe weather events in the Canary Islands. Atmospheric Research, 237, 104865. https://doi.org/10.1016/j.atmosres.2020.104865

Este primer artículo cubre los objetivos 1,2 y 5 del apartado 1.8.

Suárez-Molina, D., Fernández-González, S., Montero, G., Oliver, A., & González, J. C. S. (2021). Sensitivity analysis of the WRF model: Assessment of performance in high resolution simulations in complex terrain in the Canary Islands. Atmospheric Research, 247, 105157. https://doi.org/10.1016/j.atmosres.2020.105157

El segundo artículo cubre los objetivos 3 y 4 del apartado 1.8.

Suárez-Molina, D., Cuevas, E., Alonso-Pérez, S., Cana, L., Montero, G., & Oliver, A. (2024). Dust events characterization from visibility, trends and Dust Adversity Index in the Canary Islands for the period 1980–2022. Heliyon, 10(10), e31262. https://doi.org/10.1016/j.heliyon.2024.e31262

El tercer artículo cubre los objetivos 6 y 7 presentados en el apartado 1.8.

1.10. Bibliografía del Capítulo

[1] IPCC. (2021). Climate Change 2021: The Physical Science Basis. Contribution of Working Group I to the Sixth Assessment Report of the Intergovernmental Panel on Climate Change.

[2] World Meteorological Organization. (2021). Atlas of Mortality and Economic Losses from Weather, Climate and Water Extremes (1970–2019).

[3] Bauer, P., Thorpe, A., & Brunet, G. (2015). The quiet revolution of numerical weather prediction. Nature, 525(7567), 47-55.2.

[4] Chen, S. H., & Lin, Y. L. (2018). The critical role of data assimilation in numerical weather prediction. Journal of Geophysical Research: Atmospheres, 123(10), 4878-4895.

[5] UNDRR. (2019). The Human Cost of Disasters: An Overview of the Last 20 Years 2000-2019.

[6] Frame, D. J., Wehner, M. F., Noy, I., & Rosier, S. M. (2020). The economic costs of climate change. Nature Communications, 11(1), 329.

[7] Diffenbaugh, N. S., & Burke, M. (2019). Global warming has increased global economic inequality. Nature Climate Change, 9(2), 124-128.

[8] AEMET. (2022). Plan Meteoalerta. https://www.aemet.es/es/eltiempo/prediccion/avisos

[9] Meteoalarm. European Weather Warnings. Retrieved from https://www.meteoalarm.eu

[10] Hernández, M., Cruz, J., & Marquina, S. (2016). Economic impact of flooding in Tenerife (Canary Islands). Journal of Flood Risk Management, 9(3), 237-245.

[11] World Health Organization. (2018). Climate change and health. Retrieved from https://www.who.int/news-room/fact-sheets/detail/climate-change-and-health

[12] Díaz, J., Carmona, R., Mirón, I. J., Luna, M. Y., & Linares, C. (2015). Time trend in the impact of heat waves on daily mortality in Spain for a period of over thirty years (1983-2013). Environment International, 85, 290-298.

[13] Querol, X., Alastuey, A., Rodriguez, S., Viana, M. M., Artíñano, B., Salvador, P., ... & Cuevas, E. (2004). Levels of particulate matter in rural, urban and industrial sites in Spain. Science of the Total Environment, 334-335, 359-376.

[14] Aena. (2020). Calima February 2020: Impact on Air Traffic. https://www.aena.es/en/press-room/news/2020/calima-february-2020-impact.html

[15] Cuevas Agulló, E., Milford, C., Barreto Velasco, Á., Bustos Seguela, J. J. D., García Cabrera, R. D., Marrero, C., ... & Campo Hernández, R. D. (2021). Desert Dust Outbreak in the Canary Islands (February 2020): Assessment and Impacts.

[16] Dorta, P., Díaz, J. P., Hernández, E., & Fernández, G. (2013). Saharan dust intrusions and hospital admissions in the Canary Islands. International Journal of Environmental Health Research, 23(2), 124-134.

[17] UNDRR. Reduction of Mortality and Economic Losses from Disasters. https://www.undrr.org

[18] World Meteorological Organization. Early Warning Systems. https://public.wmo.int/en/our-mandate/focus-areas/early-warning-systems

[19] United Nations . Economic Benefits of Early Warning Systems. https://www.un.org/en/development/desa/policy/cdp/cdp_publications/2019cdppolicybriefs/early-warning-systems.pdf

[20] IOC-UNESCO. Pacific Tsunami Warning and Mitigation System. https://ioc.unesco.org/tsunami

[21] World Food Programme. . Early Warning Systems in Africa. https://www.wfp.org/early-warning

[22] Gobierno de Canarias (2012) .PEFMA: Plan Especial de Protección Civil de Fenómenos Meteorológicos Adversos. https://www.gobiernodecanarias.org/cultura/fileadmin/documentos/docs/seguridad/PEFMA.pdf

[23] National Oceanic and Atmospheric Administration. (2023). Global Forecast System (GFS). Retrieved from https://www.noaa.gov/gfs

[24] European Centre for Medium-Range Weather Forecasts. (2023). Integrated Forecast System (IFS). Retrieved from https://www.ecmwf.int/en/forecasts/dataset/ifs

[25] HIRLAM Programme. (2023). High Resolution Limited Area Model (HIRLAM). Retrieved from https://hirlam.org

[26] European Centre for Medium-Range Weather Forecasts. (2023). Advances in Numerical Weather Prediction. Retrieved from https://www.ecmwf.int/en/research/modelling-and-prediction

[27] Skamarock, W. C., Klemp, J. B., Dudhia, J., Gill, D. O., Liu, Z., Berner, J., ... & Powers, J. G. (2019). A description of the advanced research WRF model version 4. National Center for Atmospheric Research (NCAR) Technical Note.

[28] Bengtsson, L., Steinheimer, M., Bechtold, P., Geleyn, J. F., & Geiß, L. (2017). A seamless weather–climate prediction model based on variable resolution GCM. Monthly Weather Review, 145(11), 4365-4386.

[29] Brousseau, P., Berre, L., Bouttier, F., & Desroziers, G. (2016). Flow-dependent background-error covariances for a convective-scale data assimilation system. Quarterly Journal of the Royal Meteorological Society, 142(694), 1130-1140.

[30] Powers, J. G., Klemp, J. B., Skamarock, W. C., Davis, C. A., Dudhia, J., Gill, D. O., ... & Duda, M. G. (2017). The Weather Research and Forecasting Model: Overview, system efforts, and future directions. Bulletin of the American Meteorological Society, 98(8), 1717-1737.

[31] Suárez, A., & Ramis, C. (2020). Climatology of Convective Storms in the Canary Islands. Journal of Applied Meteorology and Climatology, 59(7), 1293-1307.

[32] Fernández, J., Sánchez, E., & García-Díez, M. (2018). Topographic Influence on Convective Activity in the Canary Islands. Atmospheric Research, 210, 85-94.

[33] García-Herrera, R., Gallego, D., & Hernández, E. (2019). Climate Change and Its Effects on Convection in the Canary Islands. Climate Dynamics, 53(4), 2345-2357.

[34] Pérez, L., Suárez, L., & Torres, C. (2021). Saharan Dust and Convective Storms: A Deadly Combination. Environmental Research Letters, 16(11), 113002.

[35] Quintero-Plaza, D., González-Alemán, J.J., Alejo-Herrera, C.J., Suárez-Molina, D., González-Alejandre, C., & Peñate-De La Rosa, I.S. (2024). Verification of forecasted precipitation from Tropical Storm Hermine in the Canary Islands. Weather. https://doi.org/10.1002/wea.4558

[36] Rodríguez, A., Hernández, M., & Marrero, J. (2017). Analysis of the 2015 Gran Canaria Storm: Dynamics and Impacts. Meteorological Applications, 24(3), 362-371.

[37] AEMET. (2005). Estudio de la tormenta tropical "Delta" y su transición extratropical: efectos meteorológicos en Canarias. http://hdl.handle.net/20.500.11765/1341

[38] AEMET. (2003). SITUACIÓN DE LLUVIAS TORRENCIALES EN SANTA CRUZ DE TENERIFE (31 DE MARZO DE 2002). http://hdl.handle.net/20.500.11765/1791

[39] Marrero, C., Jorba, O., Cuevas Agulló, E., & Baldasano, J. M. (2008). Sensitivity study of surface wind flow of a limited area model simulating the extratropical storm Delta affecting the Canary Islands. Advances in Science and Research, 2, 151-157. http://www.adv-sci-res.net/2/151/2008/asr-2-151-2008.html

[40] Domínguez, M., Rodríguez, E., & González, P. (2021). Performance evaluation of HARMONIE-AROME model for extreme weather events in the Canary Islands. Meteorological Applications, 28(1), e1954.

[41] Fernández, J., Sánchez, E., & García-Díez, M. (2018). Topographic influence on weather forecasting in the Canary Islands. Atmospheric Research, 210, 85-94.

[42] García-Herrera, R., Gallego, D., & Hernández, E. (2019). Climate change impacts on weather modeling in the Canary Islands. Climate Dynamics, 53(4), 2345-2357.

[43] Querol, X., Alastuey, A., Rodríguez, S., Viana, M. M., Artíñano, B., Salvador, P., ... & García Dos Santos, S. (2004). Levels of particulate matter in rural, urban and industrial sites in Spain. Science of the Total Environment, 334-335, 359-376.

[44] Pérez, C., Nickovic, S., Baldasano, J. M., Sicard, M., Rocadenbosch, F., & Cachorro, V. E. (2006). A long Saharan dust event over the western Mediterranean: Lidar, Sun photometer observations, and regional dust modeling. Journal of Geophysical Research: Atmospheres, 111(D15).

[45] Basart, S., Pérez, C., Cuevas, E., Baldasano, J. M., & Gobbi, G. P. (2012). Aerosol characterization in Northern Africa, Northeastern Atlantic, Mediterranean Basin and Middle East from direct-sun AERONET observations. Atmospheric Chemistry and Physics, 12(2), 847-875.

[46] Rodríguez, E., Guerra, J. A., & Cuevas, E. (2018). Impact of Saharan dust on the biomass and metabolism of marine phytoplankton—A mesocosm experiment in the subtropical North Atlantic. Journal of Marine Systems, 156, 71-85.

[47] Giles, D. M., Sinyuk, A., Sorokin, M. G., Schafer, J. S., Smirnov, A., Slutsker, I., Eck, T. F., Holben, B. N., Lewis, J. R., Campbell, J. R., Welton, E. J., Korkin, S. V., and Lyapustin, A. I.: Advancements in the Aerosol Robotic Network (AERONET) Version 3 database – automated near-real-time quality control algorithm with improved cloud screening for Sun photometer

aerosol optical depth (AOD) measurements, Atmos. Meas. Tech., 12, 169–209, https://doi.org/10.5194/amt-12-169-2019, 2019.

[48] Escudero, M., Stein, A. F., Draxler, R. R., Querol, X., Alastuey, A., & Castillo, S. (2021). Source apportionment for African dust outbreaks over the Western Mediterranean using the Hybrid Single-Particle Lagrangian Integrated Trajectory model (HYSPLIT) applied to PM10 data. Journal of Geophysical Research: Atmospheres, 116(D19).

[49] Molina, D. S., Fernández-González, S., González, J. C. S., & Oliver, A. (2020). Analysis of sounding derived parameters and application to severe weather events in the Canary Islands. Atmospheric research, 237, 104865. 10.1016/j.atmosres.2020.104865

2. Trabajos publicados

2.1. Analysis of sounding derived parameters and application to severe weather events in the Canary Islands

Molina, D. S., Fernández-González, S., González, J. C. S., & Oliver, A. (2020). Analysis of sounding derived parameters and application to severe weather events in the Canary Islands. Atmospheric research, 237, 104865. 10.1016/j.atmosres.2020.104865

JOURNAL CITATION REPORTS:

2020 journal Impact factor: 5.369

Rank by Journal Impact Factor:

METEOROLOGY & ATMOSPHERIC SCIENCES: 16/94 Q1 (83.51%)

Rank by Journal Citation Indicator (JCI):

METEOROLOGY & ATMOSPHERIC SCIENCES: 13/106 Q1 (88.21%)

Atmospheric Research 237 (2020) 104865

Contents lists available at ScienceDirect

Atmospheric Research

journal homepage: www.elsevier.com/locate/atmosres

Analysis of sounding derived parameters and application to severe weather events in the Canary Islands

David Suárez Molina[a], Sergio Fernández-González[a,*], Juan Carlos Suárez González[a], Albert Oliver[b]

[a] State Meteorological Agency (AEMET), Spain
[b] University Institute for Intelligent Systems and Numerical Applications in Engineering (SIANI), University of Las Palmas de Gran Canaria, Spain

ARTICLE INFO

Keywords:
Soundings
Deep convection
Subtropical atmosphere
Severe weather events

ABSTRACT

Severe weather phenomena have serious consequences in Canary Islands. This archipelago is located in the subtropical Atlantic Ocean, west of North Africa. For this reason, its climatic characteristics differ greatly from those of mainland Spain. The importance of forecasting convective precipitation mainly lies in the damage caused by flooding. Therefore, an adequate knowledge of the thresholds for the convective indices associated with severe thunderstorms in the Canary Islands is crucial for minimizing the damage that these events cause.

In this paper, 7021 soundings from the Güimar station (id = 60,018, Tenerife, Spain) during the period 2009–2018 were analysed. Observation data are used to categorize soundings as representative of conditions for no thunder episodes, general thunder, rainfall ≥15 mm/h, rainfall ≥30 mm/h and hail or wind gusts ≥120 km/h. From sounding data, several parameters were computed. For some parameters, the results show remarkable differences between categories. In the studied region, thunderstorms are not expected when CAPE values are close to 0 J/kg and the lapse rate in the 0–3 km layer is below 5 °C/km. On the other hand, heavy rainfall events (rainfall ≥30 mm/h) show the highest median of CAPE, a high median total precipitable water (TPW, close to 30 mm) and the lapse rate decreases with height. Finally, hailstorm events are characterized by High Shear (shear vector magnitude ≥35 kt) and Low CAPE (surface-based CAPE ≤500 J/kg and most unstable parcel CAPE ≤1000 J/kg) environments (HSLC).

1. Introduction

Deep convection is related to the transfer of moisture and latent heat by updrafts and downdrafts, causing meteorological risks such as strong wind gusts, heavy rain, and sometimes lightning and hail (García-Ortega et al., 2014). As a result, severe thunderstorms cause dramatic damage to properties and even fatalities every year in many regions around the world (Czernecki et al., 2016). In addition, air traffic management is strongly affected by adverse weather conditions caused by deep convection (Borsky and Unterberger, 2019). As far as aviation safety is concerned, deep convection results in problems related to turbulence, wind shear, aircraft icing, and low visibility events (Bolgiani et al., 2018). The Canary Islands are not exempt from this risk, with several cases of flash floods recorded in recent decades (Génova et al., 2015).

The analysis of the pre-convective atmospheric environment is vital when estimating the risk of severe thunderstorms events (Brooks et al., 2003). In this regard, the use of radiosonde data has proven to be useful (Sánchez et al., 2007). Thereby, the comparison between pre-convective radio soundings during severe and non-severe thunderstorm events permits the categorization of the atmospheric conditions related to deep convection (Púcik et al., 2015). In the same way, Taszarek et al. (2017) analyse the thermodynamic and kinematic variables capable of differentiating among the atmospheric conditions prone to severe and non-severe thunderstorms, distinguishing between gale-force wind gusts, large hail, and even tornadoes.

Convective storms are commonly connected with weather patterns on the synoptic scale. However, the worst effects of these events usually affect a lesser area, hindering forecasting. There are at least three essential requirements for the development of severe thunderstorms: a deep unstable layer, high moisture content in the boundary layer, and a trigger mechanism responsible for the activation of the convection process (Gascón et al., 2015). In southwestern Europe, thermal instability and low-level convergence associated with dynamic instability are the main triggers of convection (Merino et al., 2019).

The adverse effects of severe thunderstorms over human activities

* Corresponding author at: Delegación Territorial de AEMET en Cantabria, C/Ricardo Lorenzo, s/n 39012 Cueto - Santander, Cantabria, Spain.
E-mail address: sfernandezg@aemet.es (S. Fernández-González).

https://doi.org/10.1016/j.atmosres.2020.104865
Received 11 September 2019; Received in revised form 30 December 2019; Accepted 15 January 2020
Available online 16 January 2020
0169-8095/

can be diminished by having a better knowledge of this kind of meteorological phenomenon, allowing the development of early warning systems and forecasting models to minimize economic losses and even saving human lives (Bauer et al., 2015; García-Ortega et al., 2017). Due to the low performance of traditional forecasting methods in the forecast of deep convection, subjective methods based on stability indices and thermodynamic conditions were developed in order to identify the most favourable conditions for the occurrence of thunderstorms (López et al., 2007). However, no single index works best in all locations, or for all types of severe weather, such as wind, large hail, heavy precipitation or tornadoes (Doswell III, 1987). As a result, the indices calculated for a specific area cannot be extrapolated to other regions. In fact, the values of stability indices in Europe tend to be lower than in North America or tropical latitudes (López et al., 2001). It is known that the performance of convection indices is highly dependent upon the features of the specific area of the world (Charba, 1979), which suggests the need to estimate the thresholds of the indices associated with a certain severity of convective episodes in a specific region.

Stability indices can be calculated by analysing radiosonde data. Radiosondes have a high vertical resolution, capable of defining the bases and thicknesses of cloud layers and stable layers. They also give the only operationally available upper-air data with an absolute calibration (Lorenc et al., 1996). This is the methodology chosen in this research, in which ten years of radiosonde profiles were analysed, categorizing the events within 5 categories depending on the observational data. Subsequently, the thresholds of several stability indices related to different categories of convective episodes are estimated, with the aim of providing this information to bench forecasters during the decision-making process, helping them in the evaluation of risks associated to severe convection.

The paper is organized as follows. A brief description of the study area is covered in Section 2. Section 3 summarizes the database used in this research. Subsequently, Section 4 presents the main results of this research and the discussion, including an analysis of several convection indexes and an examination of case studies. Finally, the main conclusions of this paper are provided in Section 5.

2. Study area

The Canary archipelago (Fig. 1), which is located west of North Africa, consists of seven islands with a total area of about 7200 km^2, 1100 km from mainland Spain. Covering from 27°37′ to 29°25′N and from 18°10′ to 13°20′W, all islands belong to the subtropical zone. Canary Islands are under the direct influence of the trade wind belt, making the climate very stable all year. Usually, the Azores high acts as a shield, preventing Atlantic lows from affecting the area south of 30°N. Moreover the islands are surrounded by the Canary Current, coming from the north as a cold derivation of the Gulf Stream (Herrera et al., 2001). The average trade winds blow mainly against the north side of the islands, advecting wet and fresh air, which can rise over the island slopes, often leading to condensation and cloud growth that is usually obstructed by the typical vertical stratification structure (Font, 1956). Therefore, three main layers can be distinguished:

1) Relatively fresh and moist air exists at low levels, due to the cold surface water of the Canaries Current.
2) A subsidence inversion is usually found roughly between 700 and 1500 masl (meters above sea level). Temperature increases across this layer up to 6 °C, acting as a lid that obstructs any convective development, even those forced by the orography.
3) Over the inversion layer, the air is dry and clear.

In this way, water vapour is condensed at low levels, under the inversion layer, developing non precipitating thin clouds, which are called “cloud sea” when viewed from above the clouds' top. As a result, the typical weather on Canary Islands is very stable and dry. Rainy events only happen when disturbances break the inversion layer, either at surface (Atlantic lows) or at upper levels (troughs). The importance of high-level disturbances on the islands' precipitation must be emphasized. Most of the typical rainfall situations cannot be detected at surface level, and are only evident when upper levels are analysed.

2.1. Weather impact on the Canary Islands

In spite of the apparent climatic mildness, the frequency and intensity of the severe weather events have serious consequences on the Canary Islands (Dorta, 2007). To contextualize the impact that severe weather events have in the Canary Islands, statistics on fatalities due to natural hazards in the Canary Islands can be used. In the period from 1995 to 2014 there have been a total of 74 fatalities due to disasters caused by severe weather events. According to information provided by the CCS (Consorcio de Compensación de Seguros, a public organization

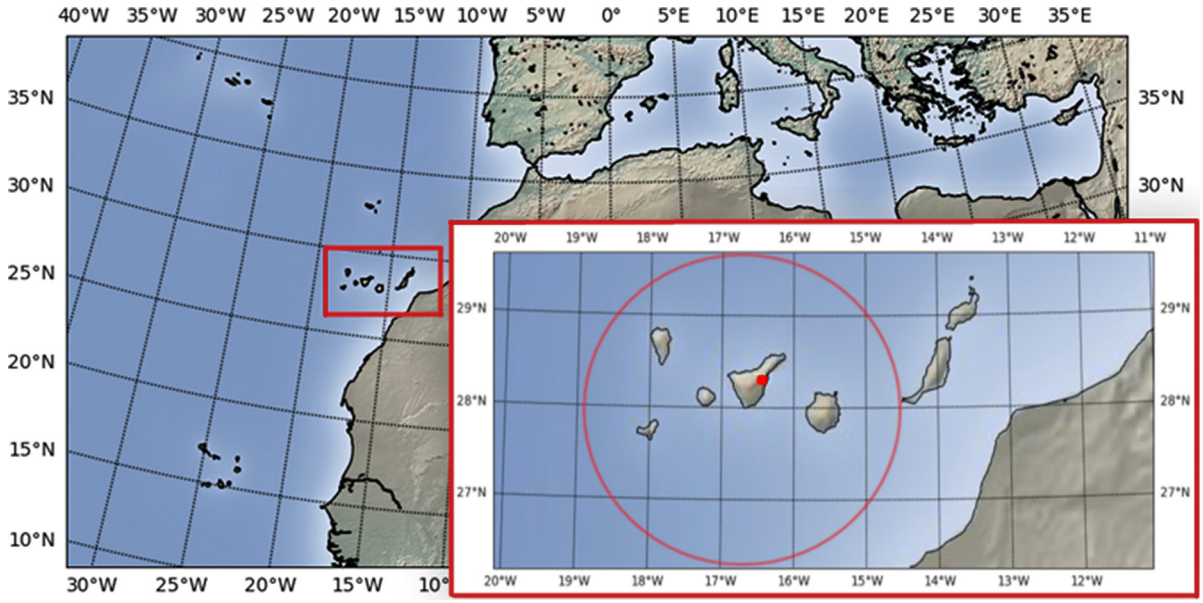

Fig. 1. Study area, with a zoom of Canary Islands. The red circle indicates the 200 km threshold of the radio sounding representativeness. The red dot highlights station number 60018 (Güimar, Tenerife). (For interpretation of the references to colour in this figure legend, the reader is referred to the web version of this article.)

funded by the Ministry of Economy, Industry and Competitiveness), the losses in economic terms due to floods and windstorms in the Canary Islands throughout the period 1996–2018, amounted to > 211 million Euros.

One of the biggest impacts is caused by flooding and landslides due to intense rainfall. Precipitation is very rare and localized, which makes them more destructive since neither the infrastructures nor the population are prepared to face them. The spatial and temporal concentration of rainfall in Canary Islands is therefore a severe hazard, which together with the high vulnerability creates extreme risk situations (Suárez-Molina et al., 2018). The origin of situations of extreme adversity must be sought in the action of high level troughs and cut-off lows, with marked thermal instability that leads to deep convection associated with some processes by which an air parcel is lifted to its level of free convection (LFC).The lift required to raise an air parcel to its LFC generally must be supplied by some processes operating at subsynoptic-scale, because the rising motions associated with synoptic-scale processes usually are too slow to lift a potentially buoyant parcel to its LFC in the required time (Doswell III, 1987). Tropical factors may have an essential role during some events, such as a disturbance of tropical origin, or indirectly, the interaction of the polar front with maritime tropical air masses of high moisture content.

3. Methods

3.1. Proximity criteria

Radio sounding data at 00 and 12 UTC from the station number 60018 located in Güimar (Tenerife) were collected for the period 2009–2018. A proximity criteria of 200 km from the sounding release location (represented by a red circle in Fig. 1) was defined, with a temporal representativeness covering the period from 09 to 15 UTC and 21–03 UTC (6 h period centred on the 00 and 12 UTC soundings). The 200 km threshold lies within the range of the 80-km used by Darkow (1969), Schaefer and Livingston (1988) and Brooks et al. (1994) and 400-km criteria utilized by Rasmussen and Blanchard (1998). The 200 km threshold was also selected because of the different behaviour of rainfall in the easternmost islands (Lanzarote and Fuerteventura) in relation to the rest of the archipelago. According to Herrera et al. (2001), annual precipitation behaviour of the five western islands is very similar, while Lanzarote and Fuerteventura form an appreciably separated cluster (Herrera et al., 2001). As a result, Güimar radiosonde is not representative of the atmospheric conditions on Lanzarote and Fuerteventura due to the proximity to the African continent and the influence of the Saharan Air Layer.

3.2. Criteria for event selection

Observational data for the period from January 1, 2009 to December 31, 2018 were used. These data were extracted from the AEMET observational database and have been used to divide the dataset into 5 categories (Table 1). The categories are exclusive, and each event was assigned using the most severe observation (i.e., a wind gust ≥120 km/h or hail event was assigned only in category 5, even if rainfall ≥30 mm /h also occurred). Therefore, an event is only included in one category, although in that event it meets several criteria. The classification criteria is exclusive and it is in descending order (category 5, category 4, category 3 and so on).

The lightning strike threshold of two or more cloud-to-ground (CG) strikes is consistent with the criteria established by Reap (1986) and Orville (1991), similar to the > 3-CG strike threshold used by Hamill and Church (2000), but much less than the > 10-CG strike criteria used by Rasmussen and Blanchard (1998).

Categories 3 and 4 agree with the 1 h rainfall thresholds established in the National Plan of Prediction and Surveillance of Adverse Meteorological Phenomena (METEOALERTA, 2018), elaborated by AEMET in coordination with Spanish Civil Protection Authorities, for the interest area. At least 2 observations are necessary in category 5 in order to avoid singular points. This is because in high areas of Tenerife (e.g., Izaña is located at 2371 m above sea level) many days wind gusts ≥ 120 km/h of non-convective origin are recorded. To illustrate this local effect, the automatic meteorological station network of the Canary Islands was used. The wind gust threshold of 120 km/h was exceeded in Izaña in 54 days. In contrast, the location with the second most threshold exceedances was La Palma airport with only 8 days.

No attempt was made to modify the soundings. It was anticipated that the effects of unrepresentative, contaminated, or erroneous data would be damped out in the statistical analysis (Craven and Brooks, 2004).

Table 1
Definitions and number of proximity soundings for the five categories.

Category	Definition	Quantity
1	No thunder or < 2 CG strikes	6791
2	General thunder (≥ 2 CG strikes)	58
3	Rainfall ≥15 mm/h	81
4	Rainfall ≥30 mm/h	34
5	Hail or wind gust ≥120 km/h at least in 2 locations	57

3.3. Sounding derived parameters

A list of the parameters computed from the sounding dataset is shown in Table 2. One often underappreciated aspect of computing CAPE is the effect of moisture on the calculation. For this reason all CAPE values were calculated using the virtual temperature correction (Doswell III and Rasmussen, 1994). Different air parcels are being used to calculate CAPE. The prefixes MU, ML and SB have been designed to identify air parcels. MU is the most unstable parcel found in the lowest 300 hPa of the atmosphere, ML represents the mean conditions in the lowest 100 hPa, while SB is the surface based parcel. The SB parcel choice uses the surface air and dew point temperatures to determine the parcel ascent path.

Although it allows a better representation of surface-based convection, calculations can be highly dependent on small time and space scales when these thermodynamic parameters display significant variations. The ML parcel choice is used to lift a parcel constituting a well-mixed layer of constant potential temperature and mixing ratio. Due to the averaging properties of the ML parcel choice, it is less variable in time and space than SB. Values of ML are typically smaller than those of SB. The ML and SB will be equal when the boundary layer is well mixed throughout the lifting layer. The MU will always produce the largest estimation of buoyancy among the three measures introduced above. There is an ongoing discussion as to what the best choice is. It seems that every forecaster has his own preference. Due to the high sensitivity

Table 2
Parameters computed from soundings (m AGL refers to meters above ground level).

Parameter	Units
MUCAPE	J/kg
MLCAPE	J/kg
SBCAPE	J/kg
0–3 km Lapse Rate	°C/km
3–6 km Lapse Rate	°C/km
700–500 hPa Lapse Rate	°C/km
850–700 hPa Lapse Rate	°C/km
LCL height (lifted condensation level)	m AGL
0–1 km Bulk shear	kt
0–3 km Bulk shear	kt
0–6 km Bulk shear	kt
Total precipitable water	mm

of CAPE for minor changes in temperature and dew point one should always be aware of which CAPE one is considering. In order to characterize and to establish CAPE thresholds to the different categories defined in Table 1 for the area of interest, ML, MU and SB parcels were used.

4. Results and Discussion

4.1. Analysis of convection indexes

In this section, box-and-whisker plots (Tukey, 1977) are used extensively to compare data in each category. Boxplot essentially presents a quick sketch of the distribution of the underlying data. Boxplots can convey a surprisingly large amount of information at a glance. Median and quartiles of the boxplot are highly robust and resistant to any outliers that might be present. One important use of box plots is the simultaneous graphical comparison of several batches of data (Wilks, 2011).

4.1.1. CAPE

During the forecasting of deep convection episodes, one of the main problems an operational forecaster faces is determining a representative value of potential instability. Deciding which parcel to "lift" in the computation of CAPE is crucial in this diagnostic process (Craven et al., 2002). The choice of different parcels for the computation of CAPE (Fig. 2) shows an overlap between categories. However, it is possible to discriminate in most cases category 1 from the rest since the values are close to 0 J/kg. There is overlap between category 1 and 5 for the MLCAPE. However, this category presents higher distribution values of MUCAPE (median = 21 J/kg) and SBCAPE (median = 17 J/kg) than category 1. Typical soundings of category 5 are called "inverted-V" since the dew point depression decreases significantly with height. These events have dry air in the lower troposphere with nearly saturated air in the middle troposphere. As will be seen later, convection tends to be high based since the Convective Condensation Level is at a high elevation. Due to negative buoyancy related to latent cooling of evaporation aloft that causes it to accelerate toward the surface, strong winds are the most common severe weather (Fernández-González et al., 2016). Hail or wind gusts higher than 120 km/h events (category 5) are characterized by low CAPE environments.

Situations categorized as type 2, 3 and 4 show the largest median differences between SBCAPE and MUCAPE. However, categories 2 and 3 have SBCAPE medians close to 0 J/kg and category 4 has a SBCAPE median of 485 J/kg. In the categories 2 and 3 low values of SBCAPE can be explained because convective storms may be sustained by air feeding the updraft from this level. It is likely to occur, when the surface layer may be substantially cooler than the air above it. In that case, it is more appropriate to calculate MUCAPE. The highest CAPE medians were found it in the category 4 (745 J/kg for MUCAPE, 485 J/kg for SBCAPE and 65 MLCAPE). These events are characterized by a temperature near dew point in all layers and the parcels can rise from surface and there is not much further latent cooling of evaporation since air is already or nearly saturated.

It is interesting to note that in > 75% of the cases, the MLCAPE, MUCAPE and SBCAPE values are below 1000 J/kg. In typical severe storm environments, CAPE values < 1000 J/kg are usually considered small (Markowski and Richardson, 2010). These results are in agreement with those obtained by Sherburn and Parker (2014), who defined low CAPE environments by surface-based CAPE ≤500 J/kg and most unstable parcel CAPE ≤1000 J/kg. The values obtained in this research are also similar to those measured in the north-west of the Iberian Peninsula during hailfall episodes (López et al., 2001). However, these results differ from those obtained by Craven and Brooks (2004), with similar CAPE values in severe storms with and without hail. CAPE values calculated in Canary Islands are lower than the ones obtained during severe thunderstorms in China (Li et al., 2018), United States (Brooks et al., 2003) and even in Europe (Brooks et al., 2007; Tuovinen et al., 2015). The lower CAPE values characteristic of Canary Islands might be connected to the dry air commonly located above the trade-wind inversion layer. This fact highlights the need to adapt the convection index thresholds to the region of interest.

4.1.2. Lapse rates

Low level (0–3 km and 850-700 hPa, Fig. 3 and Fig. 4) Environmental Lapse Rate (ELR) shows significant difference between category 1 and the rest of the categories. Category 1 shows 75% lapse rate values less than 5°C/Km, stable or absolutely stable. Conditionally unstable conditions predominate for the rest of the categories. Categories 4 and 5 show more than 75 percent of conditionally unstable conditions. This is consistent with the research carried out by Taszarek et al. (2017), in which higher lapse rates at low levels were found during hail and severe wind gust events. Our results are also in agreement with the conclusions of Jin et al. (2017), who detected that the midlevel temperature lapse rate was strongly correlated to hailfall in South Korea.

Analysing the upper layers of the atmosphere (3-6 km and 700-500hPa, Fig. 3 and Fig. 4), it is observed that instability increases with

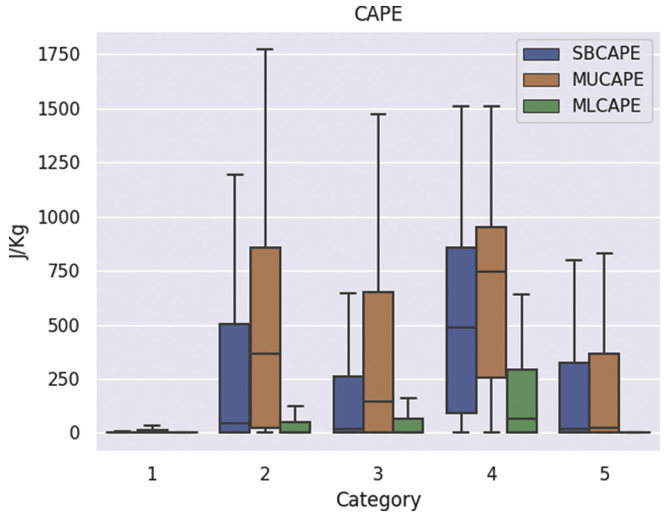

Fig. 2. Box and whisker plot of the lowest 100 hPa mean layer CAPE (J/kg), Most Unstable parcel found in the lowest 300 hPa CAPE (J/kg) and Surface Based parcel CAPE (J/kg).

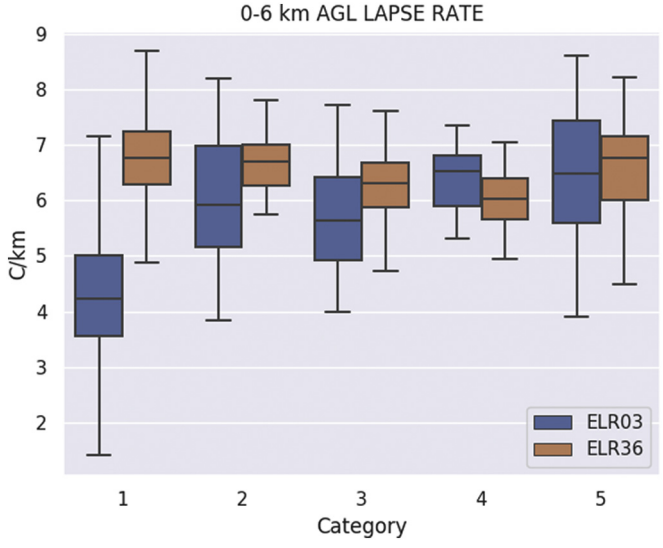

Fig. 3. Box and whisker plot of 0-3 km AGL Environmental Lapse Rate (°C/km) and 3-6 km AGL Environmental Lapse Rate (°C/km).

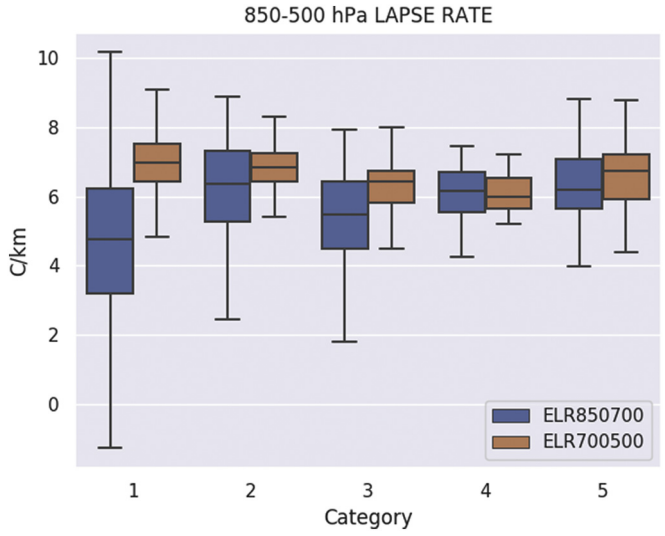

Fig. 4. Box and whisker plot of 850-700 hPa Environmental Lapse Rate (°C/km) and 700-500 hPa Environmental Lapse Rate (°C/km).

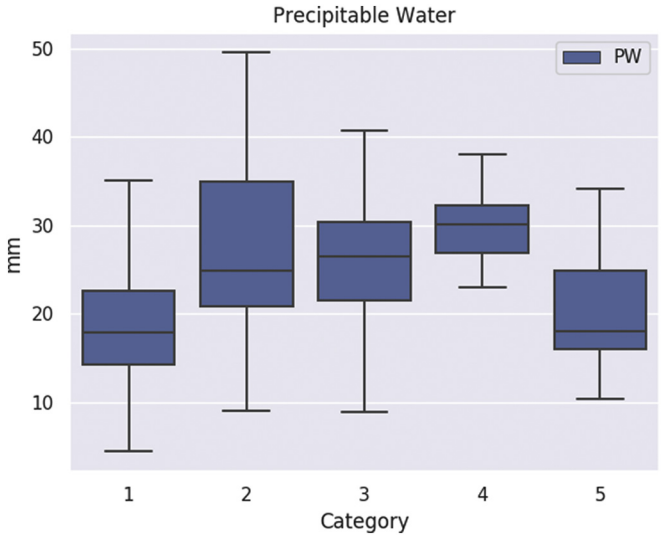

Fig. 5. Box and whisker plot of total precipitable water (mm).

height for all categories except for category 4 where the median goes from being 6.5°C/km (0-3 km AGL Lapse Rate) to 6°C/km (3-6 km AGL Lapse Rate). The results calculated for Canary Islands are consistent with those obtained by Craven and Brooks (2004) in the United States, although the no thunder category is more clearly discriminated in this research by the lapse rates between 0-3 km.

The explanation of the change in conditions from stable or absolutely stable to conditionally unstable with height in category 1, is due to the vertical structure of the atmosphere in the region under normal conditions. Trade winds, which blow towards Ecuador, come from higher latitudes and, as a result, act like cold masses. Above these winds, there is layer of the hottest and driest air in the world, so that the inversion that separates both air masses is extremely sharp and stable. However, that inversion has potential instability (also called convective instability or thermal instability), and just a column lift to subvert it. The negative lapse rates between 850-700 hPa in category 1 are related to the presence of a subsidence inversion.

According to Houston and Niyogi (2007), lapse rates are crucial in the development of convective clouds. They are connected to potential instability, which is the state of an unsaturated layer or column of air in the atmosphere with a wet-bulb potential temperature (or equivalent potential temperature) that decreases with elevation. If such a column is lifted bodily until completely saturated, it will become unstable (i.e., its temperature lapse rate will exceed the saturation-adiabatic lapse rate) regardless of its initial stratification (Saucier, 1955).

4.1.3. Total precipitable water

Total precipitable water (TPW) shows median values around 18 mm for categories 1 and 5 (Fig. 5). On the other hand, categories 2 and 3 with 75 percent exceed 20 mm while category 4 exceeds that threshold in 100 percent of the cases, placing its median around 30 mm.

Therefore, high TPW values (above 20 mm) are necessary for the occurrence of heavy rain events on the Canary Islands. Nevertheless, hailstorms can take place with TPW values below 20 mm, so it does not seem a transcendental factor in the hail development in the study area. These TPW values are slightly lower than those obtained by Li et al. (2018) during hailstorm events in China. In that research, the authors found a direct relationship between the TPW amount and the hail size. Similarly to CAPE, the reason of the TPW values in Canary Islands may be linked to the cold oceanic current that exists in the western shore of North Africa, as well as the dry air above the trade-wind inversion.

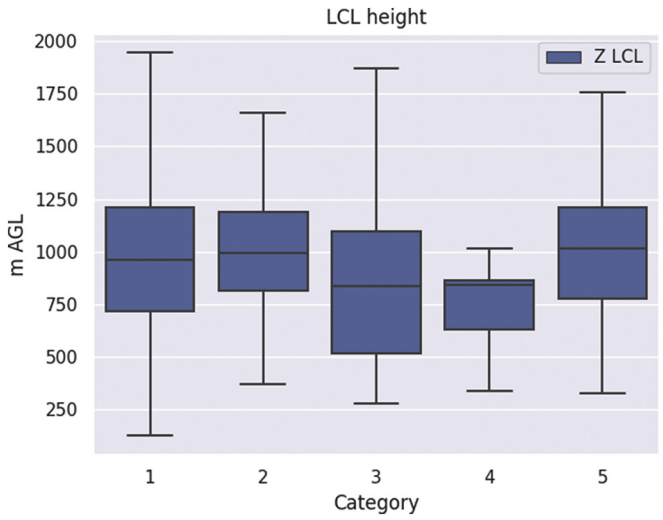

Fig. 6. Box and whisker plot of LCL height (m AGL).

4.1.4. LCL height

The median values of LCL height (Fig. 6) in the categories 1, 2 and 5 are around 1000 m AGL. Categories 3 and 4 (all related to heavy rainfall) show medians around 830 meters. Since moisture in the planetary boundary layer is related to the LCL (Li et al., 2018), these results indicate that high moisture in the boundary layer is necessary for the occurrence of heavy rain events, while it is not indispensable for the development of thunderstorms or hailstorms. Our results are in agreement with those of Taszarek et al. (2017), who claimed that large hailstorm and severe wind gusts events take place with higher cloud bases than the non-severe thunderstorm events. Since relatively low moisture in the boundary layer is related to more low-level cooling through sublimation, melting and evaporation of falling precipitation, stronger outflow are generated, increasing the likelihood of severe wind gusts (Rasmussen and Blanchard, 1998).

4.1.5. Vertical wind shear

In general, wind shear increases with height for all categories (Fig. 7).The most relevant feature is that the median values of categories 3, 4 and 5 are around 40 kt for 0-6 km layer (Fig. 7) and the category 1 can be discriminated because in more than 75 percent of the cases 0-6 km Bulk shear do not reach the 40 kt threshold. Category 5 shows the highest median of low level wind shear, (0-1 km Bulk shear,

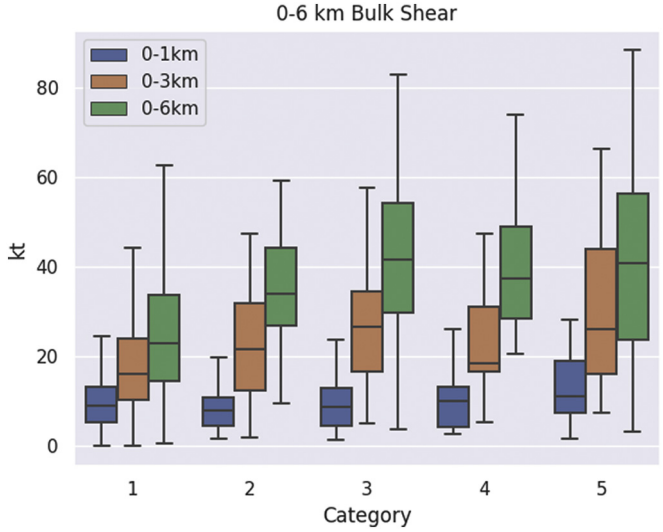

Fig. 7. Box and whisker plot of 0-1 km shear, 0-3 km shear and 0-6 km shear (kt).

Fig. 7) around 12 kt. In fact, hail or wind gust ≥ 120 km/h events are characterized by high 0–6 km bulk shear vector magnitude (Fig. 7) and Low CAPE. Our results agree with those obtained by Sherburn and Parker (2014), who linked High-Shear environments of 0–6 km shear vector magnitude ≥ 35 kt with hail events. In addition, Taszarek et al. (2017) asserted that the risk of hailstorms increase along with higher values of wind shear, being this the best parameter for assessing the severity of deep convection events. Our results are also consistent with those obtained by Jin et al. (2017), who detected a strong correlation between strong bulk wind shear and hail occurrence.

Severe weather episodes were recorded with a broad range of CAPE and shear values (Schneider and Dean, 2008). Therefore, the high dispersion observed in the box and whisper plots of bulk shear for category 5 may be related to the wide variety of meteorological conditions that can trigger strong winds during convective events (Taszarek et al., 2017). Severe convective storms in environments with large vertical wind shear but meagre instability [high-shear, low-CAPE (HSLC) environments] have received only modest attention in the literature compared to their higher-CAPE counterparts (Sherburn and Parker, 2014). However, Craven and Brooks (2004) related High-Shear environments with risk of significant tornadoes.

4.1.6. Other parameters computed

In addition to the parameters calculated in the previous subsections, other parameters were computed. In the case of storm relative helicity (0-1 km and 0-3 km, graphs not shown), no relevant conclusions were found. Nevertheless, remarkable results were obtained in the case of thicknesses analysis. Several thicknesses were calculated: 1000-850 hPa, 1000-700 hPa, 1000-500 hPa, 850-700 hPa (graphs not shown). All thicknesses computed show notable differences. The medians values for category 5 is considerably smaller than other categories. Empirical studies (e.g., Glahn and Bocchieri, 1975; Cantin and Bachand, 1993) have shown that certain values of differing thickness have shown some skill in differentiating between rain and snow.

In this way, empirical thresholds based on medians values of different thickness (from category 5 events) have been established in the Canary region as critical thickness, to distinguish between the precipitation types. Table 3 shows the critical thickness values for different atmospherics layers on the Canary Islands. These values can be used to help the precipitation type forecasting in this area. In applying these values to forecast, if thickness values are less than the critical thickness value, snow is the likely precipitation type. If thickness values are greater than the critical thickness value, rain is the likely precipitation type. Thickness values just provide a clue to the precipitation type, not the occurrence of the precipitation.

Table 3
Critical thickness in meters.

Thickness	Critical thickness values (meters)
1000-850 hPa	1365
1000-700 hPa	2936
1000-500 hPa	5550
850-700 hPa	1572

4.2. Seasonal and annual variability

The global distribution of seasonal and inter annual variations of CAPE and TPW during 2009–2018 are analyzed in this section. First, the left panel of Fig. 8 displays the monthly average values of CAPE. Medians values around 0 J/kg are obtained for much of the year, except in autumn (September, October, November), when the median increases to around 50 J/Kg. The seasonal cycle of CAPE is defined by the seasonal cycles of temperature and specific humidity. Higher values are generally found in the autumn for the Canary Islands. In contrast to the global distribution of seasonally averaged CAPE (Riemann-Campe et al., 2009), where higher values are generally found in the summer northern hemisphere (June, July, and August, JJA). These differences are due to the strength of the subsidence inversion in summer (JJA) in the Canary Islands. The inversion suppresses convection by acting as a cap. Therefore, an air parcel rising into the inversion layer would sink back to its original level because the rising parcel would be colder and denser than the air surrounding it.

Inter annual variations of CAPE (right panel of Fig. 8) show small median differences between years. However, the 75th percentile presents notable differences between years, mainly the years 2014, 2015 and 2017 where it reaches 200 J/kg. Data grouped by season (Fig. 9) highlights the winter (DJF) of 2010 and the spring (MAM) of 2017. The high values of CAPE in the winter of 2010 are in agreement with the results obtained by Núñez Mora et al. (2019), who indicated that this year was the one with the highest number of storm days in the Canary Islands, with 80 days (studied period 2007-2016).

Seasonal cycle of TPW is quite similar to CAPE's cycle. TPW median values are between 10 to 20 mm throughout the year (left panel of Fig. 10) but these values rise above that 20 mm threshold during August, September and October, and then decrease again in November. These results are in agreement with those of Romero Campos et al. (2011), who claimed that, during these months, the air in contact with the sea surface is heated and has more capacity to store water vapour. Then, the updrafts and downdrafts associated to convection spread water vapour more evenly throughout the entire column. The right panel of Fig. 10 shows inter annual variations of TPW. Note that the annual median is close to 20 mm and that there are no marked differences between years, being inter annual variability of TPW much lower than that of CAPE. As shown in Fig. 11, the TPW was also remarkably high during the winter of 2010.

4.3. Case studies

In this section, the parameters derived from the radio soundings are analysed in detail for two case studies. Both situations correspond to events before 2009 and therefore not included in the statistics calculated in the previous subsection. Case a) corresponds to a category 4 event, while case b) matches to a category 5 episode.

4.3.1. Case a (10/29/2006)

The synoptic situation was characterized by a blocking high (Fig. 12) on the north of the Iberian Peninsula extending to northern

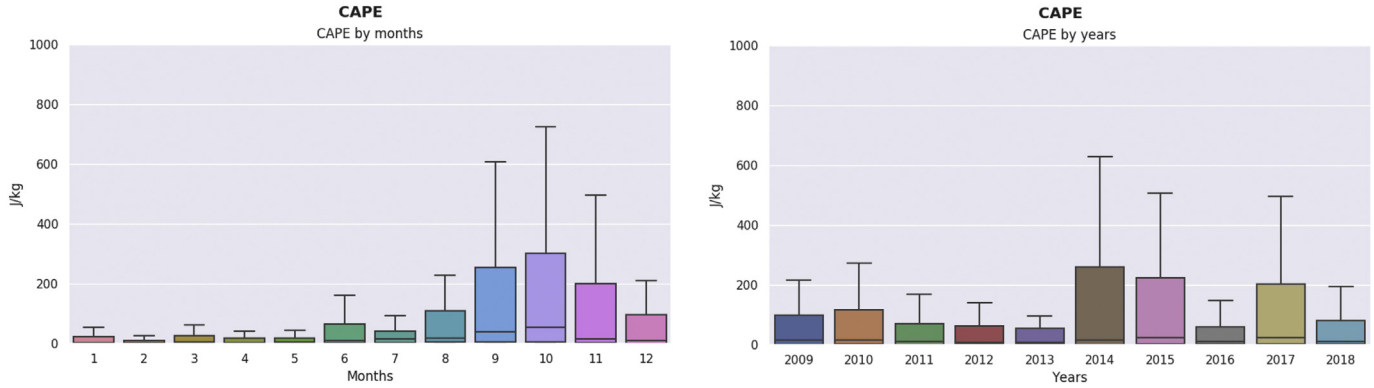

Fig. 8. Box and whisker plot of CAPE (J/kg) group by months (left) and by years (right).

Europe, while the Canary Islands were affected by a low pressure system with a minimum sea level pressure of 1012 hPa. At 500 hPa, the low system was located on the north of the Canary Islands with a core temperature around -18 °C. The heaviest rainfall in one hour (Fig. 13) occurred in the south of La Gomera (53.5 mm in an hour).

4.3.2. Case b (02/19/2004)

In case b), the Canary Islands were affected by an intense extra-tropical cyclone (with a minimum of sea level pressure of 994 hPa, Fig. 14), causing strong west-southwest wind over the region. In 500 hPa the low system was located northwest of the islands with a core temperature around -24 °C. The heaviest rainfall accumulated in one hour during this event is shown in Fig. 15. El Hierro was the most affected island (15.2 mm in an hour), being the rainfall accumulated in one hour considerably lower than that registered during episode a). Nevertheless, wind gusts were more intense in this event (Fig. 16). Although the threshold of 120 km/h was not reached, hail was observed in at least 2 locations and, as a result, this event belongs to category 5.

Table 4 shows the values of the calculated parameters for both situations. The results of case studies are of great interest because they are consistent with the results obtained for categories 4 and 5 in the previous section. Therefore, the characterization and knowledge of the different indices used in this article for the Canary Islands is relevant for operational use.

As illustrated by case a), extreme precipitation events (category 4, rainfall ≥ 30 mm /h) in the Canary Islands are characterized by high values of MUCAPE and SBCAPE compared to those obtained in the other categories in the region of interest. In addition, in these situations the lapse rate decreased with height, moving from a conditionally unstable layer (0-3 km) to a stable layer (3-6 km), and high content of TPW are presented. When a capping inversion is present but weak, or non-existent, convection can readily break out. However, in cases of stronger capping inversions, dry surfaces may be more conducive to deep convection even if there is less moisture since the larger sensible heat flux in those cases can erode the capping layer (McGinley, 1986). In these events, the precipitation intensity is related to the amount of

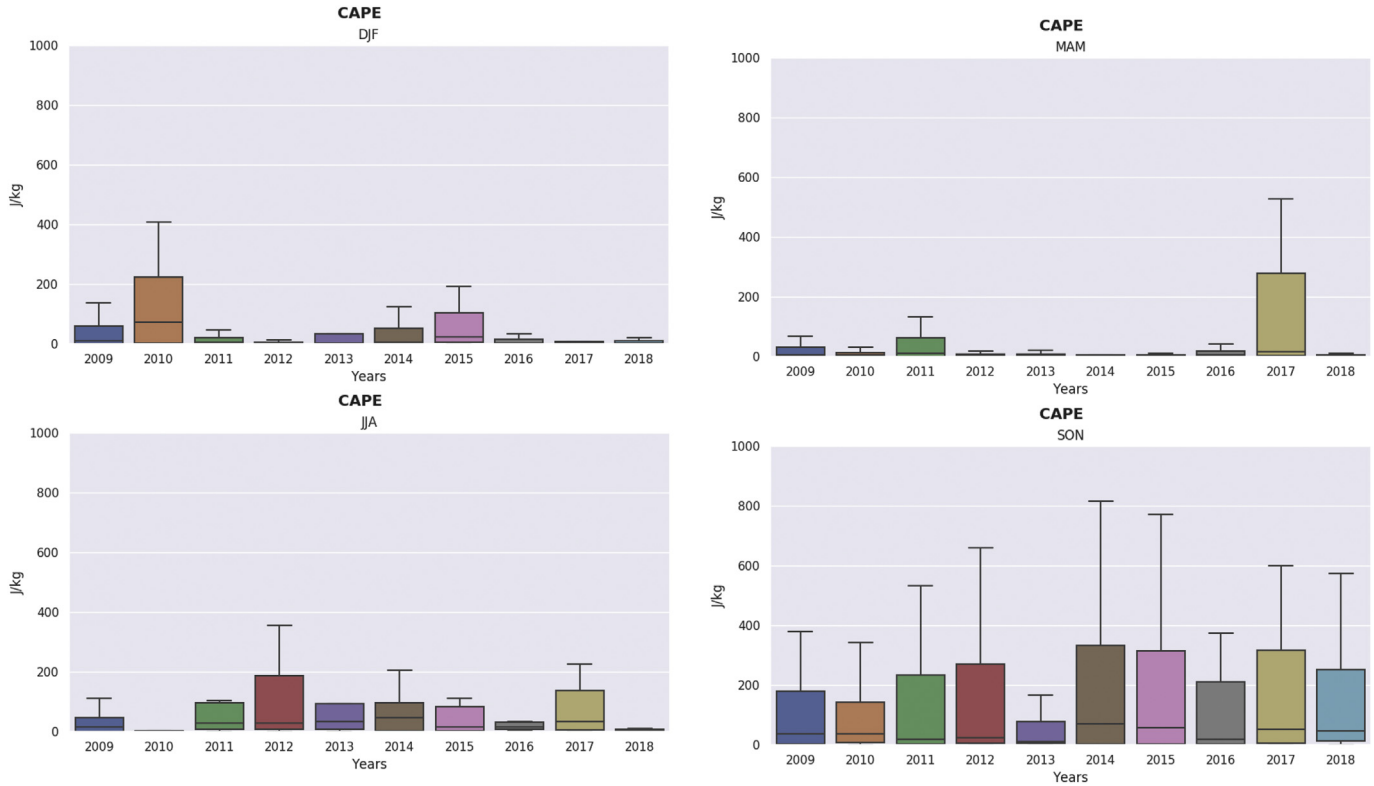

Fig. 9. Box and whisker plot of CAPE (J/kg) group by season.

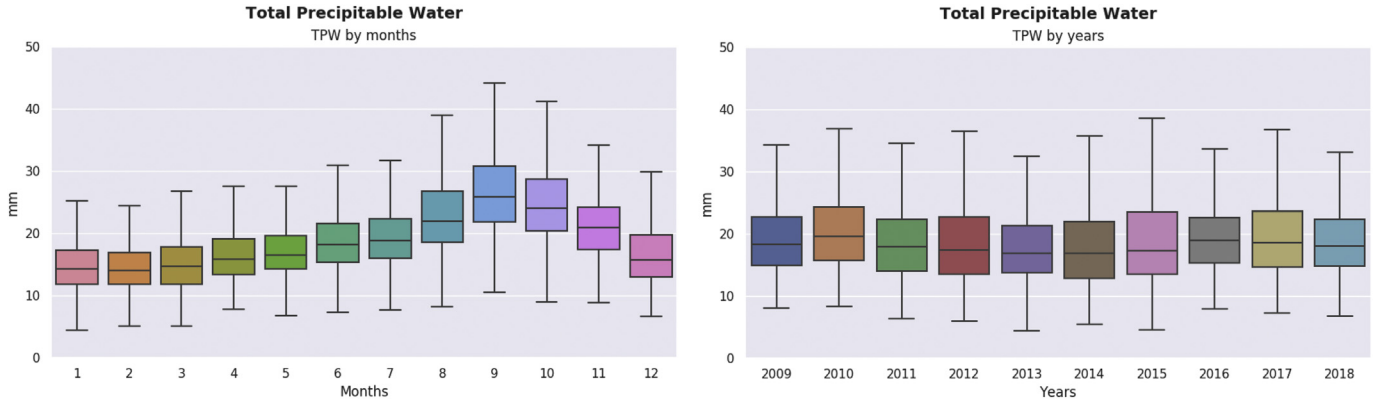

Fig. 10. Box and whisker plot of Total Precipitable Water (mm) group by months (left) and by years (right).

water vapour that is condensed in a convective updraft and the speed with which the condensation occurs. Hence, both strong instability that leads to strong updrafts and a high amount of water vapour available for condensation are important for the precipitation rate. Convection that is sustained from a deep, moist boundary layer will likely produce storms with heavy precipitation.

On the other hand, the events framed in category 5 (hail or wind gust ≥ 120 km/h), according to case study b) and the results obtained in previous section, are characterized by a high 0–6 km bulk shear vector magnitude and Low CAPE (HSLC). HSLC environments were previously defined by 0–6 km shear vector magnitude ≥ 35 kt, surface-based CAPE ≤ 500 J/kg and most unstable parcel CAPE ≤ 1000 J/kg. In addition, in these situations the lapse rate increased with height and low content of TPW are presented. These events have dry air in the lower troposphere with nearly saturated air in the middle troposphere and the convection tends to be high based.

In events of category 5, wind shear has an important influence on deep convection because it plays a role in the generation of new convective cells along the outflow of an older cell and hence influences the propagation of a storm system and it affects vertical speeds in storm updrafts and downdrafts, by causing pressure perturbations. Deep layer shear strongly influences convective organization.

4.4. Simulated soundings application

The operational forecast of convective episodes is more difficult in subtropical regions such as the Canary Islands since the performance of numerical weather prediction models is lower than in the extra-tropics (Žagar et al., 2005). The categorization carried out in this research can provide a quantification of the risk of occurrence of a certain meteorological phenomenon when the thresholds defined in the previous section are exceeded. In order to apply this technique to operational

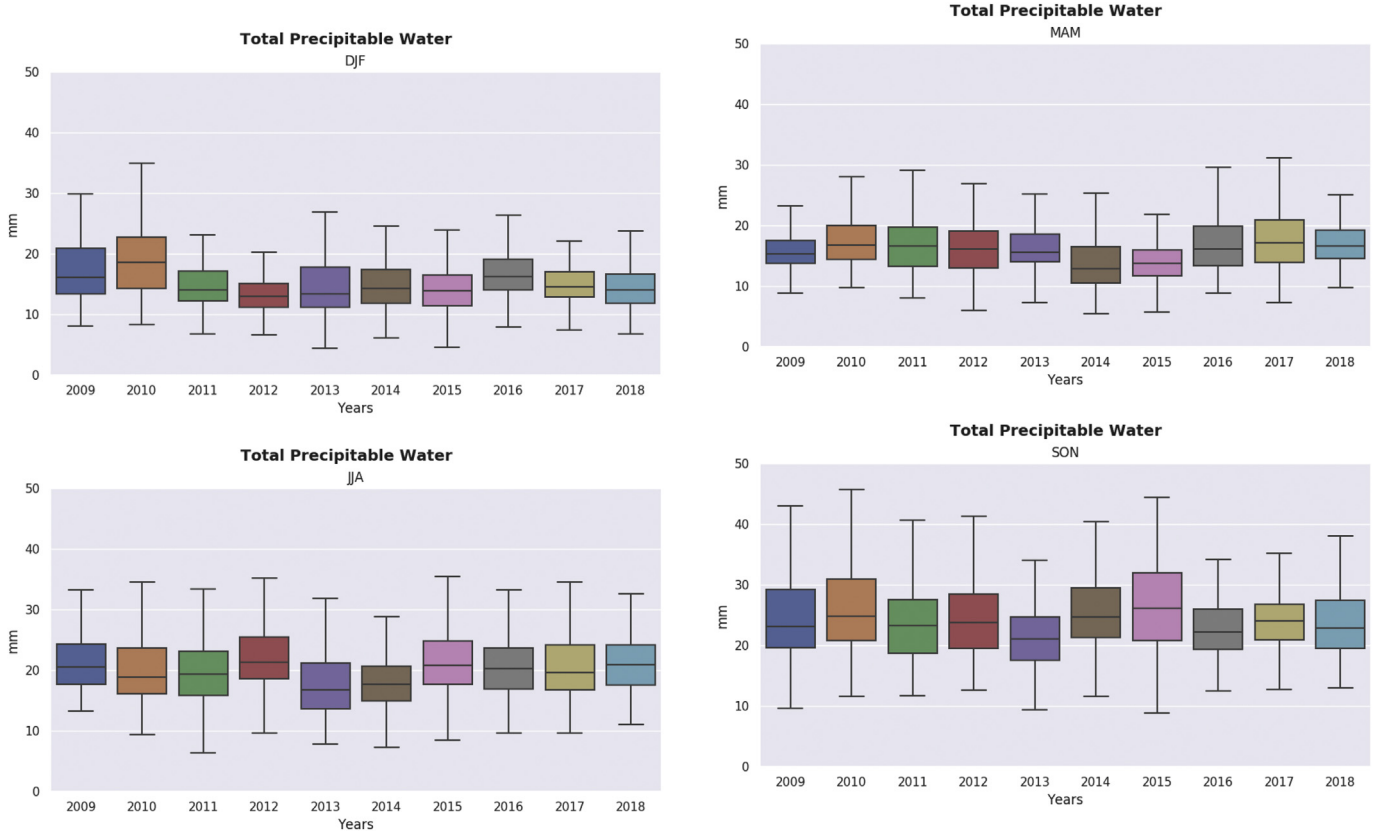

Fig. 11. Box and whisker plot of Total Precipitable Water (mm) group by season.

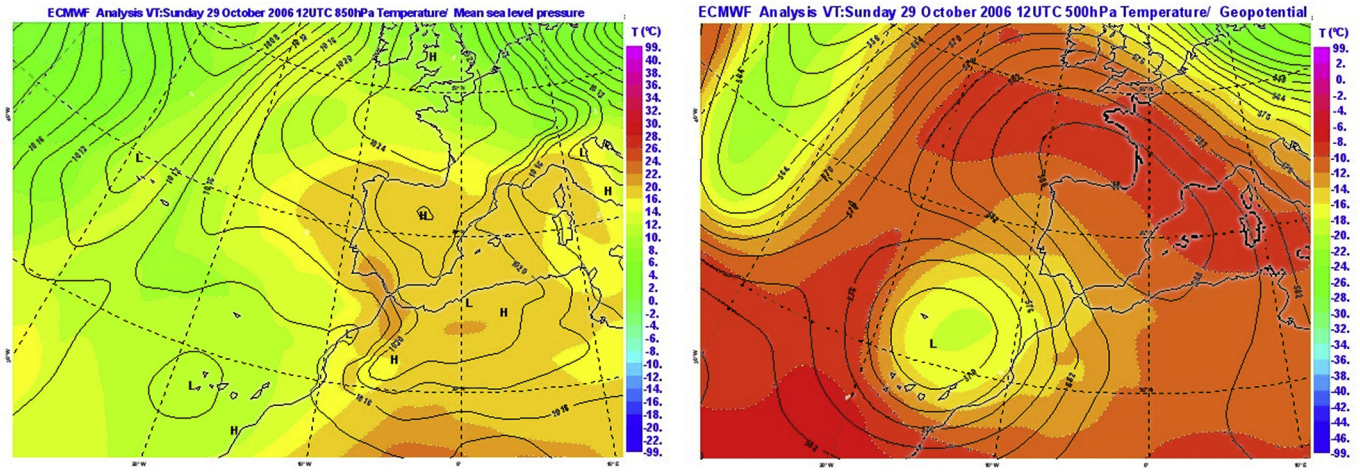

Fig. 12. Analysis from ECMWF model (29 October 2006 12 UTC). Left: Mean sea level pressure and 850 hPa temperature. Right: 500 hPa temperature and geopotential (Source: AEMET).

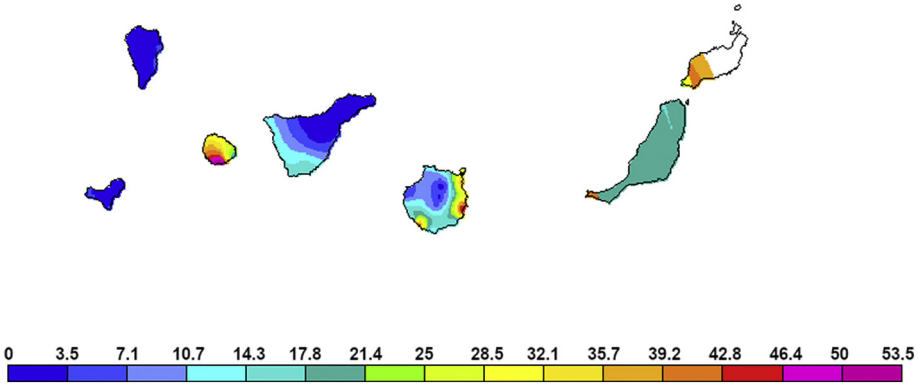

Fig. 13. Maximum 1 hour rainfall (mm) in 29 October of 2006 (Source: AEMET).

forecasting, we need to anticipate the information provided by the observed radio sounding. That is why this section presents the possibility of using forecast soundings obtained from numerical models. The soundings from high resolution models are used extensively in severe weather forecasting. Nowadays, the increase in the resolution of the numerical models makes them closer to the observation. In this regard, simulated soundings from Integrated Forecasting System (IFS) of the ECMWF for both study cases and observed sounding are shown (Fig. 17 and Fig. 18). For case study a) (Fig. 17), both soundings showed similar values of Total Precipitable Water and shear. However, CAPE's values were underestimated by simulated sounding. Due to the vertical (in 2006 operational ECMWF model had 91 levels) and horizontal resolutions the main differences have been found in low levels because the nearest grid model point is at a higher altitude than observation.

For case study b) (Fig. 18), despite the worst vertical resolution (in 2004 operational ECMWF model had only 60 levels) both soundings

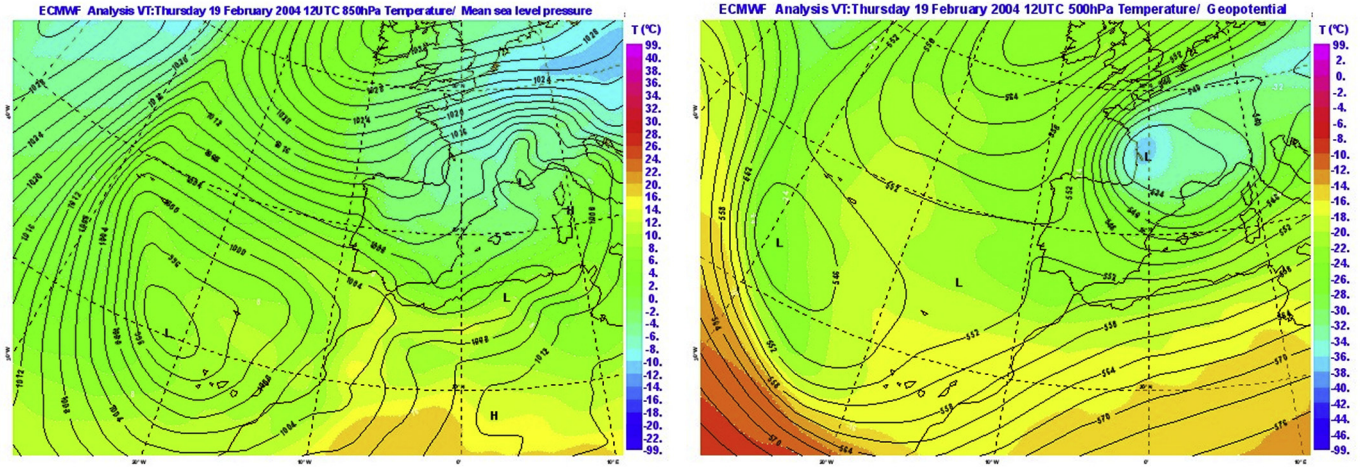

Fig. 14. Analysis from ECMWF model (19 February 2004 12 UTC). Left: Mean sea level pressure and 850 hPa temperature. Right 500 hPa temperature and geopotential (Source: AEMET).

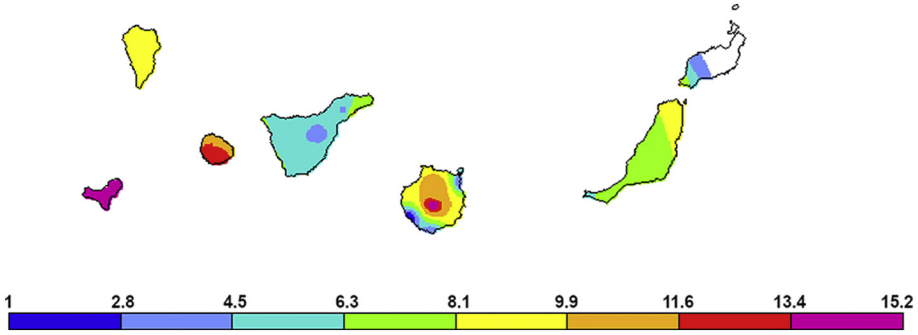

Fig. 15. Maximum 1 hour rainfall (mm) in 19 February of 2004 (Source: AEMET).

were quite similar. The low and middle levels show again the most remarkable differences. While observed sounding presents up to four temperature inversions in the low and middle levels, the simulated sounding shows only one. This is obviously due to the vertical discretization of the model.

In the first stage of convective forecasting, the operational forecaster needs data about the current weather situation to make a diagnosis. As shown above, the atmospheric conditions can be acceptably reproduced by the soundings forecasted by the IFS model. The incessant improvements in the resolution of the models make them reproduce the atmospheric conditions more precisely. In this regard, the high resolution forecast of the IFS model currently has a horizontal resolution of 9 km, and 137 vertical levels. In addition, the HARMONIE-AROME is the operative mesoscale model used in AEMET, which has a horizontal resolution of 2.5 km and 65 vertical levels. Simulated soundings provided by the HARMONIE-AROME and IFS can be really useful for making a reasonable analysis, and it can be used as a tool to predict the evolution of the weather in the short-term.

Although the performance of numerical models about the development of convective storms in subtropical regions is not very accurate, the use of convective indices obtained from forecast soundings can be useful in the diagnosis of the situation. The classification within the 5 categories defined in this research can be useful in the decision-making process when the operational forecaster has to evaluate the risk of a certain weather phenomena.

5. Conclusions

In this research, different indices from soundings were computed from the analysis of 7021 soundings from the Güimar station (id = 60018, Tenerife) during the period 2009-2018. Subsequently, a classification of the values of these indices was made according to the observed meteorological phenomena. The results can be summarised by the following remarkable conclusions:

- CAPE values were below 1000 J/kg in more than 75 percent of the cases on the Canary Islands.

Table 4
Parameters computed for both case studies.

Parameter	Case a	Case b	Units
MUCAPE	550	30	J/kg
MLCAPE	54	4	J/kg
SBCAPE	438	16	J/kg
0-3 km AGL Lapse Rate	6.1	5.7	°C/km
3-6 km AGL Lapse Rate	5.7	6.7	°C/km
LCL height (lifted condensation level)	392	932	m AGL
0-1 km Bulk shear	8.9	4.9	Kt
0-3 km Bulk shear	12.6	25.6	Kt
0-6 km Bulk shear	34.2	48.8	Kt
Total precipitable water	30	19	mm

- In the area of interest, extreme rainfall events (rainfall > 30 mm/h) are characterized by the highest median of MUCAPE and SBCAPE, a decrease of Environmental Lapse Rate with height, and high TPW. However, categories 2 and 3 showed SBCAPE median values close to 0. In addition, the analysis of CAPE values can be used to discriminate category 1 (no thunder) from the rest.
- In the Canary Islands, hail or wind gusts higher than 120 km/h events are characterized by high 0–6-km bulk Shear vector magnitude (HS) and Low CAPE (LC), besides low TPW.
- Seasonal cycle of CAPE in the Canary Islands showed differences with global distribution of CAPE. These differences are due to the strength of the subsidence inversion in summer in the Canary Islands, which acts as a lid inhibiting convection.
- The largest median values of TPW are found during August, September and October, when the highest sea surface temperatures are reached in the Canary Islands and, consequently, the air in contact with the sea surface has more capacity to store water vapour.
- In this study, it has become evident that the combination of sounding derived parameters can help the operational forecaster to evaluate the risk of adverse weather phenomenon. In order to illustrate the application of the combined use of different parameters, 2 case studies were analysed. Both cases showed similar behaviour

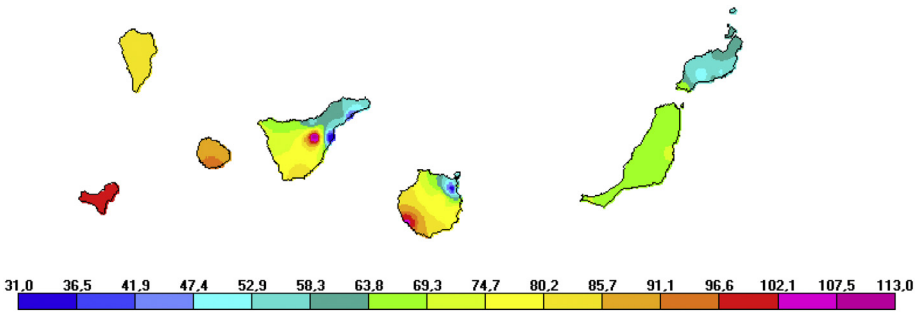

Fig. 16. Daily maximum wind gust (km/h) in 19 February of 2004 (Source: AEMET).

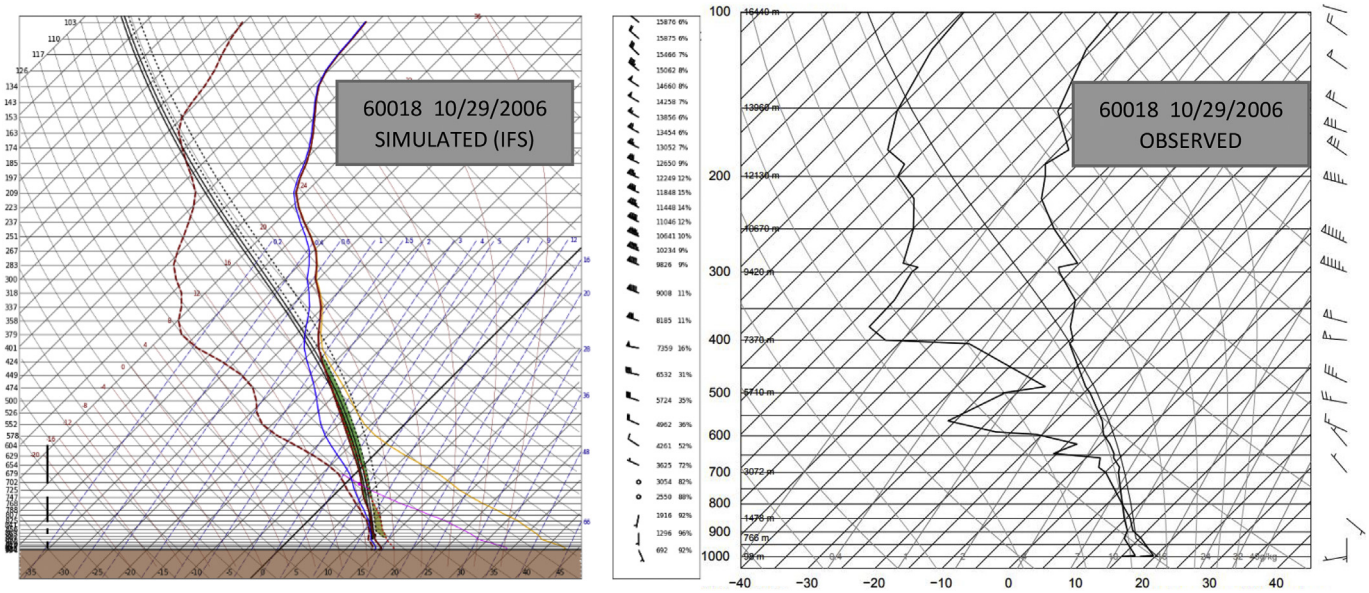

Fig. 17. Simulated and observed soundings for the case study a) (10/29/2006). Sounding forecasted by the IFS model (left panel) on the nearest grid model point to 60018 radio sounding station (Source: AEMET). Right panel shows the observed sounding from 60018 station (Source: University of Wyoming).

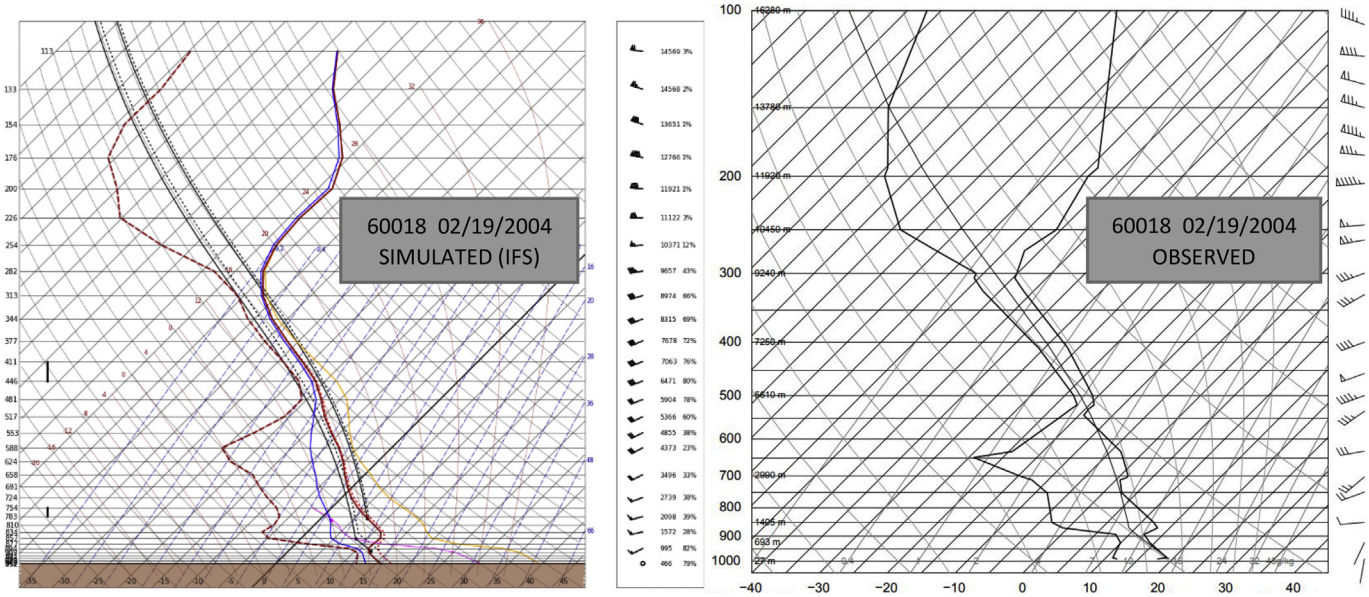

Fig. 18. Simulated and observed soundings for the case study b (02/19/2004). Sounding forecasted by the IFS model (left panel) on the nearest grid model point to 60018 radio sounding station (Source: AEMET). Right panel shows the observed sounding from 60018 station (Source: University of Wyoming).

to the results obtained with the complete data set, supporting the importance of the characterization and knowledge of environmental conditions for severe thunderstorms in the region of interest.

- Sounding data analysis can be useful to understand what kinds of atmospheric conditions are typically observed during severe thunderstorm event. They help aid forecasters in knowing when unusual conditions are occurring. In weather forecasting, it is extremely important for forecaster to recognize unusual conditions when they come together. Local studies of the frequency of occurrence of unusual conditions can be a great aid.
- In this study, forecast soundings from high resolution models showed good ability to reproduce the observed conditions. Therefore, the use of forecast soundings is recommended in order to anticipate the risk of a severe weather event.

The conclusions of this paper could significantly aid the operational forecasters of AEMET in the Canary Islands during the decision-making process of warning the population and Civil Protection Authorities about the occurrence of severe weather events, raising alerts regarding thunderstorms, heavy rain, gale-force winds and hail risk.

Author statement

The paper entitled “Analysis of sounding derived parameters and application to severe weather events in the Canary Islands” was carried out by the authors David Suárez Molina, Sergio Fernández-González, Juan Carlos Suárez González and Albert Oliver. In the following lines, the contribution of each author will be detailed:

David Suárez Molina: He is the main contributor to this paper, being the responsible of the conceptualization, design of the methodology, obtaining results, and writing.

Sergio Fernández-González has contributed in the redaction of the

paper, and supervising the research activity.

Juan Carlos Suárez González has helped with the software, data curation and formal analysis.

Albert Oliver has contributed in the second revision and the analysis of the radio soundings incorporated in this version of the manuscript.

Declaration of Competing Interest

The authors claim that there is no conflict of interest, nor any funding source that intercedes with the free publication of results obtained in this research.

Acknowledgments

Data support came from the State Meteorological Agency of Spain (AEMET). The observed soundings were supplied by University of Wyoming (http://www.weather.uwyo.edu/upperair/sounding.html). Special thanks go to the SAFEFLIGHT (CGL2016-78702-C2-1-R and CGL2016-78702-C2-2-R) and UE ERA-NET Plus NEWA (PCIN2016-080) projects.

References

Bauer, P., Thorpe, A., Brunet, G., 2015. The quiet revolution of numerical weather prediction. Nature 525, 47–55. https://doi.org/10.1038/nature14956.

Bolgiani, P., Fernández-González, S., Valero, F., Merino, A., García-Ortega, E., Sánchez, J.L., Martín, M.L., 2018. Numerical Simulation of a heavy precipitation event in the vicinity of Madrid-Barajas international airport: sensitivity to Initial conditions, domain resolution, and microphysics parameterizations. Atmosphere 9, 329. https://doi.org/10.3390/atmos9090329.

Borsky, S., Unterberger, B.C., 2019. Weather and flight delays: The impact of sudden and slow onset weather events. Econ. Transp. 18, 10–26.

Brooks, H.E., Doswell III, C.A., Cooper, J., 1994. On the environments of tornadic and nontornadic mesocyclones. Wea. Forecasting 9, 606–618.

Brooks, H.E., Lee, J.W., Graven, J.P., 2003. The spatial distribution of severe thunderstorm and tornado environments from global reanalysis data. Atmos. Res. 67-68, 73–94.

Brooks, H.E., Anderson, A.R., Riemann, K., Ebbers, I., Flachs, H., 2007. Climatological aspects of convective parameters from the NCAR/NCEP reanalysis. Atmos. Res. 83, 294–305. https://doi.org/10.1016/j.atmosres.2005.08.005.

Cantin, A., Bachand, D., 1993. Synoptic pattern recognition and partial thickness techniques as a tool for precipitation types forecasting associated with a winter storm. Centre Meteorologique du Quebec Tech. Note 93N-002, 9 pp. [Available from Environmental Weather Services Office, 100, boul. Alexis-Nihon, Suite 300, Saint-Laurent, PQ H4M 2N8, Canada].

Charba, J.P., 1979. Two-to-six hour severe local storm probabilities: An operational forecasting system. Mon. Weather Rev. 107, 268–282.

Craven, J.P., Brooks, H., 2004. Baseline climatology of sounding derived parameters associated with deep, moist convection. Natl. Wea. Dig. 28, 13–24.

Craven, J.P., Jewell, R.E., Harold, H.E., 2002. Comparison between Observed Convective Cloud-Base Heights and Lifting Condensation Level for Two Different Lifted Parcels. Weather Forecast. 17, 885–890. https://doi.org/10.1175/1520-0434(2002)017<0885:CBOCCB>2.0.CO;2.

Czernecki, B., Taszarek, M., Kolendowicz, L., Konarski, J., 2016. Relationship between human observations of thunderstorms and the PERUN lightning detection network in Poland. Atmos. Res. 167, 118–128. https://doi.org/10.1016/j.atmosres.2015.08.003.

Darkow, G.L., 1969. An analysis of over sixty tornado proximity soundings. Preprints. In: 6th Conf. on Severe Local Storms, Chicago, IL, Amer. Meteor. Soc, pp. 218–221.

Dorta, P., 2007. Catálogo de riesgos climáticos en Canarias: Amenazas y vulnerabilidad. Geographicalia, ISSN 0210-8380, N° 51, 2007. 133-160. 51. https://doi.org/10.26754/ojs_geoph/geoph.2007511118.

Doswell III, C., 1987. The Distinction between Large-Scale and Mesoscale Contribution to Severe Convection: A Case Study Example. Weather Forecast. 2, 3–16. https://doi.org/10.1175/1520-0434(1987)002<0003:TDBLSA>2.0.CO;2.

Doswell III, C., Rasmussen, E., 1994. The Effect of neglecting the virtual temperature correction on CAPE calculations. Weather Forecast. 9, 625–629. https://doi.org/10.1175/1520-0434(1994)009<0625:TEONTV>2.0.CO;2.

Fernández-González, S., Wang, P.K., Gascón, E., Valero, F., Sánchez, J.L., 2016. Latent cooling and microphysics effects in deep convection. Atmos. Res. 180, 189–199. https://doi.org/10.1016/j.atmosres.2016.05.022.

Font, I., 1956. El Tiempo Atmosférico en las Islas Canarias. Servicio Meteorológico Nacional 96.

García-Ortega, E., Hermida, L., Hierro, R., Merino, A., Gascón, E., Fernández-González, S., Sánchez, J.L., López, L., 2014. Anomalies, trends and variability in atmospheric fields related to hailstorms in north-eastern Spain. Int. J. Climatol. 34, 3251–3263. https://doi.org/10.1002/joc.3910.

García-Ortega, E., Lorenzana, J., Merino, A., Fernández-González, S., López, L., Sánchez, J.L., 2017. Performance of multi-physics ensembles in convective precipitation events over northeastern Spain. Atmos. Res. 190, 55–67. https://doi.org/10.1016/j.atmosres.2017.02.009.

Gascón, E., Merino, A., Sánchez, J.L., Fernández-González, S., García-Ortega, E., López, L., Hermida, L., 2015. Spatial distribution of thermodynamic conditions of severe storms in southwestern Europe. Atmos. Res. 164–165, 194–209. https://doi.org/10.1016/j.atmosres.2015.05.012.

Génova, M., Máyer, P., Ballesteros-Cánovas, J.A., Rubiales, J.M., Saz, M.A., Díez-Herrero, A., 2015. Multidisciplinary study of flash floods in the Caldera de Taburiente National Park (Canary Islands, Spain). CATENA 131, 22–34. https://doi.org/10.3390/geosciences8080300.

Glahn, H.R., Bocchieri, J., 1975. Objective estimation of the conditional probability of frozen precipitation. Mon. Weather Rev. 103, 3–15. https://doi.org/10.1175/1520-0493(1975)103<0003:OEOTCP>2.0.CO;2.

Hamill, T.M., Church, A.T., 2000. Conditional probabilities of significant tornadoes from RUC-2 forecasts. Wea. Forecasting 15, 461–475.

Herrera, R.G., Puyol, D.G., Martín, E.H., Presa, L.G., Rodríguez, P.R., 2001. Influence of the North Atlantic Oscillation on the Canary Islands Precipitation. J. Climate 14, 3889–3903. https://doi.org/10.1175/1520-0442(2001)014<3889:IOTNAO>2.0.CO;2.

Houston, A.L., Niyogi, D., 2007. The sensitivity of convective initiation to the lapse rate of the active cloud-bearing layer. Mon. Weather Rev. 135, 3013–3032.

Jin, H. -G., Lee, H., Lkhamjav, J., Baik, J. -J., 2017. A hail climatology in South Korea. Atmos. Res. 188, 90–99. https://doi.org/10.1016/j.atmosres.2016.12.013.

Li, M.X., Sun, J.S., Zhang, Q.H., 2018. A Statistical Analysis of Hail Events and Their Environmental Conditions in China during 2008-15. J. Appl. Meteorol. Climatol. 57 (12), 2817–2833. https://doi.org/10.1175/JAMC-D-18-0109.1.

López, L., Marcos, J.L., Sánchez, J.L., Castro, A., Fraile, R., 2001. CAPE values and hailstorms on north western Spain. Atmos. Res. 56, 147–160.

López, L., García-Ortega, E., Sánchez, J.L., 2007. A short-term forecast model for hail. Atmos. Res. 83, 176–184. https://doi.org/10.1016/j.atmosres.2005.10.014.

Lorenc, A.C., Barker, D., Bell, R.S., Macpherson, B., Maycock, A.J., 1996. On the use of Radiosonde Humidity Observations in mid-latitude NWP. Meteorol. Atmos. Phys. 60, 3–17.

Markowski, P., Richardson, Y., 2010. Mesoscale Meteorology in Midlatitudes. https://doi.org/10.1002/9780470682104.

McGinley, J.A., 1986. Nowcasting mesoscale phenomena. In: Ray, P.S. (Ed.), Mesoscale Meteorology and Forecasting. Amer. Meteor. Soc.pp. 657–688.

Merino, A., Sánchez, J.L., Fernández-González, S., García-Ortega, E., Marcos, J.L., Berthet, C., Dessens, J., 2019. Hailfalls in southwest Europe: EOF analysis for identifying synoptic pattern and their trends. Atmos. Res. 215, 42–56. https://doi.org/10.1016/j.atmosres.2018.08.006.

METEOALERTA, 2018. Plan Nacional de Predicción y Vigilancia de Fenómenos Meteorológicos Adversos. METEOALERTA. Agencia Estatal de Meteorología (AEMET). http://www.aemet.es/documentos/es/eltiempo/prediccion/avisos/plan_meteoalerta/plan_meteoalerta.pdf. (accessed 26 July 2019).

Núñez Mora, J.A., Riesco Martín, J., Mora García, M.A., 2019. Climatología de descargas eléctricas y días de tormenta en España. In: Agencia Estatal de Meteorología. Ministerio para la Transición Ecológica. Madrid. NIPO: 639-19-007-7.

Orville, R.E., 1991. Lightning ground flash density in the contiguous United States-1989. Mon. Weather Rev. 119, 573–577.

Púcik, T., Groenemeijer, P., Rýva, D., Kolár, M., 2015. Proximity soundings of severe and non-severe thunderstorms in central Europe. Mon. Weather Rev. 143, 4805–4821.

Rasmussen, E.N., Blanchard, D.O., 1998. A baseline climatology of sounding-derived supercell and tornado forecast parameters. Wea. Forecasting 13, 1148–1164.

Reap, R.M., 1986. Evaluation of cloud-to-ground lightning data from the western United States for the 1983-1984 summer seasons. J. Climate Appl. Meteor. 25, 785–799.

Riemann-Campe, K., Fraedrich, K., Lunkeit, F., 2009. Global climatology of Convective Available Potential Energy (CAPE) and Convective Inhibition (CIN) in ERA-40 reanalysis. Atmos. Res. 93, 534–545. https://doi.org/10.1016/j.atmosres.2008.09.037.

Romero Campos, P.M., Marrero de la Santa Cruz, C.L., Alonso Pérez, S., Cuevas Agulló, E., Afonso Gómez, S., Ortiz de Galisteo Marín, J.P., 2011. Una Climatología del Agua Precipitable en la Región Subtropical sobre la Isla de Tenerife basada en Datos de Radiosondeos. NT 6, Agencia Estatal de Meteorología. NIPO: 281-12-007-5.

Sánchez, J.L., López, L., Bustos, C., Marcos, J.L., García-Ortega, E., 2007. Short-term forecast of thunderstorms in Argentina. Atmos. Res. 88, 36–45.

Saucier, W.J., 1955. Principles of Meteorological Analysis. University of Chicago Press, pp. 438. https://doi.org/10.1002/qj.49708235217.

Schaefer, J.T., Livingston, R.L., 1988. The structural characteristics of tornado proximity soundings. Preprints. In: 15th Conf. on Severe Local Storms, Baltimore, MD, Amer. Meteor. Soc, pp. 537–540.

Schneider, R.S., Dean, A.R., 2008. A comprehensive 5-year severe storm environment climatology for the continental United States. Preprints, 24th Conf. on Severe Local Storms, Savannah, GA, Amer. Meteor. Soc., 16A.4. [Available online at https://ams.confex.com/ams/pdfpapers/141748.pdf].

Sherburn, K.D., Parker, M.D., 2014. Climatology and Ingredients of Significant Severe Convection in High-Shear, Low-CAPE Environments. Wea. Forecasting 29, 854–877. https://doi.org/10.1175/WAF-D-13-00041.1.

Suárez-Molina, D., Fernández-Monistrol, J.A., Uriel-González, A.E., 2018. Catálogo-guía de fenómenos meteorológicos que afectan a la isla de Gran Canaria. Agencia Estatal de.

Taszarek, M., Brooks, H.E., Czernecki, B., 2017. Sounding-Derived Parameters Associated with Convective Hazards in Europe. Mon. Weather Rev. 145, 1511–1528.

Tukey, J.W., 1977. Exploratory Data Analysis. Addison Wesley 599.

Tuovinen, J.-P., Rauhala, J., Schultz, D.M., 2015. Significant-Hail-producing storms in Finland: convective-Storm environment and mode. Wea. Forecasting 30, 1064–1076. https://doi.org/10.1175/WAF-D-14-00159.1.

Wilks, D.S., 2011. Statistical Methods in the Atmospheric Sciences, 3rd ed. Academic Press, Oxford; Waltham, MA.

Žagar, N., Andersson, E., Fisher, M., 2005. Balanced tropical data assimilation based on study of equatorial waves in ECMWF short-range forecast errors. Q. J. R. Meteorol. Soc. 131, 987–1011.

2.2. Sensitivity analysis of the WRF model: Assessment of performance in high resolution simulations in complex terrain in the Canary Islands

Suárez-Molina, D., Fernández-González, S., Montero, G., Oliver, A., & González, J. C. S. (2021). Sensitivity analysis of the WRF model: Assessment of performance in high resolution simulations in complex terrain in the Canary Islands. Atmospheric Research, 247, 105157. DOI: 10.1016/j.atmosres.2020.105157

JOURNAL CITATION REPORTS:

2021 journal Impact factor: 5.965

Rank by Journal Impact Factor

METEOROLOGY & ATMOSPHERIC SCIENCES: 18/94 Q1 (81.38%)

Rank by Journal Citation Indicator (JCI)

METEOROLOGY & ATMOSPHERIC SCIENCES: 14/108 Q1 (87.50%)

Atmospheric Research 247 (2021) 105157

Contents lists available at ScienceDirect

Atmospheric Research

journal homepage: www.elsevier.com/locate/atmosres

Sensitivity analysis of the WRF model: Assessment of performance in high resolution simulations in complex terrain in the Canary Islands

David Suárez-Molina[a], Sergio Fernández-González[a,*], Gustavo Montero[b], Albert Oliver[b], Juan Carlos Suárez González[a]

[a] State Meteorological Agency (AEMET), Spain
[b] University Institute for Intelligent Systems and Numerical Applications in Engineering (SIANI), University of Las Palmas de Gran Canaria, Spain

ARTICLE INFO

Keywords:
WRF
Sensitivity analysis
Complex terrain
PBL
Microphysics
Canary Islands

ABSTRACT

Canary Islands and other regions have been greatly damaged by weather events during the last decades. For this reason, the main duty of National Meteorological Services is to minimize socio-economic losses by forecasting adverse weather episodes with enough time in advance. To achieve this goal, the use of numerical weather prediction models is highly relevant. And, even more crucial, is to comprehend the model accuracy.

In this paper, an exhaustive sensitivity analysis of the Weather Research and Forecasting (WRF) model over the Canary Islands has been carried out. The complex terrain of the archipelago makes the islands a test bench of high interest. Four scores were used to assess the accuracy of the model configurations: Bias, mean absolute error (MAE), root of the Mean Squared Error (RMSE), and the correlation coefficient (r). Initially, twenty-five WRF model configurations were considered. However, a preliminary test discarded inadequate configurations, and reduced the number to six. The variables of interest were air temperature at 2 m (T2m), maximum 1-h wind gust at 10 m and 3-h rainfall accumulation. The results indicated a systematic wind speed underestimation. This underestimation is related to the influence of the location and the complex orography. The most accurate wind forecasts were obtained using the Mellor-Yamada-Janjic Planetary Boudary Layer (PBL) scheme with the WSM6 microphysics (MP) scheme. Another major conclusion is that, for precipitation, the PBL scheme has a greater impact than the MP scheme. Finally, the results show that the Boulac – Thompson combination is the most accurate regarding T2m forecast.

1. Introduction

Extreme weather events have negative impacts on transportations and communications, consequently resulting in catastrophic effects on distinct aspects of people's lives and economy. Despite the apparent climatic mildness, the frequency and intensity of the severe weather events have serious consequences on the Canary Islands (Dorta, 2007). To understand this impact, statistics show that severe weather events caused 74 fatalities between 1995 and Eiserloh, 2014 (Suárez-Molina et al., 2018). According to the CCS ("Consorcio de Compensación de Seguros", a public organization funded by the Ministry of Economy, Industry and Competitiveness of the Spanish Government), between 1996 and 2018, floods and windstorms in the Canary Islands produced more than 211 million Euros in losses (Suárez-Molina et al., 2020).

The accuracy of Numerical Weather Prediction (NWP) models in complex terrain is lower than over flat and homogeneous terrain. This discrepancy is attributed to the fact that boundary-layer processes in complex terrain are not well represented by NWP models. Previous studies have evaluated the performance of different planetary boundary layer (PBL) parameterization schemes in locations known for complex atmospheric situations (Pérez et al., 2006; Bossioli et al., 2009). Microphysics schemes in numerical models play a key role in simulating the formation of cloud droplets, precipitation, and land surface temperature. It also takes into account the interactions and energy fluxes between the atmosphere and the surface, which is considered a key parameter in many hydrological, meteorological and environmental studies (Anderson et al., 2011).

In recent years, the use of the Weather Research and Forecasting (WRF) model in operational mode has increased. For instance, since 2017, the National Centers for Environmental Prediction (NCEP) use in operational mode the Hurricane Weather Research and Forecast (HWRF) system (Biswas et al., 2018). In addition, the WRF model has been used by other authors in operational mode with different purposes (Hsiao et al., 2012; Hamill, 2014; Sahoo et al., 2019). The WRF model is

* Corresponding author.
E-mail address: sfernandezg@aemet.es (S. Fernández-González).

https://doi.org/10.1016/j.atmosres.2020.105157
Received 19 June 2020; Received in revised form 13 July 2020; Accepted 22 July 2020
Available online 25 July 2020
0169-8095/

also being used in γSREPS, an Ensemble Prediction System developed by AEMET, the Spanish Meteorological Agency (Callado et al., 2019).

Although other studies have used WRF in the Canary Islands for particular phenomena (Marrero et al., 2008; Jorba et al., 2015; Quitián-Hernández et al., 2018), a comprehensive sensitivity analysis has not been carried out before. Such study is essential to determine the most convenient model setup for this geographical domain (Borge et al., 2008). In addition, it should be taken into consideration that the operational forecast of convective episodes is more problematic in subtropical regions such as the Canary Islands (Žagar et al., 2005).

The purpose of this work is to evaluate the quality of WRF forecasts in the Canary Islands. The fields analyzed–air temperature at 2 m (T2m), maximum 1-h wind gust at 10 m and 3-h rainfall accumulation–are of vital importance for issuing meteorological warnings (METEOALERTA, 2018). The period analyzed (15 days in February 2018) includes various weather patterns; therefore, the sensitivity analysis will evaluate the model performance under different atmospheric conditions.

This paper is structured as follows: Section 2 describes the study area, the configuration of the WRF experiments and the observational dataset used to evaluate the model performance. Section 3 presents the results of the performance evaluation. Finally, Section 4 summarizes the paper conclusions.

2. Methodology

2.1. Study area and dataset

This research is focused on the Canary Islands (Fig. 1). This archipelago is in front of the west coast of North Africa in the subtropical zone (27°37′–29°25′N and 18°10′–13°20′W). The archipelago is formed by seven islands of volcanic origin that present a complex orography. The highest point is Mount Teide (3718 m) on Tenerife (TF). With Tenerife being by far the highest island, La Palma (LA), Gran Canaria (GC), La Gomera (GO) and El Hierro (HI) constitute a medium cluster with highest heights of: 2423 m (Roque de los Muchachos, LA), 1948 m (Pico de Las Nieves, GC), 1501 m (Pico de Malpaso, HI) and 1487 m (Garajonay, GO). Lanzarote (LZ) and Fuerteventura (FV) are much flatter with maximum heights of 671 m and 807 m, respectively.

2.1.1. Episode selection

Analysis is conducted for two periods of February 2018: from February 1st at 00 h UTC to February 11th at 12 h UTC, and from February 23rd at 00 h UTC to February 28th at 12 h UTC. This approach allows the evaluation of the meteorological model under different atmospheric conditions. The synoptic situation during the different episodes of the study period will be described below:

1–4 February 2018: High pressure system centered north of the Azores Islands with central pressures exceeding 1038 hPa. Northeasterly winds were predominant. During February 1st and 2nd, a cut-off low system affected the Canary Islands.
5 February **2018:** Low pressure system of 1008 hPa over Algeria generated weak pressure gradient across Canary archipelago
6–11 February 2018: Strong high pressure system centered near to Azores Islands with central pressures about 1040 hPa. The Canary Islands were located eastwards of the ridge.
23–28 February 2018: Different low pressure systems moving from Azores to the Canary Islands with central pressures about 966–1000 hPa. A cold front affected the islands on February 24 and 25. The prevailing winds were from the west.

2.2. WRF model configurations

The model used is the version 3.9.1 of the Advanced Research version of WRF (ARW), a fully compressible and nonhydrostatic model. Two different vertical coordinate systems are available: terrain-following coordinate (TFC) and hybrid vertical coordinate (HVC) hydrostatic pressure coordinate. The Arakawa C-grid staggering is used. The model includes the Runge-Kutta 2nd and 3rd order time integration schemes, and 2nd to 6th order advection schemes in both horizontal and vertical directions. It also applies a time-split small step for acoustic and gravity-wave modes. Dynamics conserves scalar variables. This model is described in more detail in Skamarock et al. (2008).

Boundary conditions and initial starting conditions were derived from the Operational Dataset HRES-IFS (High Resolution-Integrated Forecasting System, from ECMWF) with 0.09° x 0.09° spatial resolution and temporal resolution of 3 h. Each of the 15 days analyzed were run individually, following recommendations of similar sensitivity analysis (Evans et al., 2012; Johnson and Wang, 2012; Fernández-González et al., 2015, 2017; García-Ortega et al., 2017). The lead time of the simulations is 36 h, considering the first 12 h as spin-up time; hourly outputs were generated.

The simulations consist of three nested domains (Fig. 2) following a two-way nesting strategy, with spatial resolutions of 9 (d01), 3 (d02) and 1 km (d03), respectively. Forty sigma levels in the vertical axis

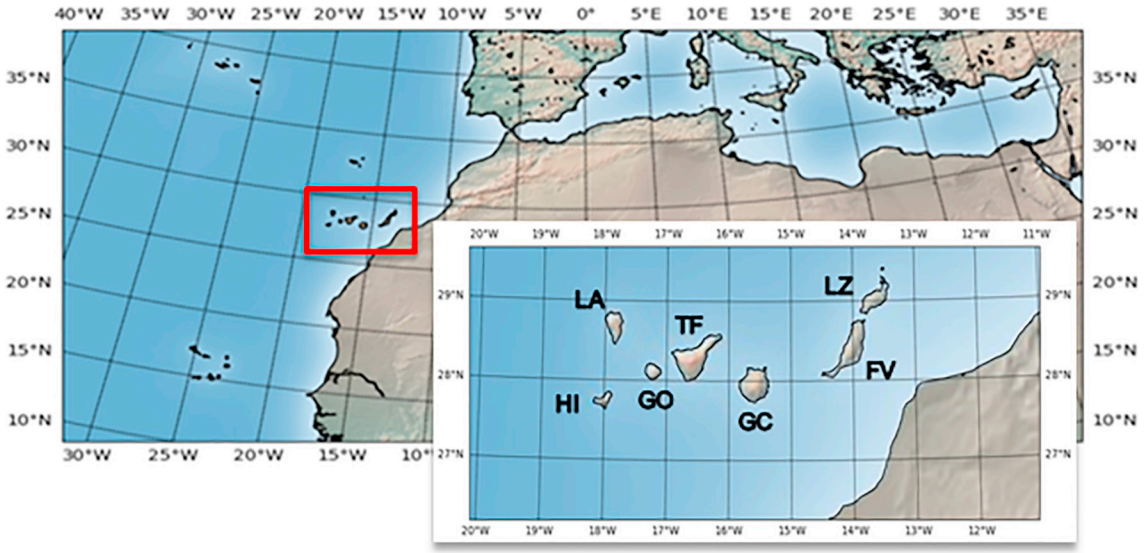

Fig. 1. Location of Canary Islands in the Subtropical Eastern Atlantic. The zoom shows the study area in more detail.

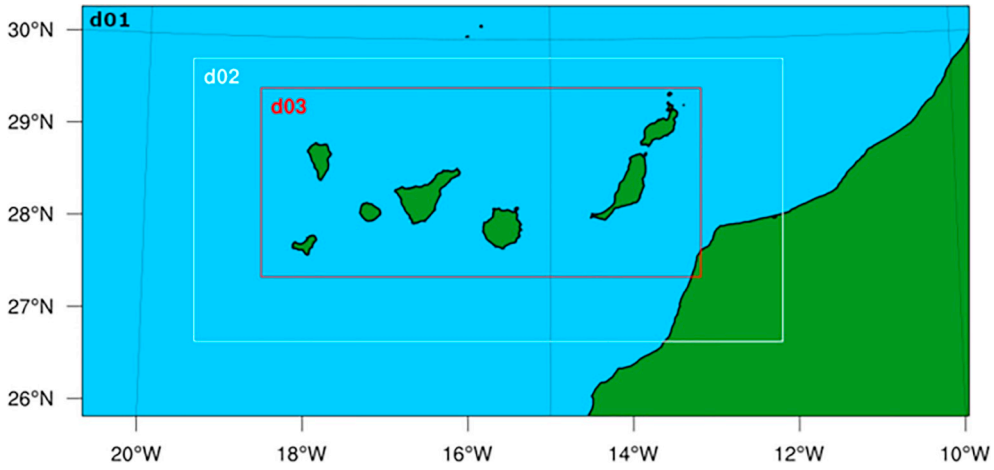

Fig. 2. Domains with spatial resolutions of 9 (d01), 3 (d02) and 1 km (d03).

were selected.

The WRF model offers several options to configure physics schemes, enabling optimization of the model for specific weather phenomenon and study area. The parameterization schemes were selected based upon previous works with similar conditions of complex terrains (Moya-Alvarez et al., 2018; González Rocha et al., 2017; Evans et al., 2012).

For radiation, the RRTMG (Iacono et al., 2008) longwave and shortwave schemes were used. It is a new version of RRTM (added in WRF Version 3.1) and includes the MCICA method of random cloud overlap. Radiation was called every 10 min. The surface processes were parameterized by the Noah Land Surface Model (NLSM), a four-layer soil temperature and moisture scheme that provides data of sensible and latent heat fluxes in the PBL (Chen and Dudhia, 2001).

The WRF Model determines surface heat, momentum, and moisture fluxes mainly via the PBL scheme, which estimates wind shear and friction at the subgrid-scale (Fernández-González et al., 2018). For this reason, five PBL scheme are evaluated to determine which one achieves the most realistic simulation for the variables of interest: the Yonsei University (YSU) (Hong et al., 2006), the Mellor-Yamada-Janjic (MYJ) (Janjic, 1994), the Mellor-Yamada-Nakanishi-Niino (MYNN2) (Nakanishi and Niino, 2006), The Asymmetric Convective Models (ACM2) (Pleim, 2007), and the BouLac (Bougeault and Lacarrere, 1989).

The YSU scheme is a first-order scheme that calculates turbulent fluxes using non-local eddy diffusivity coefficients. MYJ is an eta operational scheme with a one-dimensional prognostic turbulent kinetic energy scheme with local vertical mixing. MYNN2 predicts sub-grid TKE terms (new in Version 3.1 with a significant update in V3.8). ACM2 is the Asymmetric Convective Model with non-local upward mixing and local downward mixing. The BouLac PBL scheme is a one-and-a-half order, local closure scheme with a TKE prediction option designed for use with the BEP (Building Environment Parameterization) multi-layer, urban canopy model (Martilli et al., 2002). BouLac diagnoses PBL height as the height where the prognostic TKE reaches a sufficiently small value (in the current version of WRF is 0.005 $m^2 s^{-2}$).

All these PBL schemes require the Monin-Obukhov (MO) surface-layer scheme, except MYJ that requires Eta similarity (MOJ). MO (MM5 similarity) is based on Monin-Obukhov with Carlson-Boland viscous sub-layer and standard similarity functions from look-up tables. In contrast, MOJ is based on Monin-Obukhov with Zilitinkevich thermal roughness length and standard similarity functions from look-up tables.

In addition, five different microphysics (MP) schemes are evaluated: Kessler (Kessler, 1969), WSM6 (Hong and Lim, 2006), Goddard (Tao et al., 1989), Thompson (Thompson et al., 2008) and Morrison (Morrison et al., 2009). Kessler is a warm-rain (i.e., no ice) scheme. WSM6, Goddar and Thompson are schemes with ice, snow and graupel processes suitable for high-resolution simulations. Morrison is a double-moment ice, snow, rain and graupel scheme for cloud-resolving simulations.

Cumulus parameterizations are not recommended for high horizontal resolutions. Therefore, in domains d02 and d03, the convective processes were resolved explicitly. On the other hand, the new Kain-Fritsch cumulus scheme (Kain, 2004) was applied to domain d01.

2.2.1. Initial test

Five different PBL and five different microphysics schemes were evaluated (Table 1) in order to know its impact in the T2m, precipitation and wind gust forecast. Twenty-five simulations (5 PBL × 5 MP_PHYSICS) were run for one day (these 25 experiments were called initial test). Initial test was chosen randomly. Then, according to bias and root squared mean error (RMSE), the best configurations were selected to run the remaining 14 days, avoiding increased computational cost. The selected configurations showed in average better results for all variables in initial test. The largest differences were obtained for wind gust. Bias for the selected configurations were about −3 km/h, while for the discarded configurations, the wind gust bias reached −7.50 km/h (for the combination MYNN2-Thompson). The combinations YSU-WSM6 and MYNN2-Kessler presented the largest bias for temperature (1 °C), whereas the selected configurations exhibited temperature bias closed to −0.6 °C). The selected configurations presented precipitation bias closed to 0 mm/h in initial test, while the largest bias was found for ACM2-Goddard (−0.25 mm/h).

2.2.2. Better performing configurations

The initial test discarded inadequate combinations of parameterizations, keeping only six valid configurations for the sensitivity analysis. These valid configurations are the combination of three PBL schemes (MYJ, ACM2 and BouLac) with two microphysics schemes (WSM6 and Thompson); see Table 2.

Table 1
Summary of schemes used in initial test simulations.

Radiation (shortwave/ longwave)	Land surface model	PBL scheme - Surface layer	Microphysics scheme
RRTMG/RRTMG	NLSM	YSU-MO MYJ-MOJ MYNN2-MO ACM2-MO BouLac-MO	Kessler WSM6 Goddard Thompson Morrison 2-Moment

Table 2
Summary of combination of PBL and microphysics schemes selected.

Setting code	PBL scheme - Surface layer	Microphysics (MP) scheme
Configuration 1	MYJ-MOJ	WSM6
Configuration 2	ACM2-MO	WSM6
Configuration 3	BouLac-MO	WSM6
Configuration 4	MYJ-MOJ	Thompson
Configuration 5	ACM2-MO	Thompson
Configuration 6	BouLac-MO	Thompson

2.3. Sensitivity analysis methodology

In order to verify the model results, observational data have been used. The observation data come from the AEMET observational network. This network is composed of 68 automatic meteorological stations (Fig. 3) across the Canary Islands. The data used in this paper are T2m, maximum 1-h wind gust at 10 m and 3-h rainfall accumulation. To evaluate the accuracy of the six model configurations, forecast verification of continuous predictands was carried out.

An hourly comparison between simulation results and observations (at the 68 automatic meteorological stations) was performed, except for precipitation where the 3-h rainfall accumulation was compared. For a given observational site, the simulation result is the closest grid point to the observational location. The validation was performed on D03, ensuring that the distance between the observation site and the closest grid point will always be less than 500 m. Although this can lead to representativeness errors, such errors are systematic in all simulations and do not play a significant role in the assessment of the relative model performance across model configurations (Jiménez et al., 2010).

According to other researchers (Pereira et al., 2013; Zhao and Zhang, 2018), a threshold for the 3-h rainfall accumulation validation should be established because there is a minimum measurable precipitation amount for the operational tipping bucket rain gauges. In this paper, it has been set to 0.2 mm in 3 h.

In this research, the AFWA (the Air Force Weather Agency) diagnostic variable has been used for the maximum 10-m wind speed (afwa_diag_opt = 1). AFWA has made available to the WRF model a suite of diagnostics used in its operational Mesoscale Ensemble Prediction Suite (MEPS). The WSPD10MAX variable is used to parameterize surface wind gust (https://www2.mmm.ucar.edu/wrf/users/docs/AFWA_Diagnostics_in_WRF.pdf) applying the Weibull distribution .

Four scores were used to assess the accuracy of the model configurations: Bias, mean absolute error (MAE), root of the Mean Squared Error (RMSE), and the correlation coefficient (r). The model evaluation in the complex terrain will be presented by means of summary tables with overall results, scatter plots and through subsections lead time, geographical and vertical influence.

Bias represents the mean error and is the average of the difference between the forecast and the observation in each station and instant of time. The bias shows if the model overestimates the prediction (Bias > 0) or underestimates it (Bias < 0). It is important to note that it is not an accuracy measure, since it does not calculate the magnitude of individual forecast errors. It is computed as,

$$bias = \frac{1}{TN}\sum_{t=1}^{T}\sum_{i=1}^{N}(F_{i,t} - O_{i,t})$$

where $F_{i,\,t}$ corresponds to the forecast value and $O_{i,\,t}$ to the observed value, both at the i^{th} station in time t. The term T is the total number of hours and N the total number of stations.

Similarly, MAE is the arithmetic average of the absolute values of the differences between the members of each pair. MAE is zero for a perfect forecast and increases as discrepancies between the forecast and observations become larger. MAE can be interpreted as a typical magnitude for the forecast error in a given verification data set. The MAE formula is,

$$MAE = \frac{1}{TN}\sum_{t=1}^{T}\sum_{i=1}^{N}|F_{i,t} - O_{i,t}|$$

RMSE is the square root of the Mean Squared Error (MSE). MSE is the average squared difference between the forecast and observation pairs. Since the MSE is computed by squaring forecast errors, it will be more sensitive to larger errors than the MAE, and, thus, to outliers. RMSE has the same physical dimensions as forecasts and observations and can be considered a magnitude for forecast errors. The formula for RMSE is,

$$RMSE = \sqrt{\frac{1}{TN}\sum_{t=1}^{T}\sum_{i=1}^{N}(F_{i,t} - O_{i,t})^2}$$

Finally, r is a good measure of linear association or phase error. The correlation measures the distance between the points of a scatter plot and the diagonal. It does not take into account forecast bias; therefore, a forecast with large errors may have a good correlation coefficient; however, the correlation coefficient is sensitive to outliers. It is computed as:

$$r = \frac{\sum_{t=1}^{T}\sum_{i=1}^{N}(F_{i,t} - \overline{F})(O_{i,t} - \overline{O})}{\sqrt{\sum_{t=1}^{T}\sum_{i=1}^{N}(F_{i,t} - \overline{F})^2}\sqrt{\sum_{t=1}^{T}\sum_{i=1}^{N}(O_{i,t} - \overline{O})^2}}$$

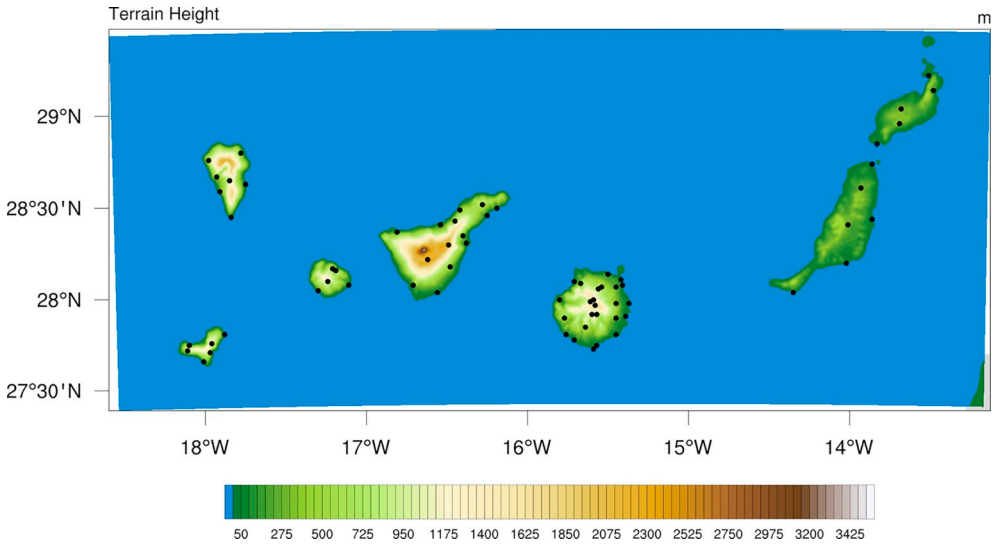

Fig. 3. Altitude within the domain 3 of the WRF model simulation. Automatic meteorological stations across the Canary Islands are marked by black dots.

Table 3
Average values of Bias, MAE, RMSE and correlation for 3-h rainfall accumulation.

	BIAS	MAE	RMSE	r
configuration 1	0.062831	3.895269	6.589668	0.587587
configuration 2	−0.504090	4.243970	7.298406	0.495282
configuration 3	0.181209	4.206904	7.073962	0.500969
configuration 4	−0.754269	3.666305	6.137176	0.557184
configuration 5	−1.666448	3.812989	6.456754	0.557064
configuration 6	−0.374882	4.131263	7.041159	0.453620

where $\overline{F}$ corresponds to the mean of forecasted values and $\overline{O}$ the mean of observed values.

3. Results and discussion

The results section is structured as follows; in Section 3.1 we will present the results of the sensitivity analysis where we discuss the different scores for the six configurations; then, we will study the dependency to the lead time (Section 3.2), to the location (Section 3.3), and altitude (Section 3.4).

3.1. Sensitivity analysis

The main objective of this study is to characterize model errors and to know the forecast accuracy in complex terrain. For these reasons, an overall evaluation has been carried out. Tables 3, 4 and 5 summarize estimated average values of the sensitivity analysis for all model configurations. The best values by score are highlighted in gray.

3.1.1. Precipitation

The recorded mean (maximum) precipitation during the period studied oscillated from 1 to 10 (110) mm/day across the archipelago.

The different scores show some differences (Table 3). Configuration 1 was practically unbiased, while configuration 3 overestimated (bias > 0), and the rest underestimated (bias < 0). The best correlation between forecast and observation was also found in configuration 1. The lowest MAE and RMSE values were obtained in configuration 4. However, there are no large differences between all configurations (the differences are less than 1 mm in 3 h). Configurations 1 and 4 showed the best scores overall. Both have in common the PBL scheme (MYJ-MOJ) but differ in the MP scheme: WSM6 (configuration 1) and Thompson (configuration 4). All model configurations presented flow dependence and therefore the model skill depends on synoptic forcing. In general, the different model configurations overestimated the precipitation during weak synoptic forcing or under trade winds influence while underestimation occurred under strong synoptic forcing. In fact, the worse model performance was found under intense cold front event. According to other authors, the precipitation forecast accuracy depends on the intensity of the precipitation events (Moya-Álvarez et al., 2018).

The scatter plot (Fig. 4) shows the correspondence between forecast and observations. An accurate forecast will have points on or near the diagonal. For 3-h rainfall accumulation, most values are below 10 mm/3 h. The plot shows more missed events with forecast values lower than 10 mm/3 h, while observed precipitation was higher than 20 mm/3 h. It is interesting to remark that no model configuration was able to forecast the 50 mm/3 h rainfall accumulation event. The predictability on the precipitation over complex terrain is limited (Hohenegger et al., 2006). This low predictability is due the role of the interactions of the moist flow with orography and the uncertainties in microphysics (Garvert et al., 2005; Colle et al., 2005). The impact of orography on precipitation will be discussed in Section 3.3.

Table 4
Average values of Bias, MAE, RMSE and correlation for T2m.

	BIAS	MAE	RMSE	r
configuration 1	−1.108372	1.905499	2.45724	0.869723
configuration 2	−1.103388	1.841778	2.387194	0.878208
configuration 3	−1.042808	1.802495	2.340985	0.879837
configuration 4	−1.107951	1.901527	2.45491	0.869747
configuration 5	−1.092369	1.831298	2.378982	0.87844
configuration 6	−1.038473	1.795847	2.332715	0.880667

Table 5
Average values of Bias, MAE, RMSE and correlation for wind gust.

	BIAS	MAE	RMSE	r
configuration 1	−4.827238	10.802053	14.748979	0.684739
configuration 2	−8.289803	12.124696	16.130221	0.67946
Configuration 3	−5.571593	11.338342	15.244262	0.673237
configuration 4	−4.886065	10.808923	14.791971	0.68299
configuration 5	−8.262815	12.149721	16.18515	0.675455
configuration 6	−5.601049	11.349421	15.268025	0.671952

3.1.2. Temperature at 2 m

In contrast with 3-h rainfall accumulation, results obtained for T2m show that configuration 6 obtains the best score. All model configurations underestimate the temperature by 1 °C approximately (bias ≈ −1) and show great correlation with r values higher than 0.86. Temperature underestimation can be justified partly by the method of the soil temperature initialization in the WRF Surface Land Model (SLM) (Cheng and Steenburgh, 2005).

The values obtained in the current work are similar to those obtained by Banks et al. (2016), where the BouLac scheme shows the best performance for T2m.

The scatter plot (Fig. 5) shows, in general, a strong correlation between forecast and observations. The worse correspondences are found when the observed T2m is higher than 15 °C or lower than 0 °C. In the first case (T2m > 15 °C), the model underestimates T2m while in the other case (T2m < 0 °C), the model overestimates it.

3.1.3. Maximum 1-h wind gust

Maximum 1-h wind gust shows the worst verification score. The bias presents significant differences that point to two groups: configurations 2 and 5, and the rest. Configuration 2 and 5 show the largest negative bias; this may be due to the PBL scheme used in both: ACM2. The ACM2 scheme is a hybrid scheme that combines non-local upward closure with local downward closure techniques. Its poor performance suggests that some eddies, present on the days tested, were not large enough to be considered non-local, presenting conditions that could be better resolved by the local schemes used in the rest of configurations (MYJ and BouLac).

The MAE and RMSE are higher than 10 km/h. These significant errors can have important consequences in the decision-making process, for instance, in the weather warnings issuance process. Nevertheless, r values are higher than 0.67. Configurations 1 and 4 present the best overall results. Both configurations use the MYJ PBL scheme (with MOJ surface layer), confirming the importance of the PBL scheme in wind forecast.

The scatter plot (Fig. 6) shows a systematic model negative bias and remarks the model inability to forecast wind gust > 100 km/h. This error can be explained by the inability of the PBL schemes to accurately predict the wind field due to the difficulty to represent the variability of the observations (Dandou et al., 2017). This difficulty is particularly relevant in the Canary Islands, given the orographic conditions of the inland stations (Cana et al., 2020).

3.2. Lead time dependence

Figs. 7 to 9 show how the different scores vary with time. In general,

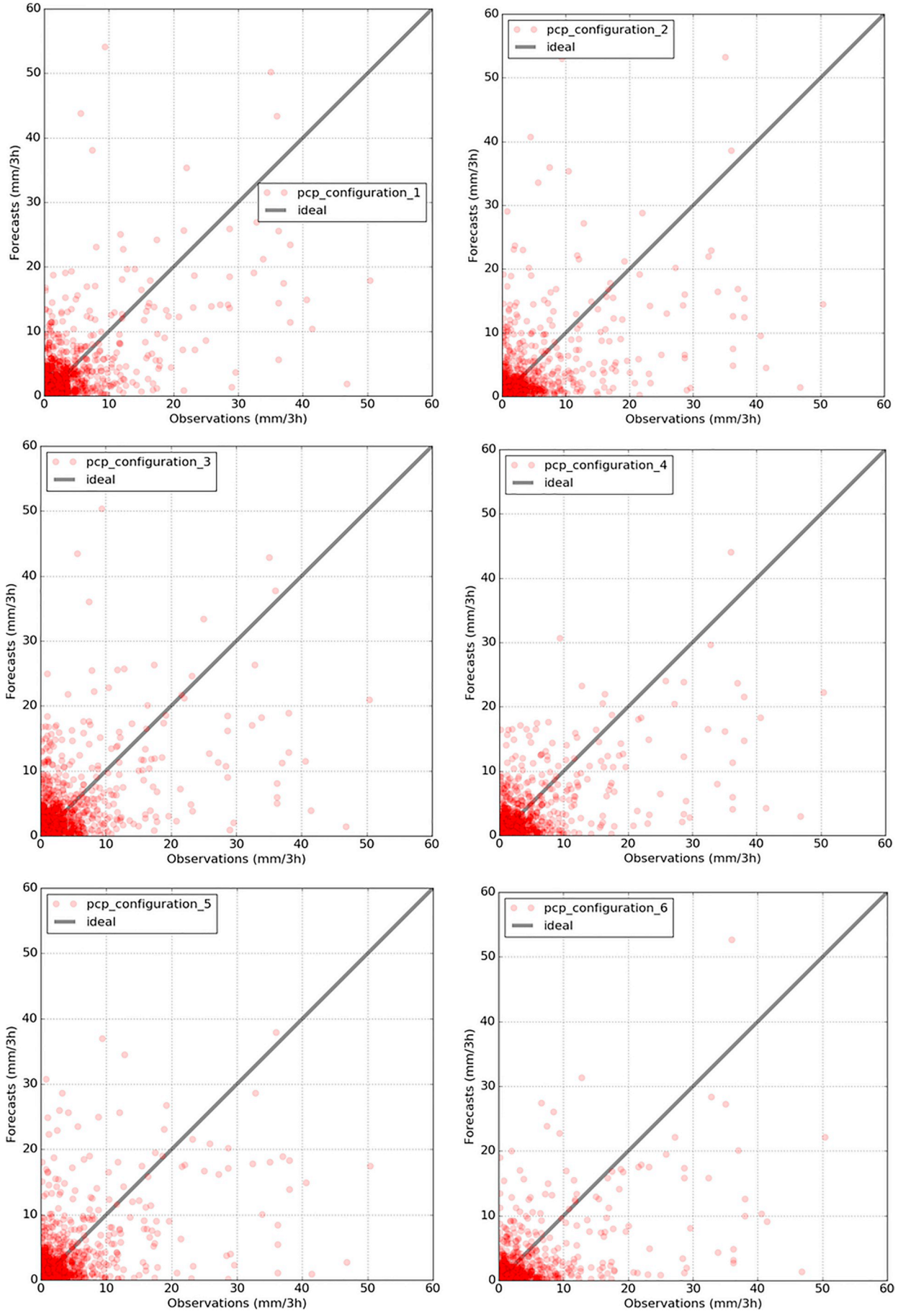

Fig. 4. Scatter plot panel for 3-h rainfall accumulation.

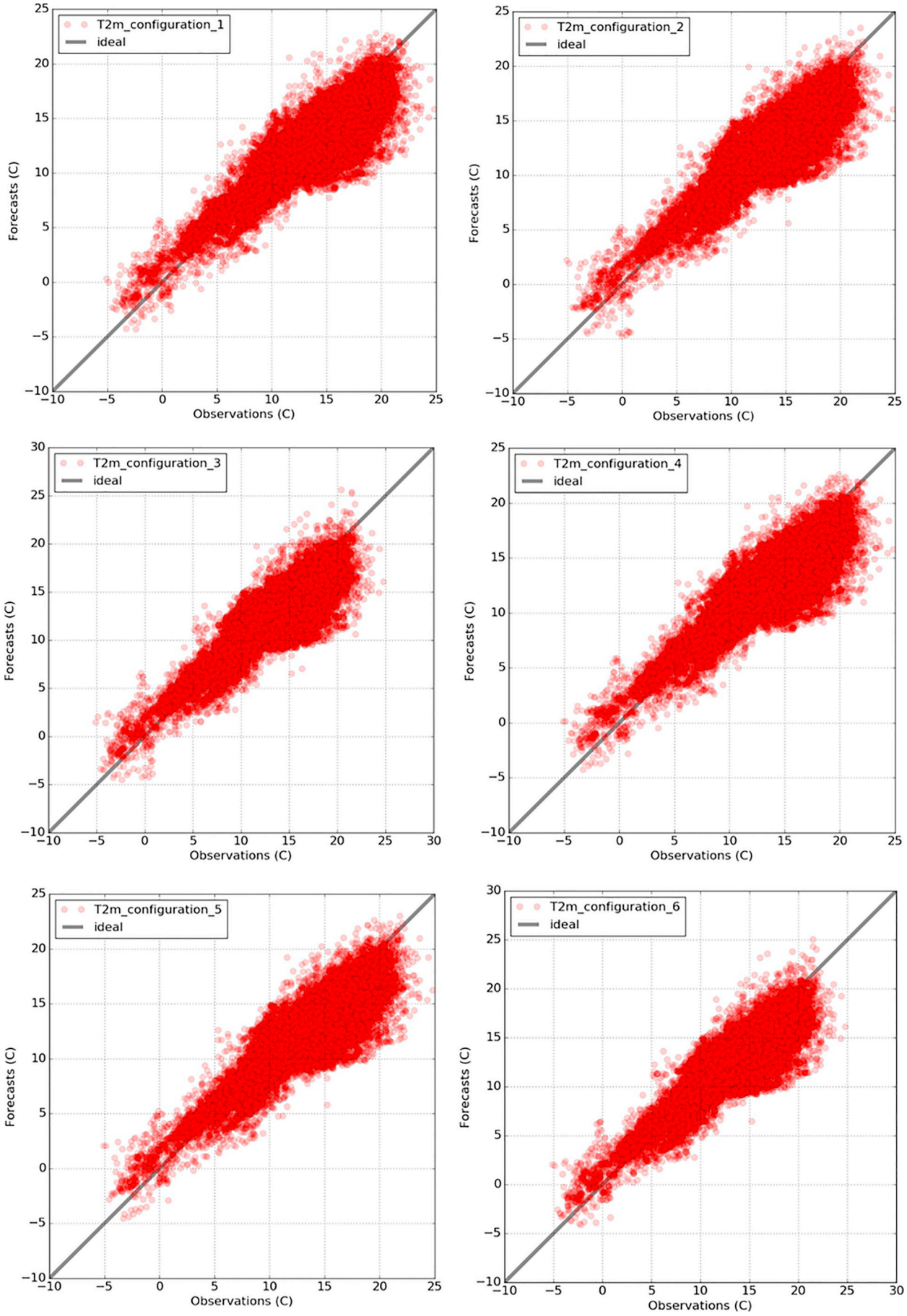

Fig. 5. Scatter plot panel for T2m.

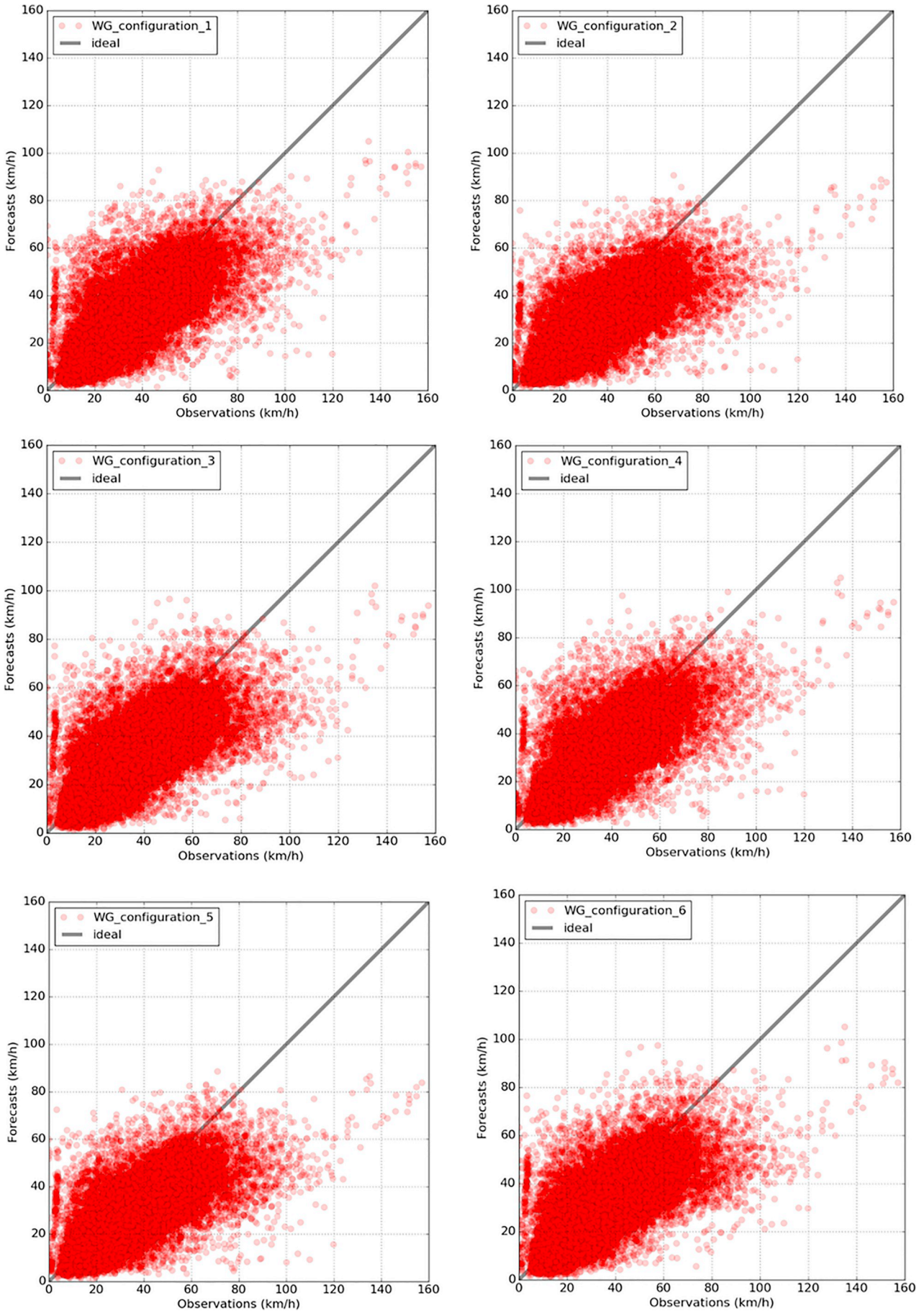

Fig. 6. Scatter plot panel for the maximum 1-h wind gust.

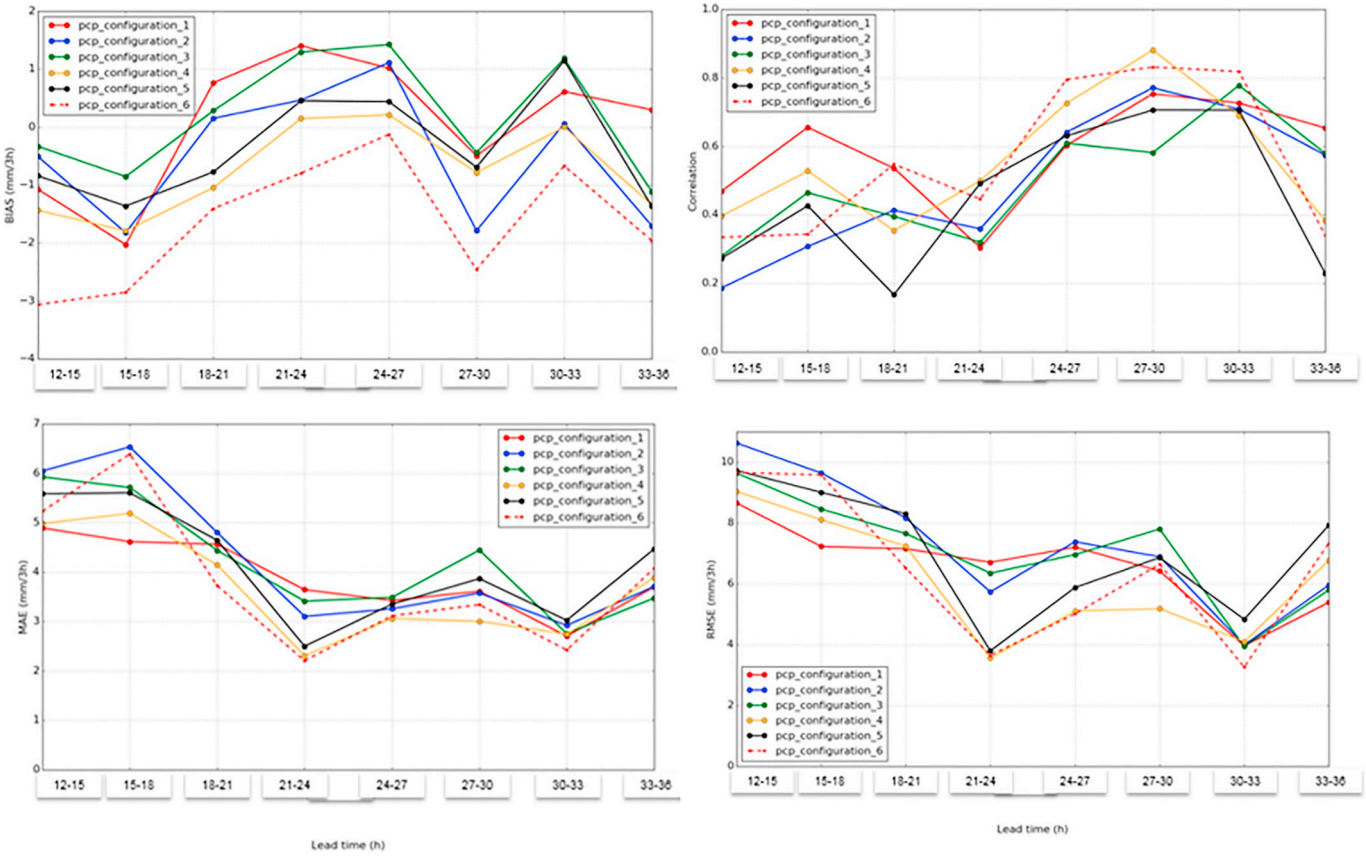

Fig. 7. Bias, correlation, MAE and RMSE for 3-h rainfall accumulation.

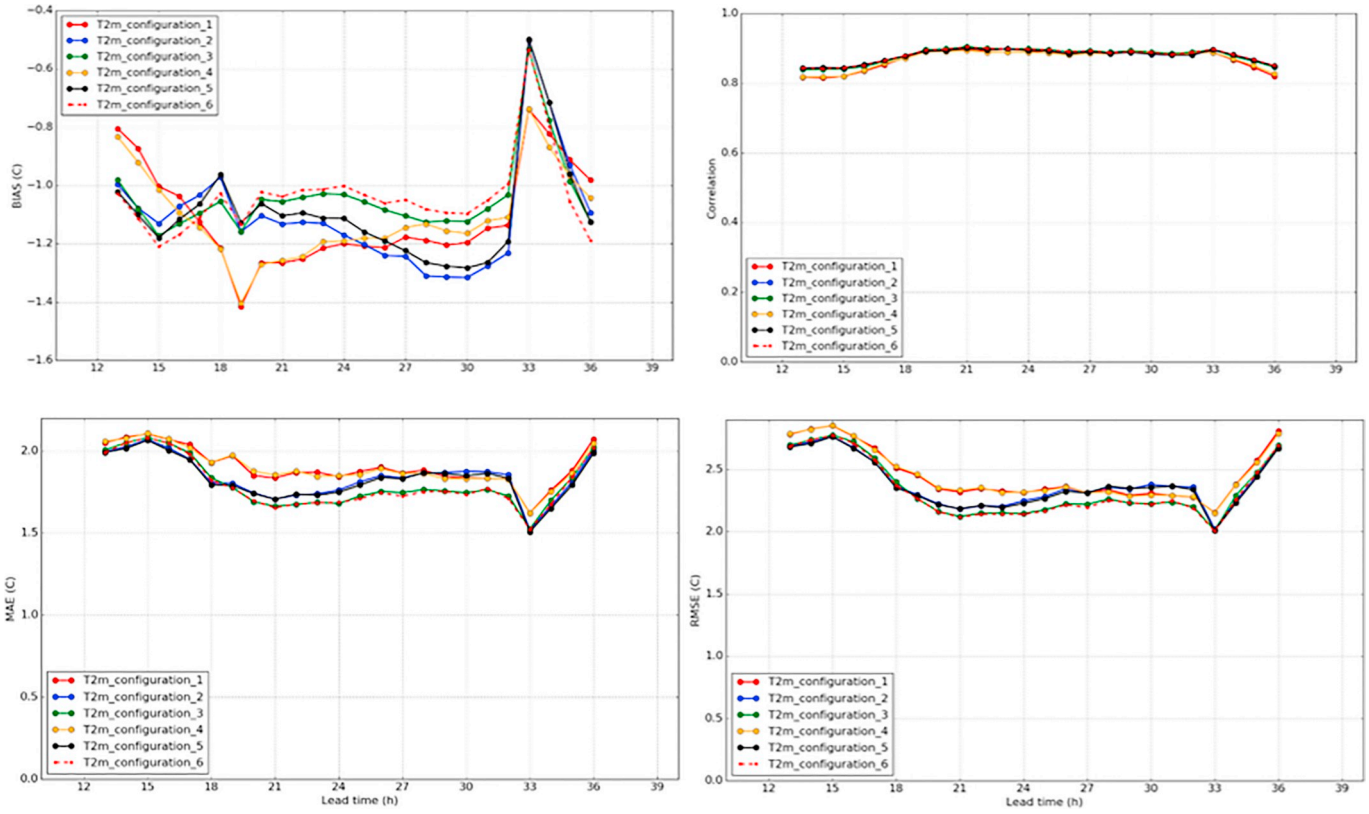

Fig. 8. Bias, correlation, MAE and RMSE for T2m.

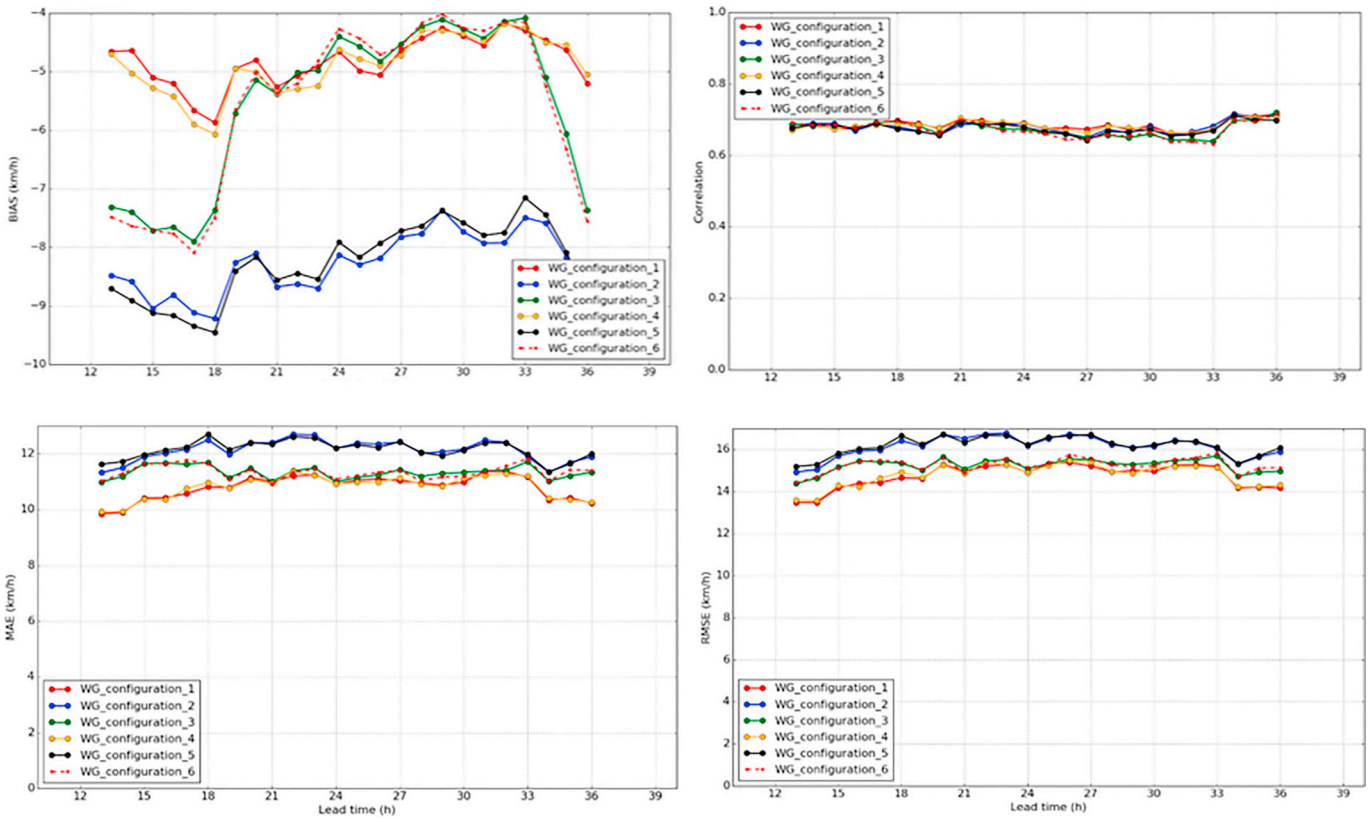

Fig. 9. Bias, correlation, MAE and RMSE for the maximum 1-h wind gust.

all scores change similarly with time and the most relevant difference between all model configurations have been found in wind gust bias. As mentioned before, configuration 2 and 5 present the largest negative bias, due to the impact of the PBL scheme used.

In general, the different scores present better results between lead times 18 and 33 h. This suggests that the lead time should be selected carefully when optimizing a WRF configuration in high-resolution models (Jee and Kim, 2017).

a) Precipitation (Fig. 7)

The precipitation correlation increased for all model configuration with time from 0.2 (configuration 2) to higher than 0.8 (configuration 4). The best correlations between observations and forecasts were found during night time and early morning. The precipitation MAE exhibited maxima (close or higher than 5 mm/3 h) during afternoon time (lead time 12–18 h). After, the precipitation MAE decreased from 21 to 33 h of lead time and showed the minima (close to 2 mm/3 h for the configurations 4 and 6) from 21 to 24 h of lead time. The best results were obtained during night time by the fact that the most intense rainfall took place during 12–18 h. As it was seen in the Fig. 4, the forecast of extreme precipitation is still a challenge. The Boulac-Thompson combination (configuration 6) predicted the lowest precipitation quantities for all lead time.

b) Temperature (Fig. 8)

Fig. 8 shows that all model configurations presented cold temperature bias values around −0.5 °C and − 1.4 °C. The temperature MAE showed three clusters with similar behaviors (configuration 1 and 4, configuration 3 and 6 and configuration 2 and 5) conditioned by the PBL scheme selected. Initially, the temperature MAE was close to 2 °C for all configurations and decreased until 1.5 °C at 33 h. The temperature scores displayed influence of the transition from night to day. All configurations showed more realistic forecast during early morning (33 to 35 h of lead time), while during night time worst results were obtained. It could be related to surface energy fluxes, cloud cover and boundary layer height. As other authors point out (Jousse et al., 2016) inaccurate representation of boundary layer height has a significant implication in the realism of WRF in a stratocumulus region.

c) Wind (Fig. 9)

Fig. 9 shows the behavior of the different model configurations for wind gust throughout the day. Observed mean wind gust displays diurnal variations, with lower speeds during night. All model configurations follow the trends of daily evolution, but configurations 1 and 4 are more realistic. Unlike mean wind gust, the observed maximum wind gust presents higher values during night time with differences between day and night of 20–30 km/h and no model configuration was able to forecast the nocturnal low level jet that forms at night above a temperature inversion. The wind gust correlation was quite similar for all configurations at around 0.67. The lower bias was found for configurations 1 and 4, while configurations 2 and 5 presented larger bias during all period. Configurations 3 and 6 exhibited better result during night time and early morning (from 21 to 33 h).

3.3. Location influence

Figs. 10, 11 and 12 show RMSE in observation stations for all model configurations and fields. The main goal of these plots is to find the influence of the location on the forecast accuracy.

Regarding precipitation (Fig. 10), the lowest RMSEs have been obtained in Fuerteventura, Lanzarote and north coasts of Gran Canaria and Tenerife. All configurations present the larger RMSEs in the south and southeast of Tenerife, and in one location of La Gomera. Also, large RMSEs are found in the center of Gran Canaria. The large RMSEs in these locations are due to orographic enhancement of precipitation on

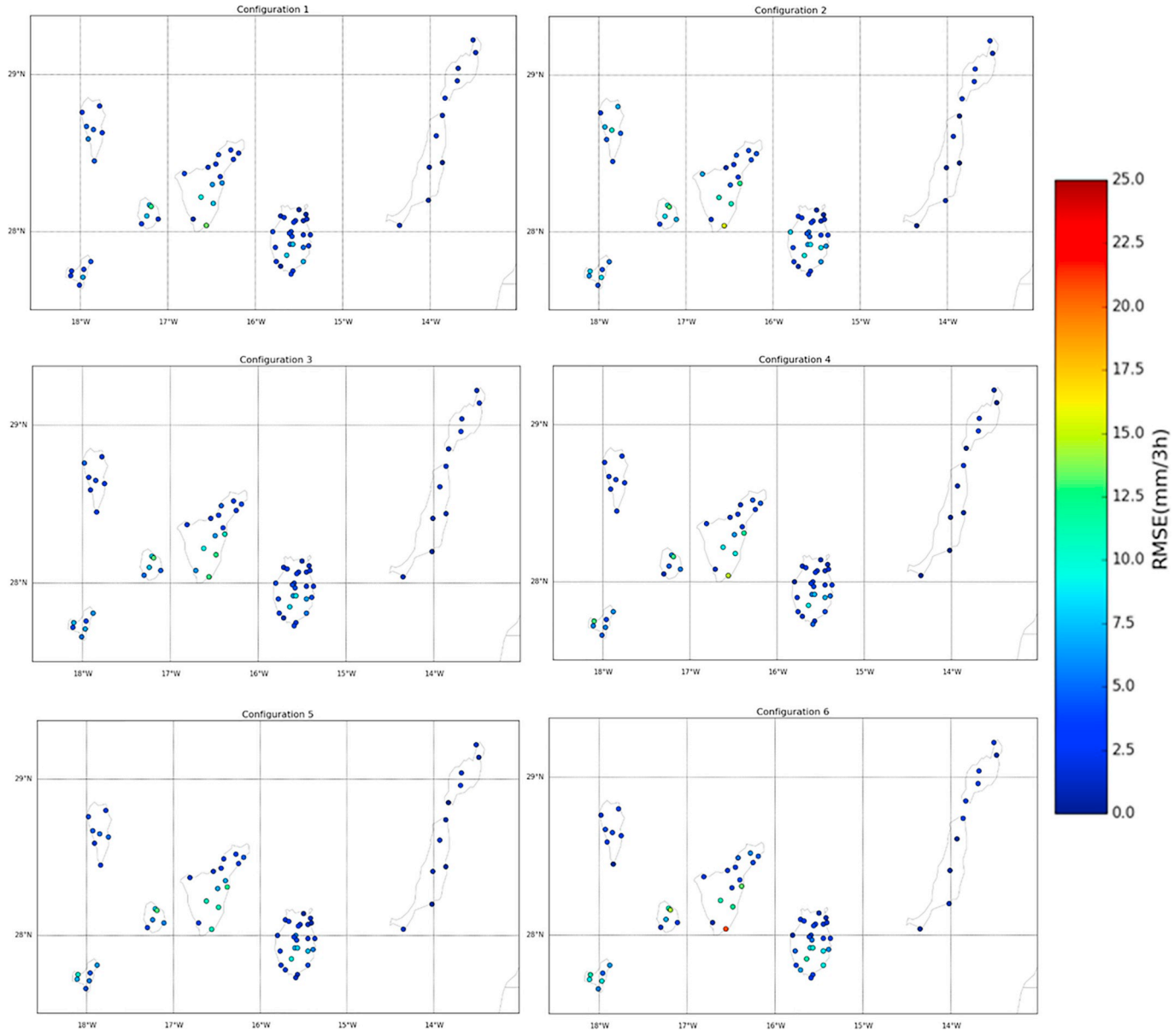

Fig. 10. Map of RMSE for 3-h rainfall accumulation by location.

the windward slope during extratropical cyclone and cold front events. Despite the convection is explicitly resolved, the orographic precipitation is underestimated; this result is in line with other studies (Hong and Lee, 2009; Eiserloh, 2014; Moya-Álvarez et al., 2019). The forecast of orographic precipitation is a challenge for NWP models as a consequence of the complexity of thermodynamic, cloud microphysics, and dynamic processes in complex terrain (Chow et al., 2013).

In contrast with precipitation, the larger RMSEs for T2m (Fig. 11) are obtained in the east of Fuerteventura, at La Palma airport (east of the island), and at El Hierro airport (northeast of the island). All of them are very close to the sea (less than 500 m) and all of them are located at an altitude lower than 33 m. For these locations, decomposition of RMSE into systematic and unsystematic components evidenced the model's linear (or systematic) error. The cold temperature bias (and the temperature RMSE) oscillated with time between −2.5 °C and − 7.8 °C (and from 3 °C to 8 °C for RMSE) depending on location. However, the worst results were found during days with prevailing intense SW to S winds, with peaks above 100 km/h. Specifically, the largest temperature RMSE was observed at Fuerteventura airport. Under these conditions (strong coast parallel southerly winds), the sea surface temperature (SST) decreases as a reaction to the Coast Low Level Jet (CLLJ) due to upwelling (Fig. 12). The cold current of Portugal–Canary is a potential area of occurrence of CLLJ (Winant et al., 1988). The increase of the temperature RMSE during CLLJ activity enables the unsystematic component and may imply the model impossibility/inability to resolve the phenomenon properly.

In the case of wind gust (Fig. 13), there are two stations with remarkable large RMSE: Izaña (Tenerife) and Vallehermoso (La Gomera). These errors are related to the intense wind gusts observed in these locations, and the model inability to forecast wind gusts over 100 km/h (as described in Section 3.1.3). The cause of this inability, and the resulting large RMSE, may be related to the complex orography. In these locations, synoptic winds are channeled and terrain-forced flows are produced. Low accuracy wind gust forecast in complex areas is partially justified by the mismatch between real and model topography.

3.4. Altitude dependence

In order to find out the altitude dependence, heatmaps exposing the RMSE as a function of altitude (y-axis) and model configurations (x-

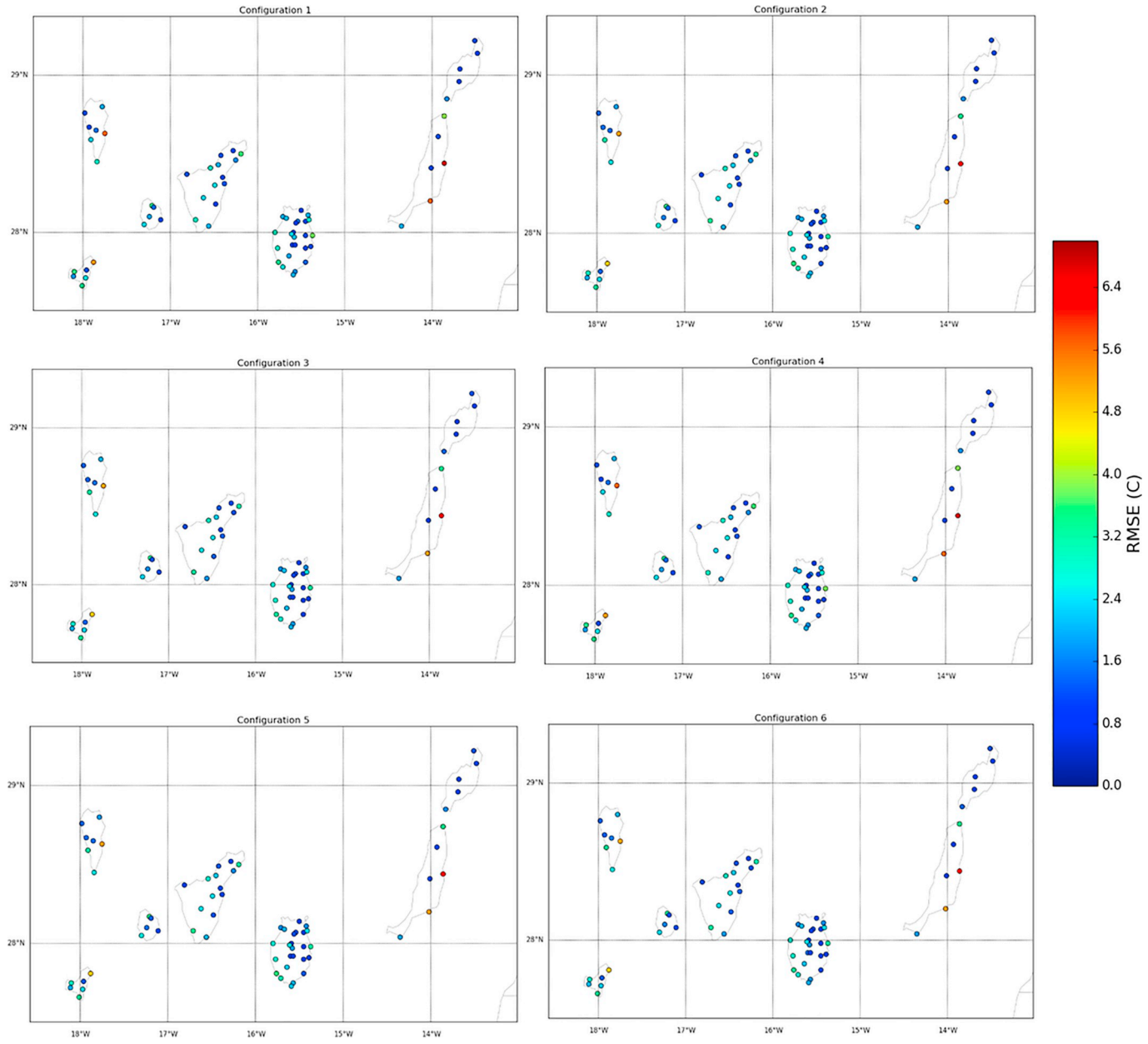

Fig. 11. Map of RMSE for T2m by location.

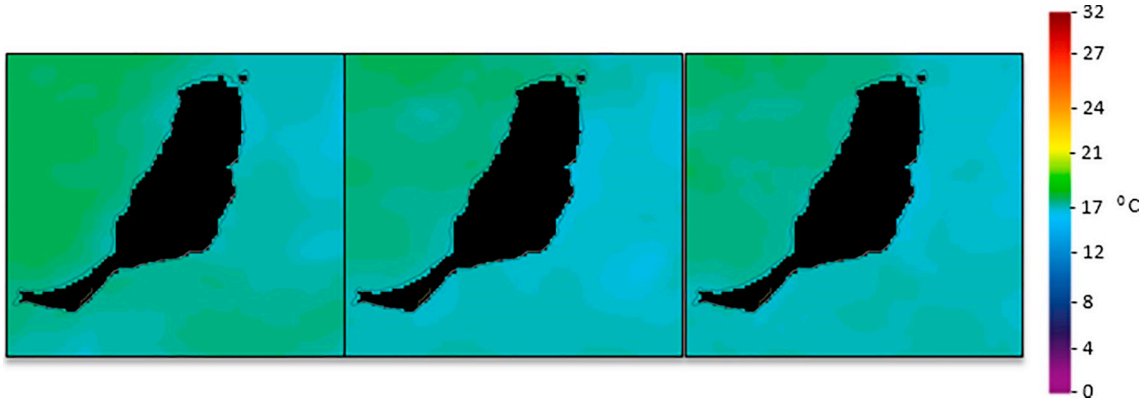

Fig. 12. Sea Surface Temperature around Fuerteventura from the Group for High Resolution Sea Surface Temperature (GHRSST). Under upwelling conditions (February 26 and 27, center and right image) SST is lower (blue color) on the east coast than under trade wind conditions (green color) (February 16, left image) (https://worldview.earthdata.nasa.gov/ SST). (For interpretation of the references to color in this figure legend, the reader is referred to the web version of this article.)

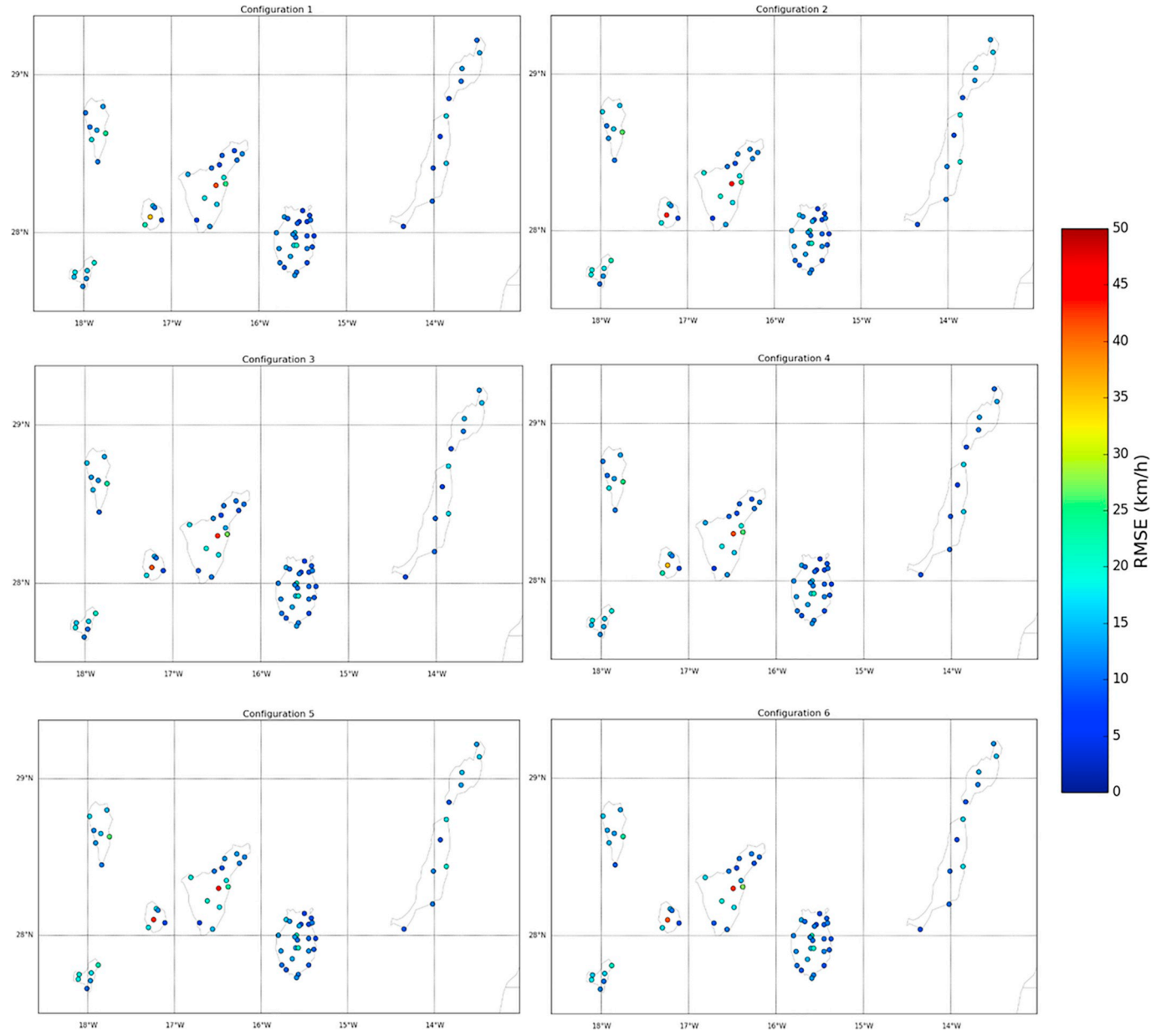

Fig. 13. Map of RMSE for maximum 1-h wind gust by location.

axis) are shown in Fig. 14 (rainfall), 15 (T2m) and 16 (wind gust). Each row represents one station except at 0 m, where there are 5 stations. In this case, heatmap shows the average RMSE. For precipitation, 60 out of 68 stations (4 stations at 0 m) were used to make heatmap. The discarded stations did not reach the threshold of 0.2 mm. Red color shows high RMSE, whereas blue color shows low RMSE.

The precipitation RMSE increased with the altitude from 0 to 12 mm/3 h (Fig. 14). However, the largest precipitation RMSE (between 15 and 24 mm/3 h) were found below 170 m. These high values of precipitation RMSE at low altitude were due to a singular maximum peak (44.6 mm/3 h accumulated in an hour) at Tenerife Sur airport under low pressure system and cold front conditions. Although the configuration model 5 reproduced better the peak, the difference between observation and forecast was 20 mm/3 h. Finally, we must consider that, in locations characterized by shallow cumulus regimes, such as the Canary Islands, the existing PBL parametrizations in the WRF model are unable to produce fully accurate results (Huang et al., 2013; Carrillo et al., 2016; Jousse et al., 2016; Gunwani and Mohan, 2017; Cana et al., 2020).

T2m does not show a direct relationship between altitude and RMSE. However, the worst results, as explained before (Fig. 15), are found at low altitudes. Analyzing different strata, in average the highest T2m RMSE (from 2 to 4.2 °C) was found at 0–50 m, highly influenced by the larger RMSE due to location influence. The strata at 50–500, 500–1000, and 1000–1500 m presented similar T2m RMSE (in average between 1.5 and 2.5 °C). Nevertheless, station at higher than 1500 m presented great variability of T2m RMSE. In high mountain areas (altitude above 1500 m) larger T2m RMSE were obtained during days with great thermal oscillation with minimal temperatures of −5 °C and maximum temperatures of 12 °C.

Regarding wind gust, RMSE increase with altitude in all cases (Fig. 16). The increase of RMSE with altitude is related to sub-grid terrain features and its impact on the wind gust (see Section 3.3).

4. Conclusions

Sensitivity analysis can be used to determine optimum WRF model configurations. However, the best configuration depends on location

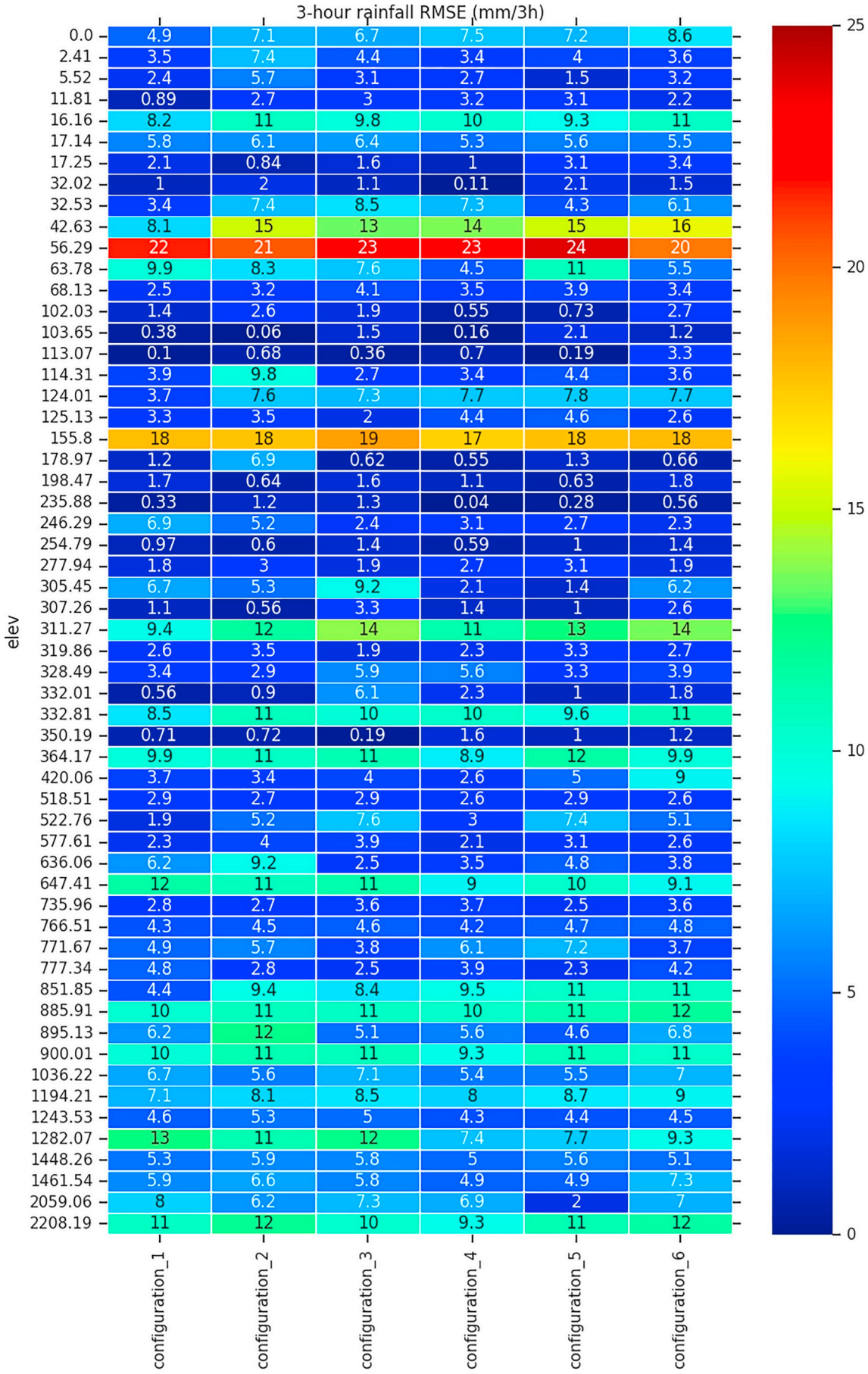

Fig. 14. Heatmap of RMSE for 3-h rainfall by altitude and configuration.

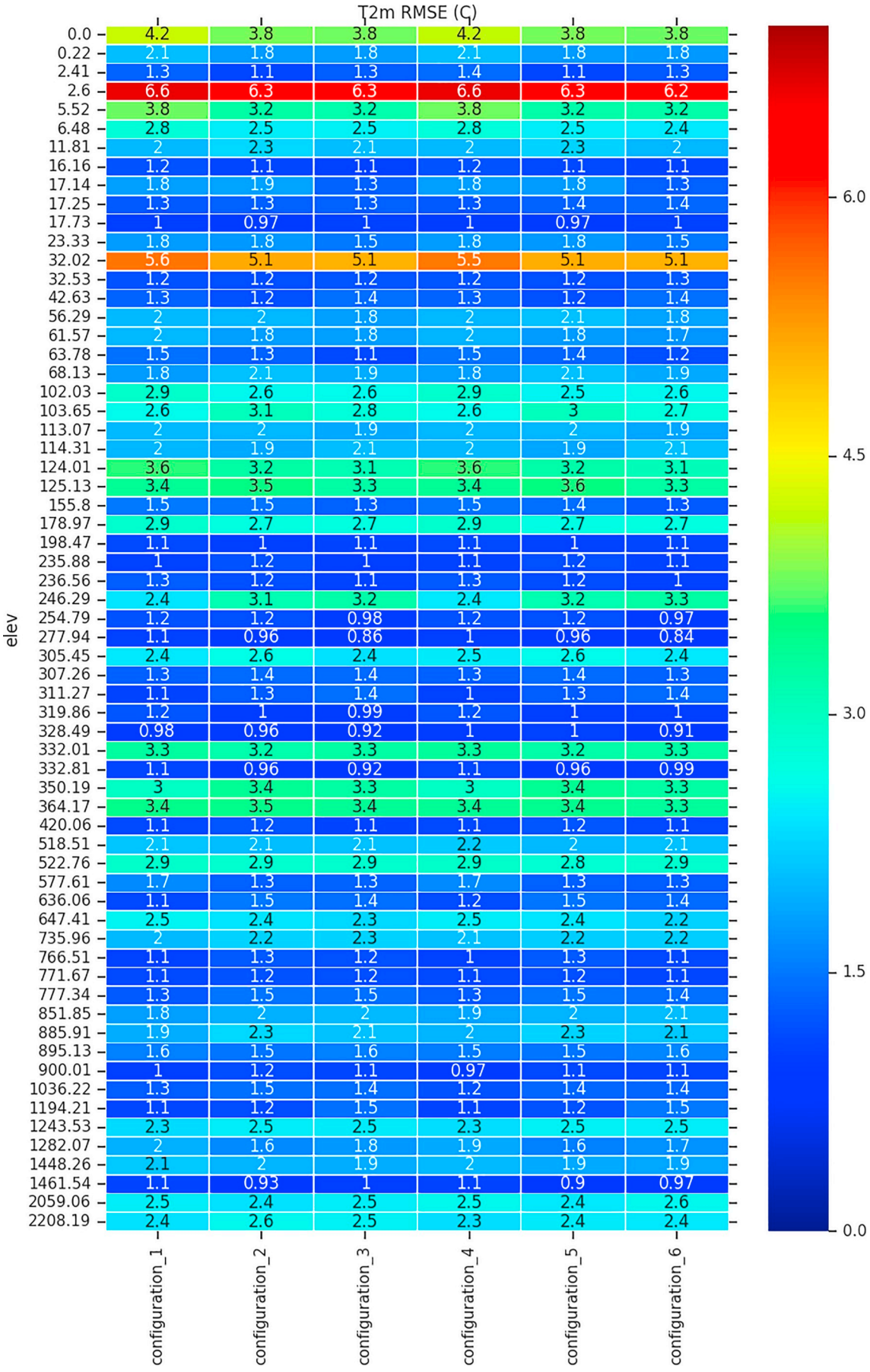

Fig. 15. Heatmap of RMSE for T2m by altitude and configuration.

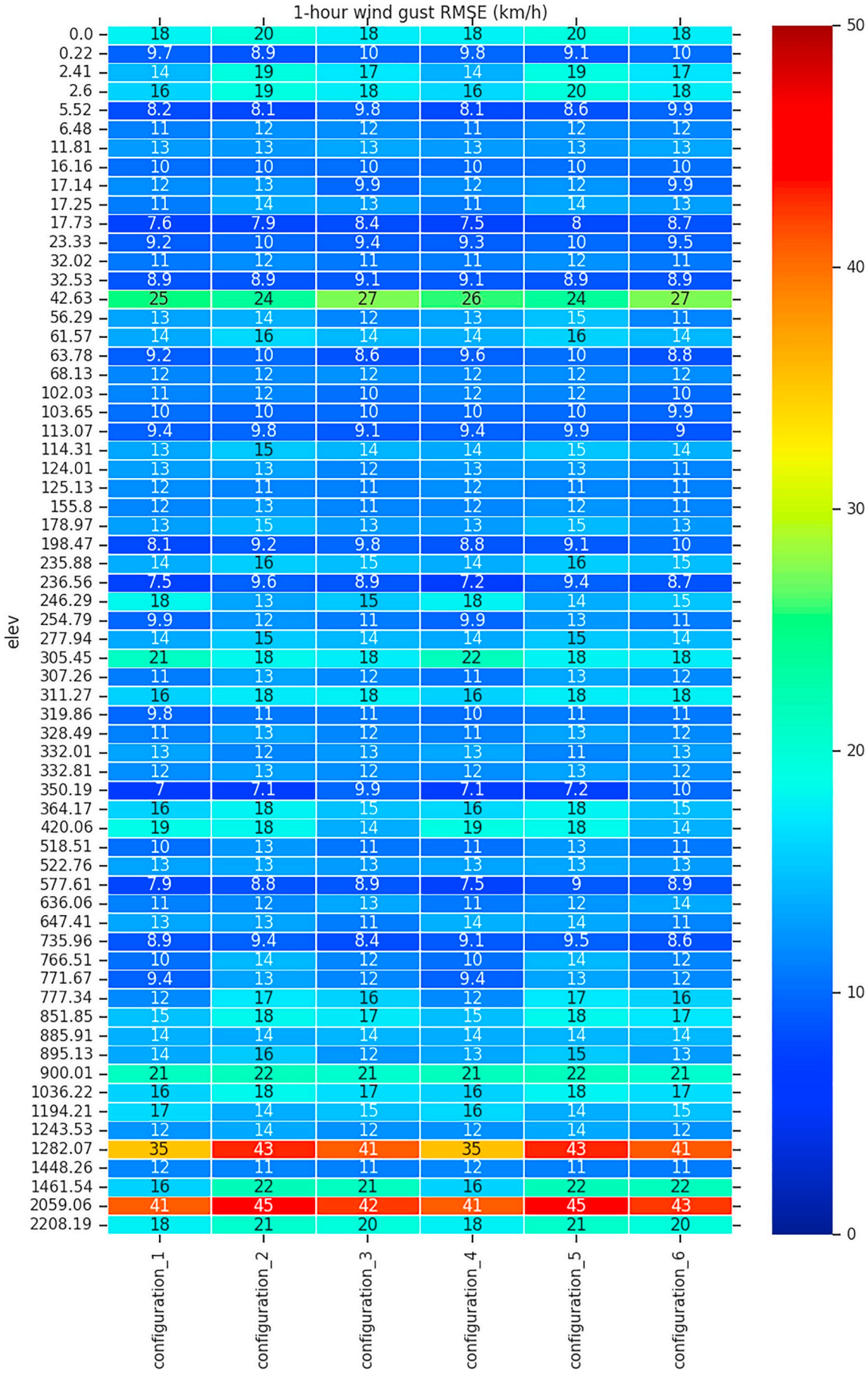

Fig. 16. Heatmap of RMSE for wind gust by altitude and configuration.

and meteorological conditions. In this research, a comprehensive sensitivity analysis has been carried out in the Canary Islands. Due to the impact on the socio-economic activities, the analysis has been focused on T2m, wind gust and 3-h rainfall accumulation. Subsequently, the most relevant conclusions are summarized:

- This research allowed discarding inappropriate WRF model configurations. The discarded configurations were the combinations of YSU, MYNN2 PBL schemes with Kessler, Goddard and Morrison 2-Moment MP schemes.
- Regarding the 3-h rainfall accumulation on the Canary Islands, the PBL scheme selected had a greater impact than the MP scheme used. The MYJ PBL scheme reached the best performance for precipitation. The ability of the model configurations to forecast precipitation was influenced by the daytime.
- The BouLac-Thompson combination presented the best results for T2m.
- The combination of MYJ-WSM6 showed the best results for the maximum 1-h wind gust. All model configurations followed the trends of daily evolution for mean wind gust. However, none was able to forecast nocturnal low level jet. Although the MYJ PBL scheme presented more stable results for wind gust with time, the Boulac PBL scheme exhibited better results during night time and early morning.
- All fields presented better results between lead time 18 and 33 h.
- The influence of the location was proved. The worst overall results were obtained in complex terrain areas. Worst T2m results arose in the land-sea transition zones on the eastern coasts of the islands. Also, for 3-h rainfall accumulation and maximum 1-h wind gust, the forecast error increased with altitude.

There was a systematic wind speed underestimation in all configurations. This underestimation suggests that, to obtain better results, either other configurations should be tested, or post processing techniques should be explored. The results obtained in this article show the difficulty to obtain accurate forecasts in complex orography areas. Therefore, in these areas, resources must be invested to test the models and achieve an optimal configuration. The results reached in this study can be taken as the basis for future WRF configurations in operational mode within AEMET for the Canary Islands domain.

Author statement

The paper entitled “Sensitivity analysis of the WRF Model: Assessment of performance in high resolution simulations in complex terrain in the Canary Islands” was carried out by the authors David Suárez-Molina, Sergio Fernández-González, Gustavo Montero, Albert Oliver and Juan Carlos Suárez González. In the following lines, the contribution of each author will be detailed:

David Suárez-Molina: He is the main contributor to this paper, being the responsible of the conceptualization, design of the methodology, obtaining results, and writing.

Sergio Fernández-González has contributed in the redaction of the paper, and supervising the research activity.

Gustavo Montero and Albert Oliver have contributed in the research design, and collaborated in the redaction of the paper.

Juan Carlos Suárez González has helped with the software, data curation and formal analysis.

Declaration of Competing Interest

The authors claim that there is no conflict of interest, nor any funding source that intercedes with the free publication of results obtained in this research.

Acknowledgements

Observational data are provided by the State Meteorological Agency of Spain (AEMET). The authors are grateful to the Weather Forecast Research Team for developing “Verif” software. Special thanks go to the SAFEFLIGHT (CGL2016-78702-C2-1-R and CGL2016-78702-C2-2-R) and UE ERA-NET Plus NEWA (PCIN2016-080) projects.

References

Eiserloh, Arthur John, 2014. WRF-Model Data Assimilation Studies of Landfalling Atmospheric Rivers and Orographic Precipitation Over Northern California. https://doi.org/10.31979/etd.5wgq-5vkc. Master's Theses. 4461. https://scholarworks.sjsu.edu/etd_theses/4461.

Anderson, M.C., Norman, J.M., Diak, G.R., Kustas, W.P., Mecikalski, J.R., 2011. A two-source time integrated model for estimating surface fluxes using thermal infrared remote sensing. Remote Sens. Environ. 60 (2), 195–216. https://doi.org/10.1016/s0034-4257(96)00215-5.

Banks, R.F., Tiana-Alsina, J., Baldasano, J.M., Rocadenbosch, F., Papayannis, A., Solomos, S., Tzanis, C.G., 2016. Sensitivity of boundary-layer variables to PBL schemes in the WRF model based on surface meteorological observations, lidar, and radiosondes during the HygrA-CD campaign. Atmos. Res. 176–177, 185–201. https://doi.org/10.1016/j.atmosres.2016.02.024.

Biswas, M.K., Bernardet, L., Abarca, S., Ginis, I., Grell, E., Kalina, E., Zhang, Z., 2018. Hurricane Weather Research and Forecasting (HWRF) Model: 2017 Scientific Documentation (No. NCAR/TN-544+STR). https://doi.org/10.5065/D6MK6BPR.

Borge, R., Alexandrov, V., del Vas, J.J., Lumbreras, J., Rodríguez, E., 2008. A comprehensive sensitivity analysis of the WRF model for air quality applications over the Iberian Peninsula. Atmos. Environ. 42 (37), 8560–8574. https://doi.org/10.1016/j.atmosenv.2008.08.032.

Bossioli, E., Tombrou, M., Dandou, A., Athanasopoulou, E., Varotsos, K.V., 2009. The role of planetary boundary-layer parameterizations in the air quality of an urban area with complex topography. Bound. Layer Meteorol. 131, 53–72. https://doi.org/10.1007/s10546-009-9349-7.

Bougeault, P., Lacarrere, P., 1989. Parameterization of orography-induced turbulence in a mesobeta–scale model. Mon. Weather Rev. 117 (8), 1872–1890. https://doi.org/10.1175/1520-0493(1989)117<1872:pooiti>2.0.co;2.

Callado, A., Escribà, P., Gil, D., Compte., M, Martínez, M., González, S., Quintero, D., García-Moya, J.A., 2019. AEMET-γSREPS en operaciones. Sexto Simposio Nacional de Predicción, Memorial Antonio Mestre. http://hdl.handle.net/20.500.11765/10995.

Cana, L., Grisolía-Santos, D., Hernández-Guerra, A., 2020. A Numerical Study of a Sea Breeze at Fuerteventura Island, Canary Islands, Spain. Bound.-Layer Meteorol. 175 (2), 277–296. https://doi.org/10.1007/s10546-020-00506-z.

Carrillo, J., Guerra, J.C., Cuevas, E., Barrancos, J., 2016. Characterization of the marine boundary layer and the trade-wind inversion over the sub-tropical North Atlantic. Boundary-Layer Meteorol. 158, 311–330. https://doi.org/10.1007/s10546-015-0081-1.

Chen, F., Dudhia, J., 2001. Coupling an advanced land surface–hydrology model with the Penn State–NCAR MM5 modeling system. Part I: model implementation and sensitivity. Mon. Weather Rev. 129 (4), 569–585. https://doi.org/10.1175/1520-0493(2001)129<0569:caalsh>2.0.co;2.

Cheng, W.Y.Y., Steenburgh, W.J., 2005. Evaluation of Surface Sensible Weather forecasts by the WRF and the Eta Models over the Western United States. Weather Forecasting 20, 812–821. https://doi.org/10.1175/WAF885.1.

Chow, F.K., De Wekker, S.F.J., Snyder, B.J., 2013. Mountain Weather Research and Forecasting. Springer Atmospheric Scienceshttps://doi.org/10.1007/978-94-007-4098-3.

Colle, B.A., Garvert, M.F., Wolfe, J.B., Mass, C.F., Woods, C.P., 2005. The 13–14 December 2001 IMPROVE-2 event. Part III: simulated microphysical budgets and sensitivity studies. J. Atmos. Sci. 62 (10), 3535–3558. https://doi.org/10.1175/jas3552.1.

Dandou, A., Tombrou, M., Kalogiros, J., Bossioli, E., Biskos, G., Mihalopoulos, N., Coe, H., 2017. Investigation of turbulence parametrization schemes with reference to the atmospheric boundary layer over the Aegean Sea during etesian winds. Boundary-Layer Meteorol. 164, 303–329. https://doi.org/10.1007/s10546-017-0255-0.

Dorta, P., 2007. Catálogo de riesgos climáticos en Canarias: Amenazas y vulnerabilidad. Geographicalia 133–160, 51. https://doi.org/10.26754/ojs_geoph/geoph.2007511118. ISSN 0210-8380, N° 51.

Evans, J.P., Ekström, M., Ji, F., 2012. Evaluating the performance of a WRF physics ensemble over South-East Australia. Clim. Dynam. 39 (6), 1241–1258. https://doi.org/10.1007/s00382-011-1244-5.

Fernández-González, S., Valero, F., Sánchez, J.L., Gascón, E., López, L., García-Ortega, E., Merino, A., 2015. Numerical simulations of snowfall events: Sensitivity analysis of physical parameterizations. J. Geophys. Res.-Atmos. 120 (19), 10–130. https://doi.org/10.1002/2015jd023793.

Fernández-González, S., Martín, M.L., Merino, A., Sánchez, J.L., Valero, F., 2017. Uncertainty quantification and predictability of wind speed over the Iberian Peninsula. J. Geophys. Res.-Atmos. 122 (7), 3877–3890. https://doi.org/10.1002/2017jd026533.

Fernández-González, S., Martín, M.L., García-Ortega, E., Merino, A., Lorenzana, J., Sánchez, J.L., Rodrigo, J.S., 2018. Sensitivity analysis of the WRF model: wind-resource assessment for complex terrain. J. Appl. Meteorol. Clim. 57 (3), 733–753.

https://doi.org/10.1175/jamc-d-17-0121.1.
García-Ortega, E., Lorenzana, J., Merino, A., Fernández-González, S., López, L., Sánchez, J.L., 2017. Performance of multi-physics ensembles in convective precipitation events over northeastern Spain. Atmos. Res. 190, 55–67. https://doi.org/10.1016/j.atmosres.2017.02.009.
Garvert, M.F., Woods, C.P., Colle, B.A., Mass, C.F., Hobbs, P.V., Stoelinga, M.T., Wolfe, J.B., 2005. The 13–14 December 2001 IMPROVE-2 event. Part II: Comparisons of MM5 model simulations of clouds and precipitation with observations. J. Atmos. Sci. 62 (10), 3520–3534.
González Rocha, S., Juárez-Pérez, F., Aguilar-Meléndez, A., Cristobalsalas, A., Calderón-Ramón, C., Escalante-Martínez, J., Baldasano, J., 2017. Planet Boundary Layer Parameterization in Weather Research and forecasting (WRFv3.5): Assessment of Performance in High Spatial Resolution Simulations in complex Topography of Mexico. Computacion y Sistemas. 21, 35–44. https://doi.org/10.13053/CyS-21-1-2581.
Gunwani, P., Mohan, M., 2017. Sensitivity of WRF model estimates to various PBL parameterizations in different climatic zones over India. Atmos. Res. 194, 43–65. https://doi.org/10.1016/j.atmosres.2017.04.026.
Hamill, T.M., 2014. Performance of Operational Model Precipitation Forecast Guidance during the 2013 Colorado Front-Range Floods. Mon. Weather Rev. 142, 2609–2618. https://doi.org/10.1175/MWR-D-14-00007.1.
Hohenegger, C., Lüthi, D., Schär, C., 2006. Predictability mysteries in cloud-resolving models. Mon. Weather. Rev. 134 (8), 2095–2107. https://doi.org/10.1175/mwr3176.1.
Hong, Song-You, Lee, Ji-Woo, 2009. Assessment of the WRF model in reproducing a flash-flood heavy rainfall event over Korea. Atmos. Res. 93 (4), 818–831. https://doi.org/10.1016/j.atmosres.2009.03.015.
Hong, S.Y., Lim, J.O.J., 2006. The WRF single-moment 6-class microphysics scheme (WSM6). Asia Pac. J. Atmos. Sci. 42 (2), 129–151.
Hong, S.Y., Noh, Y., Dudhia, J., 2006. A new vertical diffusion package with an explicit treatment of entrainment processes. Mon. Weather Rev. 134 (9), 2318–2341. https://doi.org/10.1175/mwr3199.1.
Hsiao, L., Chen, D., Kuo, Y., Guo, Y., Yeh, T., Hong, J., Fong, C., Lee, C., 2012. Application of WRF 3DVAR to Operational Typhoon Prediction in Taiwan: Impact of Outer Loop and Partial Cycling Approaches. Weather Forecasting 27, 1249–1263. https://doi.org/10.1175/WAF-D-11-00131.1.
Huang, H.-Y., Hall, A., Teixeira, J., 2013. Evaluation of the WRF PBL parameterizations for marine boundary layer clouds: cumulus and stratocumulus. Mon. Weather Rev. 141, 2265–2271. https://doi.org/10.1175/mwr-d-12-00292.1.
Iacono, M.J., Delamere, J.S., Mlawer, E.J., Shephard, M.W., Clough, S.A., Collins, W.D., 2008. Radiative forcing by long-lived greenhouse gases: Calculations with the AER radiative transfer models. J. Geophys. Res.-Atmos. 113, D13. https://doi.org/10.1029/2008jd009944.
Janjic, Z.I., 1994. The step-mountain eta coordinate model: further developments of the convection, viscous sublayer and turbulence closure schemes. Mon. Weather Rev. 122, 927–945. https://doi.org/10.1175/1520-0493(1994)122<0927:tsmecm>2.0.co;2.
Jee, J.B., Kim, S., 2017. Sensitivity study on high-resolution WRF precipitation forecast for a heavy rainfall event. Atmosphere 8 (6), 96. https://doi.org/10.3390/atmos8060096.
Jiménez, P.A., González-Rouco, J.F., García-Bustamante, E., Navarro, J., Montávez, J.P., de Arellano, J.V.-G., Dudhia, J., Muñoz-Roldan, A., 2010. Surface Wind Regionalization over Complex Terrain: Evaluation and Analysis of a High-Resolution WRF simulation. J. Appl. Meteorol. Clim. 49, 268–287. https://doi.org/10.1175/2009JAMC2175.1.
Johnson, A., Wang, X., 2012. Verification and calibration of neighborhood and object-based probabilistic precipitation forecasts from a multimodel convection-allowing ensemble. Mon. Weather Rev. 140 (9), 3054–3077. https://doi.org/10.1175/mwr-d-11-00356.1.
Jorba, O., Marrero, C., Cuevas, E., Baldasano, J.M., 2015. Numerical Modelling of the Extratropical storm Delta over Canary Islands: Importance of High Resolution. In: Klapp, J., Ruíz, Chavarría G., Medina, Ovando A., López, Villa A., Sigalotti, L. (Eds.), Selected Topics of Computational and Experimental Fluid Mechanics. Environmental Science and Engineering. Springer, Cham. https://doi.org/10.1007/978-3-319-11487-3_7.
Jousse, A., Hall, A., Sun, F., Teixeira, J., 2016. Causes of WRF surface energy fluxes biases in a stratocumulus region. Clim. Dyn. 46, 571–584. https://doi.org/10.1007/s00382-015-2599-9.
Kain, J.S., 2004. The Kain–Fritsch convective parameterization: an update. J. Appl. Meteorol. 43 (1), 170–181. https://doi.org/10.1175/1520-0450(2004)043<0170:tkcpau>2.0.co;2.
Kessler, E., 1969. On the distribution and continuity of water substance in atmospheric circulations. In: On the Distribution and Continuity of Water Substance in Atmospheric Circulations. American Meteorological Society, Boston, MA, pp. 1–84. https://doi.org/10.1007/978-1-935704-36-2_1.
Marrero, C., Jorba, O., Cuevas, E., Baldasano, J.M., 2008. Sensitivity study of surface wind flow of a limited area model simulating the extratropical storm Delta affecting the Canary Islands. Adv. Sci. Res. 2, 151–157. https://doi.org/10.5194/asr-2-151-2008.
Martilli, A., Clappier, A., Rotach, M.W., 2002. An urban surface exchange parameterisation for mesoscale models. Boundary-layer Meteorol. 104 (2), 261–304. https://doi.org/10.1023/a:1016099921195.
METEOALERTA, 2018. Plan Nacional de Predicción y Vigilancia de Fenómenos Meteorológicos Adversos. METEOALERTA. Agencia Estatal de Meteorología (AEMET). http://www.aemet.es/documentos/es/eltiempo/prediccion/avisos/plan_meteoalerta/plan_meteoalerta.pdf.
Morrison, H., Thompson, G., Tatarskii, V., 2009. Impact of cloud microphysics on the development of trailing stratiform precipitation in a simulated squall line: Comparison of one-and two-moment schemes. Mon. Weather Rev. 137 (3), 991–1007. https://doi.org/10.1175/2008mwr2556.1.
Moya-Alvarez, A.S., Martínez-Castro, D., Flores, J.L., Silva, Y., 2018. Sensitivity study on the influence of parameterization schemes in WRF_ARW model on short-and medium-range precipitation forecasts in the Central Andes of Peru. Adv. Meteorol. https://doi.org/10.1155/2018/1381092.
Moya-Álvarez, A.S., Gálvez, J., Holguín, A., Estevan, R., Kumar, S., Villalobos, E., Martínez-Castro, D., Silva, Y., 2018. Extreme rainfall forecast with the WRF-ARW model in the Central Andes of Peru. Atmosphere 9, 362. https://doi.org/10.3390/atmos9090362.
Moya-Álvarez, A.S., Martínez-Castro, D., Kumar, S., 2019. Response of the WRF model to different resolutions in the rainfall forecast over the complex Peruvian orography. Theor Appl. Climatol 137, 2993–3007. https://doi.org/10.1007/s00704-019-02782-3.
Nakanishi, M., Niino, H., 2006. An improved Mellor–Yamada level-3 model: its numerical stability and application to a regional prediction of advection fog. Boundary-Layer Meteorol. 119 (2), 397–407. https://doi.org/10.1007/s10546-005-9030-8.
Pereira, C.S., Carvalho, A.C., Ferreira, J., Nunes, J.P., Keizer, J.J., Rocha, A., 2013. Simulation of a persistent medium-term precipitation event over the Western Iberian Peninsula. Hydrol. Earth Syst. Sci. Discuss. 10. https://doi.org/10.5194/hessd-10-1423-2013.
Pérez, C., Jiménez, P., Jorba, O., Sicard, M., Baldasano, J.M., 2006. Influence of the PBL scheme on high-resolution photochemical simulations in an urban coastal area over the Western Mediterranean. Atmos. Environ. 40, 5274–5297. https://doi.org/10.1016/j.atmosenv.2006.04.039.
Pleim, J.E., 2007. A combined local and nonlocal closure model for the atmospheric boundary layer. Part I: Model description and testing. J. Appl. Meteorol. Climatol. 46 (9), 1383–1395. https://doi.org/10.1175/jam2539.1.
Quitián-Hernández, L., Fernández-González, S., González-Alemán, J.J., Valero, F., Martín, M.L., 2018. Analysis of sensitivity to different parameterization schemes for a sub-tropical cyclone. Atmos. Res. 204, 21–36. https://doi.org/10.1016/j.atmosres.2018.01.001.
Sahoo, B., Bhaskaran, P.K., Pradhan, A.K., 2019. Application of weather forecasting model WRF for operational electric power network management—a case study for Phailin cyclone. Theor. Appl. Climatol. 137, 871–891. https://doi.org/10.1007/s00704-018-2639-6.
Skamarock, W.C., Klemp, J.B., Dudhia, J., Gill, D.O., Barker, D., Duda, M.G., Powers, J.G., 2008. A Description of the Advanced Research WRF Version 3 (No. NCAR/TN-475+STR). University Corporation for Atmospheric Researchhttps://doi.org/10.5065/D68S4MVH.
Suárez-Molina, D., Fernández-Monistrol, J.A., Uriel-González, A.E., 2018. Catálogo-guía de fenómenos meteorológicos que afectan a la isla de Gran Canaria. Agencia Estatal de Meteorología. Ministerio para la Transición Ecológica, Madrid, pp. 101 NIPO: 014-18-005-8.
Suárez-Molina, D., Fernández-González, S., Suárez González, J.C., Oliver, A., 2020. Analysis of sounding derived parameters and application to severe weather events in the Canary Islands. Atmos. Res. 237, 104865. https://doi.org/10.1016/j.atmosres.2020.104865.
Tao, W.K., Simpson, J., McCumber, M., 1989. An ice-water saturation adjustment. Mon. Weather Rev. 117 (1), 231–235. https://doi.org/10.1175/1520-0493(1989)117<0231:aiwsa>2.0.co;2.
Thompson, G., Field, P.R., Rasmussen, R.M., Hall, W.D., 2008. Explicit forecasts of winter precipitation using an improved bulk microphysics scheme. Part II: Implementation of a new snow parameterization. Mon. Weather Rev. 136 (12), 5095–5115. https://doi.org/10.1175/2008mwr2387.
Winant, C.D., Dorman, C.E., Friehe, C.A., Beardsley, R.C., 1988. The marine layer off northern California: an example of supercritical channel flow. J. Atmos. Sci. 45, 3588–3605.
Nedjeljka, Žagar, Andersson, Erik, Fisher, Michael, 2005. Balanced tropical data assimilation based on study of equatorial waves in ECMWF short-range forecast errors. Quarterly Journal of the Royal Meteorological Society 131, 987–1011. https://doi.org/10.1256/qj.04.54.
Zhao, B., Zhang, B., 2018. Assessing Hourly Precipitation Forecast Skill with the Fractions Skill score. J. Meteorol. Res. 32 (1), 135–145. https://doi.org/10.1007/s13351-018-7058-1.

2.3. Dust Events Characterization from Visibility, Trends and Dust Adversity Index in the Canary Islands for the Period 1980-2022.

Suárez-Molina, D., Cuevas, E., Alonso-Pérez, S., Cana, L., Montero, G., & Oliver, A. (2024). Dust events characterization from visibility, trends and Dust Adversity Index in the Canary Islands for the period 1980–2022. Heliyon, 10(10), e31262. https://doi.org/10.1016/j.heliyon.2024.e31262

JOURNAL CITATION REPORTS:

2022 journal Impact factor: 4.0

Rank by Journal Impact Factor

MULTIDISCIPLINARY SCIENCES: 23/73 Q2 (69.2%)

Rank by Journal Citation Indicator (JCI)

MULTIDISCIPLINARY SCIENCES: 34/134 Q2 (75.00%)

Heliyon 10 (2024) e31262

Contents lists available at ScienceDirect

Heliyon

journal homepage: www.cell.com/heliyon

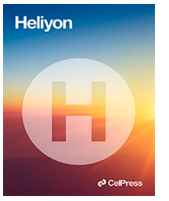

Research article

Dust events characterization from visibility, trends and Dust Adversity Index in the Canary Islands for the period 1980–2022

D. Suárez-Molina [a,*], E. Cuevas [b], S. Alonso-Pérez [c,d], L. Cana [e], G. Montero [f], A. Oliver [f]

[a] Territorial Delegation of AEMET in the Canary Islands, State Meteorological Agency of Spain (AEMET), Las Palmas, 35017, Spain
[b] Izaña Atmospheric Research Center (IARC), State Meteorological Agency of Spain (AEMET), Santa Cruz de Tenerife, 38001, Spain
[c] Departamento de Ingeniería Industrial, Universidad de La Laguna (ULL). Avenida San Francisco de Paula, s/n, 38200, La Laguna (Tenerife), Spain
[d] Instituto Universitario de Estudios de las Mujeres. Universidad de La Laguna (ULL), La Laguna (Tenerife), Spain
[e] Unidad Océano y Clima, Instituto de Oceanografía y Cambio Global, IOCAG, Universidad de Las Palmas de Gran Canaria, ULPGC, Unidad Asociada ULPGC-CSIC, Canary Islands, Spain
[f] University Institute for Intelligent Systems and Numerical Applications in Engineering (SIANI), University of Las Palmas de Gran Canaria, Spain

A B S T R A C T

Dust events in the Canary Islands have been documented since the late 19th century. However, during the past few years, several severe dust episodes have occurred in the Canary Islands, resulting in significant impacts on various sectors, such as aviation, air quality, and health, among others. These recent severe events have drawn the attention of both scientists and the general population, raising questions about whether these episodes are now more frequent and more severe. This study analyzes 483 dust events recorded in the Canary Islands over the last 40 years.

Data analysis reveals that the average number of dust event days per year is approximately 24 days, and these events have an average duration of 1.8 days, both of which show a statistically significant decreasing trend over the series. Seasonal examination indicates that events occurring in the first and fourth quarters of the year have twice the duration of those in the other quarters. Furthermore, on an annual basis, events in the first quarter exhibit negative trends in both average and minimum visibilities. This suggests that dust events in the Canary Islands are becoming shorter in duration but more intense in terms of visibility.

In this article, the Dust Adversity Index (DAI) is introduced to objectively compare the severity of events. Finally, anomalies in geopotential have been utilized to determine the prevailing synoptic patterns during dust events. It is evident that the dominant synoptic pattern during the first and fourth quarters of the year consists of a low cut-off system located to the west of the Canary Islands and a high-pressure system to the north of the Iberian Peninsula.

1. Introduction

Desert dust holds significant importance in terms of atmospheric aerosol contributions by mass [1–3]. Various arid regions on Earth serve as sources of this dust, with North Africa accounting for around 50 % of the annual emission and deposition rates of 1.2–3.1 $\times$ 10^3 Tg yr^{-1} from all source regions [4,5].

Dust exerts diverse impacts, including risks to human health [6–8], influence on Earth's climate [6,9,10] (; effects on air quality [11,12]), implications for air traffic [13], consequences for agriculture [14], impacts on terrestrial and marine ecosystems [15], and effects on cloud microphysics and precipitation [16]. Given its broad impacts across various socioeconomic sectors and health, significant efforts have been dedicated to enhancing knowledge, monitoring, and forecasting [17]. The World Meteorological

* Corresponding author
E-mail address: dsuarezm@aemet.es (D. Suárez-Molina).

https://doi.org/10.1016/j.heliyon.2024.e31262
Received 26 December 2023; Received in revised form 27 April 2024; Accepted 14 May 2024
Available online 17 May 2024

Organization (WMO) initiated the Sand and Dust Storm Warning Advisory and Assessment System (SDS-WAS) in 2007. Presently, SDS-WAS comprises three regional nodes: (a) North Africa, Middle East, and Europe, (b) Asia and Central Pacific, and (c) Pan-America. These regional centers, facilitated by the SDS-WAS Steering Committee [18], constitute a global network of research, operational centers, and users.

Various variables (such as visibility, concentration, and aerosol optical depth (AOD)) characterize a dust event, and authors like [19,20] have proposed some indices to gauge intensity. However, not all variables possess sufficiently long time series for robust conclusions.

Dust events in the Canary Islands have been documented since the late 19th century [21], which is lógical, given the archipelago's proximity to the primary source of desert dust on Earth [22]. Intrusions of Saharan dust constitute a prominent weather pattern in the Canary Islands [23].

Prior studies have subjectively analyzed favorable atmospheric patterns for desert mineral aerosol transport from North Africa to the Canary Islands [24–34]. These authors generally concur that desert mineral aerosol intrusions in the Canary Islands align with a high-pressure system in North Africa [35] identify three preferred intrusion periods, with winter being the most impactful in terms of air quality deterioration and aeronautical effects.

Given the intensity and impact of recent dust episodes in the Canary Islands (e.g., the February 2020 event; [13]), questions regarding the frequency, intensity, and climate change-related connection of these episodes have arisen from the media, public, social networks, and professionals.

This paper's objectives encompass the characterization of dust intrusions using extended visibility series, analysis of their evolution, seasonal and yearly variations, and trends over the past 42 years. The data comes from the six main Canarian airports, since wer're concerned about the significant impact of reduced visibility on aeronautical operations. The data's length and quality enable firm conclusions. Additionally, due to challenges in objectively assessing dust event severity, an index is will be proposed to gauge intensity quantitatively. Lastly, this study analyzes the synoptic patterns that caused dust events in the Canary Islands from 1980 to March 31, 2022.

The paper's structure involves an introduction to the region of interest and the data in section 2, detailing the methodology. Section 3 delves into results and discussions, followed by the presentation of key conclusions in Section 4.

2. Data and methods

2.1. Area of interest

This study has been conducted within the Canary Islands, an archipelago comprised of 7 islands situated in the subtropical Atlantic, west of Africa, spanning from coordinates 27°37′ to 29°25′ N and 18°10′ to 13°20' W (Fig. 1). These islands are positioned approximately 100 km off the Moroccan coast and 1100 km from mainland Spain. The complex topography of the islands contributes to a diverse climatic range. The higher islands exhibit B, C, and D climatic types [36], while the lower islands, Lanzarote and Fuerteventura, are predominantly characterized by type B climates according to the Köppen-Geiger classification [37].Renowned scholarsauthors like Font Tullot [23,38], in their island-focused publications, have identified 8 primary weather patterns that significantly affect this archipelago. For the analysis of the synoptic patterns (see section 2.3.4), the geographical domain analyzed was (20° N, 50° N; 35° W, 10° E)

For this study, we have employed observational data gathered from the six principal airports across the archipelago: Fuerteventura (GCFV), Lanzarote (GCRR), Gran Canaria (GCLP), Tenerife Norte (GCXO), Tenerife Sur (GCTS), and La Palma (GCLA).

2.2. Data

2.2.1. Observation data

We have used visibility data derived from the 13 UTC (Universal Time Coordinated) surface synoptic observations (SYNOP) together with relative humidity measurements from the six airports. The data spans from January 1, 1980, to March 31, 2022. The quantification of visibility aligns with the protocols defined by the World Meteorological Organization, as stipulated in Refs. [39,40]. Likewise, relative humidity has been measured through HMP155 sensor models manufactured by Vaisala.

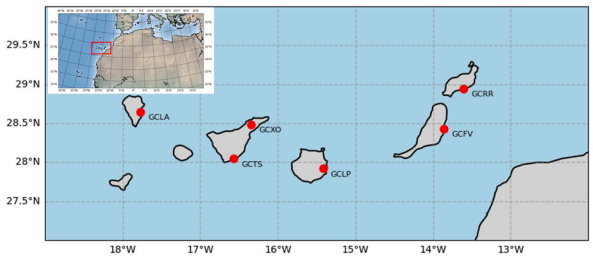

Fig. 1. Area of interest. Red box highlights the Canary Islands. On the islands the location of the airports is marked with their indicatives. (For interpretation of the references to colour in this figure legend, the reader is referred to the Web version of this article.)

These data sets have been sourced from the National Climatic Data Bank, administered by the State Meteorological Agency of Spain (AEMET). It is important to note that rigorous validation procedures have been employed to ensure the accuracy and reliability of the data.

2.2.2. Reanalysis data

To identify the most frequent meteorological patterns that encourage African dust intrusions over the Canary Islands, daily reanalysis daily of geopotential height anomalies at 925, 850, 700 and 500 hPa are used. The data comes from the NCEP/NCAR Reanalysis 1 project [41] provided by the National Centers for Environmental Protection (NCEP) and the National Centre for Atmospheric Research (NCAR). The standard reference climatology time period for the anomalies calculation is 1991–2020. The geopotential height anomalies are calculated as the difference between the geopotential height daily mean for a certain day and the geopoptential height monthly mean of the corresponding month for the standard reference period. The spatial resolution is $2.5^\circ \times 2.5^\circ$.

2.3. Method

2.3.1. Dust event definition

In this study, a "dust event" occurs when the presence of dust reduces the horizontal visibility to less than 10 km in at least two aerodromes simultaneously. This ten kilometres threshold is chosen because it is the one used in METAR (Meteorological Aerodrome Report) and TAF (Terminal Aerodrome Forecast) reports [42]. To determine if the visibility reduction is due to dust, we consider that a relative humidity measurement below 70 %. This threshold is introduced to exclude possible influence of fog or mist events, thus ensuring that the reduction in visibility is due to dust.

2.3.2. Trend analysis

We use the Mann-Kendall test [43–45] to detect potential trends within the time series data. This statistical test, widely adopted for environmental time series analysis [46], evaluates the rejection of the null hypothesis (H0) in favor of the alternative hypothesis (Ha). The null hypothesis states the absence of a monotonic trend, while the alternative hypothesis asserts its presence. The R package "Kendall" is utilized, with a significance level set at $\alpha = 0.05$.

2.3.3. Dust Adversity Index (DAI)

The adversity of a dust event in an area of interest is determined by the reduction in visibility (there is a relationship between visibility and dust mass concentration, see for exemple [47]), the affected area (number of affected stations) and the persistence of the event (number of days of duration). It is easy to find precipitation records that have been measured in a specific place, or the extreme temperatures registred for a specific location. However, it is more complex to determine a ranking of dust events based on their intensity in an area of interest.

Severity indices can be found in the literature to determine the intensity of dust events [48–50]. These indices have some limitations, as some of them only take visibility into account, or in other cases they are based on AOD, or they are based on number of affected stations and visibility. However, none of them contain information on dust concentration, area affected and persistence of the event. This is the reason why we introduce the Dust Adversity Index (DAI), with the aim of encapsulate key characteristics of dust events and facilitate comparisons between different occurrences to ascertain their relative adversity.

The DAI is defined as shown in equation (1):

$$DAI = s/s_T * x/x_r * d * 10^4/v_m \quad (1)$$

Where.

- "s" represents the number of stations affected by the dust event, with potential values ranging from 2 to 6. The role of "s" in the index is to take into account that the greater the number of affected stations, the evidently the dust event has a less local character and is more widespread.
- "s_T" is the total number of stations in the area of interest. For the present study, s_T is equal to 6.
- "d" is the duration factor, which takes values between 1 and 5 determined by percentiles of the dust event duration. This tabulation is done to minimize the impact on the DAI of the outlaiers. Table 1 shows the relationship.
- "V_m" is mean visibility of dust event in m. It is calculated as the average of the visibility of all stations during the entire event.

Table 1
Values of the "d" parameter as a function of the percentile of the dust event duration.

Dust event duration (in days)	d value
1–2	1
3(P72) - 4(P86)	2
5 (P95)	3
6-8 (P98)	4
>8 (P99)	5

- "x/x_r" To guarantee comparability of results across various regions, we have introduced a term that represents the maximum separation distance between the analyzed stations. In this study, we use the variable "x" to denote the maximum distance between the furthest stations, while "x_r" represents the reference distance (xr = 406.79 km), which corresponds to the distance between GCRR and GCLA. Therefore, in our case, the ratio "x/xr" is equal to 1.

2.3.4. K-means

The K-means clustering algorithm, as introduced in Ref. [51], is a widely recognized and robust technique employed for the categorization of data into distinct clusters.We use this algorithm to calculate the main patterns of geopotential height anomalies in the area and time period of study, for all the tropospheric levels considered, and grouping the days of dust events into four quarters. We adopt a methodological approach similar to the one employed in Ref. [34].

3. Results and discussion

Using the methodology outlined in section 2.3.1, an examination spanning from 1980 to 2022 reveals a total of 483 instances of dust events in the Canary Islands. Among these occurrences, 46 events exhibit an average visibility of 5000 m or less.

It is worth noting that of the 46 events with an average visibility equal to or lower than 5000 m, only 9 dust events (1983-01-17; 1983-12-27; 1988-12-27; 1992-01-03; 1998-02-12; 2004-03-03; 2013-02-04; 2020-02-22; 2022-01-28) affected the 6 main airports of the Canary Islands. As shown in Fig. 2, these events had a different duration but were characterised by their intensity (low average visibility) and their wide extension (all stations were affected). As will be shown in section 3.2 variously, within these 9 dust events are the most intense ones.To encapsulate these 46 events, Fig. 2 serves as an illustrative summary. The height of the bar represents the event's average visibility, while the width represents its duration. Each bar is accompanied by a label denoting the number of airports influenced by the event.

3.1. Basic statistics and trend tests

To present and analyze all the dust events, we group them into five distinct periods. The first one, the Annual group, includes all the data. The other four are grouped by quarters: Q1 includes all the dust events that occurred during January, February, and March; Q2 has all the events that happened during April, May, and June; Q3 has all the events that happened during July, August, and September; and finally, Q4, has all the events that happened during October, November, and December.

For each group, we want to analyze the duration of the events, their visibility (both mean and minimum values), and the number of days of dust events in the period. Table 2 shows the mean, median, standard deviation (SD), the slope of trends (τ), and the p-value of all these values for each group. The slope of the trends (τ) distinguishes between rising ($\tau > 0$) and falling ($\tau < 0$) trends. The p-value detects statistically significant trends; greyed rows represent the significant ones ($p < \alpha$).

Following, we present an in-depth analysis of each group.

3.1.1. Annual analysis

In the study period there have been 24.12 ± 12.15 (with a median of 22.50 days per year) days of dust events annually. The average

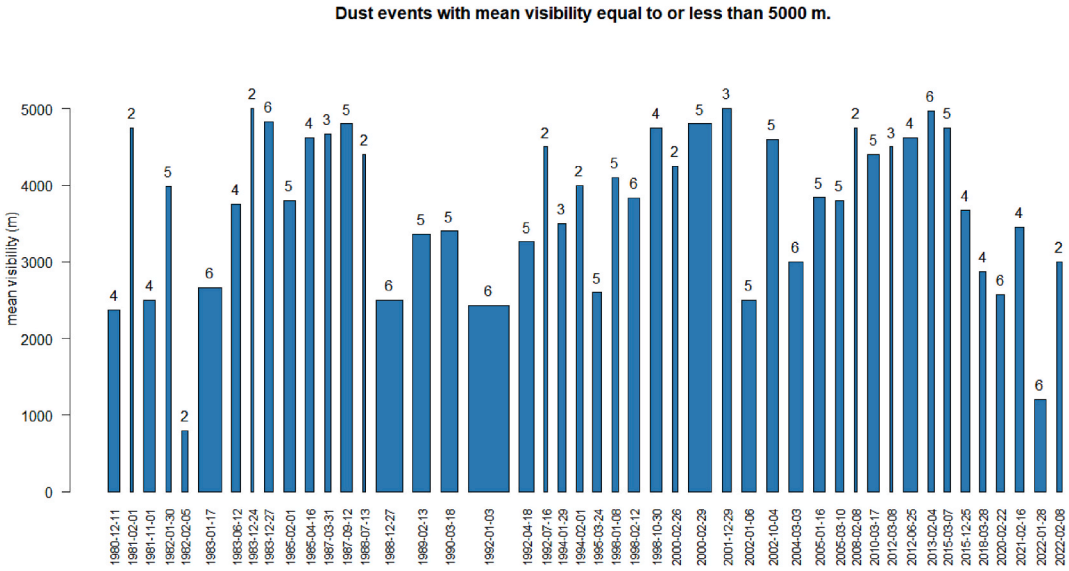

Fig. 2. Summary of the 46 most intense dust events that occurred in the Canary Islands (average visibility equal to or less than 5000 m).

Table 2
Statistical results and trend test for different periods. (January, February, and March (Q1); April, May and June (Q2); July, August and September (Q3) and October, November and December (Q4)).

	mean	median	sd	Ƭ	p-vaule
Annual duration (days)	1.81	1.8	0.35	-0.238	**0.028343**
Annual mean visibility (m)	8141	8069	640	-0.157	0.14644
Annual mínimum visibility (m)	7165	7094	832	-0.123	0.25507
Number of annual dust event days	24.12	22.50	12.15	-0.627	**7.28E-05**
Q1 duration (days)	1.93	1.8	0.91	-0.158	0.14679
Q1 Mean visibility (m)	7359	7339	1410	-0.115	0.28103
Q1 minimum visibility (m)	6062	6033	2012	-0.0958	0.37334
Q1 days of dust events	8.42	8	4.92	-0.205	0.060002
Q2 duration (days)	1.44	1,.58	0.81	-0.278	**0.013941**
Q2 Mean visibility (m)	9085	9242	912	0.172	0.12074
Q2 mínimum visibility (m)	8531	8708	1383	0.124	0.27177
Q2 days of dust events	4.02	3.50	3.05	-0.433	**0.00010466**
Q3 duration (days)	1.85	1.95	0.97	-0.375	**0.00063657**
Q3 Mean visibility (m)	8964	8881	694	0.061	0.57979
Q3 mínimum visibility (m)	8011	8000	1193	-0.0771	0.48647
Q3 days of dust events	8.10	7	6.45	-0.528	**1,45E-02**
Q4 duration (days)	1.30	1.50	0.87	0.078	0.50065
Q4 Mean visibility (m)	8190	8333	1554	0.0661	0.55447
Q4 mínimum visibility (m)	7149	7500	2344	0.0836	0.45629
Q4 days of dust events	3.07	3	2.68	-0.165	0.14686

duration of these dust events over the years is 1.81 ± 0.35 days (with a median of 1.80 days). The annual mean (median) visibility is 8141 ± 640 m (8069 m), and the annual mean (median) minimum visibility is 7165 ± 832 m (7094 m). During this period, both the number of days with dust events and the duration of these events have decreased, with Ƭ values of −0.627 and −0.238, respectively, as indicated by the results of the trend test (see Table 2 and Fig. 3). These trends are statistically significant at a significance level of $\alpha = 0.05$. Despite these downward trends, annual variability is observed. The results obtained here are in line with previous studies [52, 53]. These studies examine the annual trends and variability of dust over North Africa. The authors state that periods favorable for dust production, such as the late 1980s, are caused by abnormally high winds and low soil moisture [6,54,55]. According to Ref. [53], the decreasing trend observed between 1986 and 2000 was due to a decrease in wind intensity and an increase in soil moisture, which contributed to dust suppression. Since 2011, there has been an increase in dust activity in North Africa. This can be attributed to a

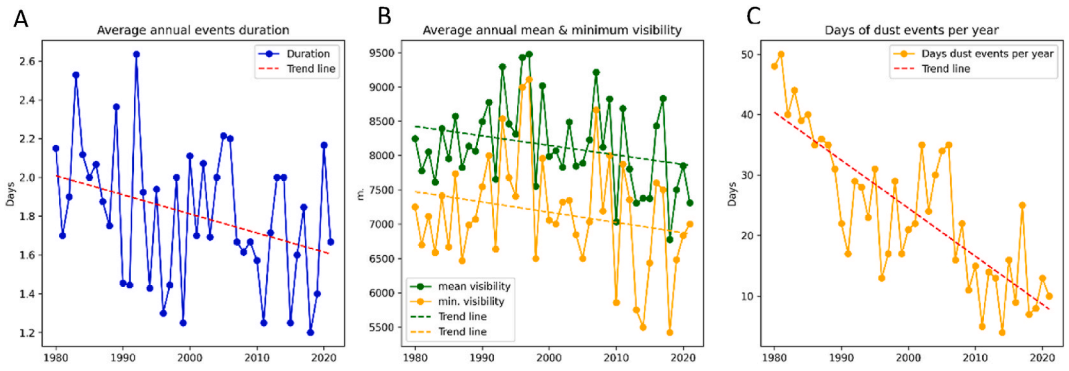

Fig. 3. Annual evolution of the variables: A) Annual average duration of dust events. B) Annual average of mean and minimum visibility. C) Number of days of dust events.

decrease in soil moisture and an increase in wind intensity [53].

The annual average visibility (both mean and minimum visibility) has shown negative trends. This suggests that the events have become more intense, resulting in further reductions in visibility. However, these trends are not statistically significant.

3.1.2. Monthly analysis

Fig. 4 depicts the monthly average of the duration and the visibility (mean and minimum). The longest events occur in January and February, spanning 2.10 and 2.11 days, respectively. In contrast, the shortest dust events manifest in November, lasting 1.48 days. Regarding visibility, the most intense events occur in February, December, and January, with mean visibility levels of 6963, 7101, and 7252 m, respectively. However, the minimum visibility levels occur in December, February, and October, with values of 5550, 5563, and 5708 m, respectively. Analyzing both the mean and minimum visibility values we can conclude that the least intense dust events occur from April to September.

3.1.3. Seasonal analysis

A first analysis of Table 2 and Fig. 5 shows us that, on average, there are twice as many occurrences in the Q1 and Q3 quarters as in the other two quarters. In Q1 and Q3 the occurrence is slightly higher than 8 days (8.42 and 8.10 respectively), while in Q2 and Q4 the values are between 3 and 4 days (4.02 and 3.07). The analysis of the average visibility reveals that the most severe events occur in the Q1 quarter, with an average visibility of 7359 $\pm$ 1410 m. In contrast, the least affected quarter is Q2, with an average visibility of 9085 $\pm$ 912 m. The above is also consistent when examining the average minimum visibility, where the Q1 quarter also presents the most reduced visibility with an average of 6062 $\pm$ 2021 m.

Considering the τ, it is discernible that all variables exhibit negative values during the Q1 quarter, suggesting shorter yet more intense events. However, the trends lack statistical significance at a confidence level of $\alpha = 0.05$. In the Q2 quarter, events show a negative τ in duration and days of occurrence, but a positive τ in visibility (both mean and minimum). Noteworthy is the statistical significance of the duration and days of occurrence trends during this quarter. For Q3, significant negative τ manifest in duration and event days, while visibility τ diverge with mean visibility showing an upward trend and minimum visibility showing a downward trend. In contrast, the τ for visibility variables (mean and minimum) remain statistically insignificant during the Q1 quarter. During Q4, all variables except the number of event days show a positive trends. However, these trends lack statistical significance.

To complete the seasonal analysis of dust events in the area of interest, the methodology of section 2.3.4 has been applied to determine the synoptic patterns during dust events occurring in each quarter. During the first quarter (Fig. 6), dust events manifest under the influence of a well-defined dipole pattern characterized by a low cut-off (more profound in 52 % of instances, clusters 2 and 4) to the western region of the Canary Islands, juxtaposed with a high-pressure system centered to the north-northeast of the Iberian Peninsula at the 500 hPa level.

Across the other atmospheric levels (700 hPa, 850 hPa, and 925 hPa), the meteorological configuration exhibits parallels, although the drop in height is less marked in the lower levels of the troposphere. This atmospheric pattern generates an east-southeast flow at lower altitudes, facilitating the transport of mineral-laden desert aerosols from the African landmass into the Atlantic domain. The interplay with the low-pressure cutoff positioned to the west of the Canary Islands moves the dust particles upwards, subsequently entrapping them. This phenomenon forces a recirculation of air over the islands Cuevas et al. (2021) concluded that this weather pattern produces the most severe dust events in the Canary Islands. Due to the significance of this pattern in dust episodes in the Canary Islands, it will be referred to in the following quarters.

During the second quarter (Fig. 7), a high-pressure system is present either in the northwest (approximately 82 % of the time) or in the west (approximately 18 %) of the Iberian Peninsula at the 500 hPa atmospheric level.Furthermore, the geopotential anomalies are less marked at the 925 hPa level, except within cluster 1 (approximately 33 %), where the high-pressure configuration mirrors the customary disposition observed at the 500 hPa level.

In this quarter, only a situation similar to the predominant one in Q1, a dipole of low pressure (located west of the Canary Islands) and high pressure (located north of the Iberian Peninsula), appears at the 850 hPa level (approximately 46 % of events).

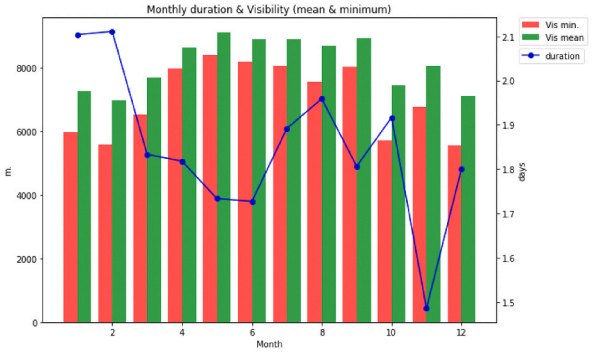

Fig. 4. Monthly average of duration (blue line), mean (green bar) and minimum visibility (red bar). (For interpretation of the references to colour in this figure legend, the reader is referred to the Web version of this article.)

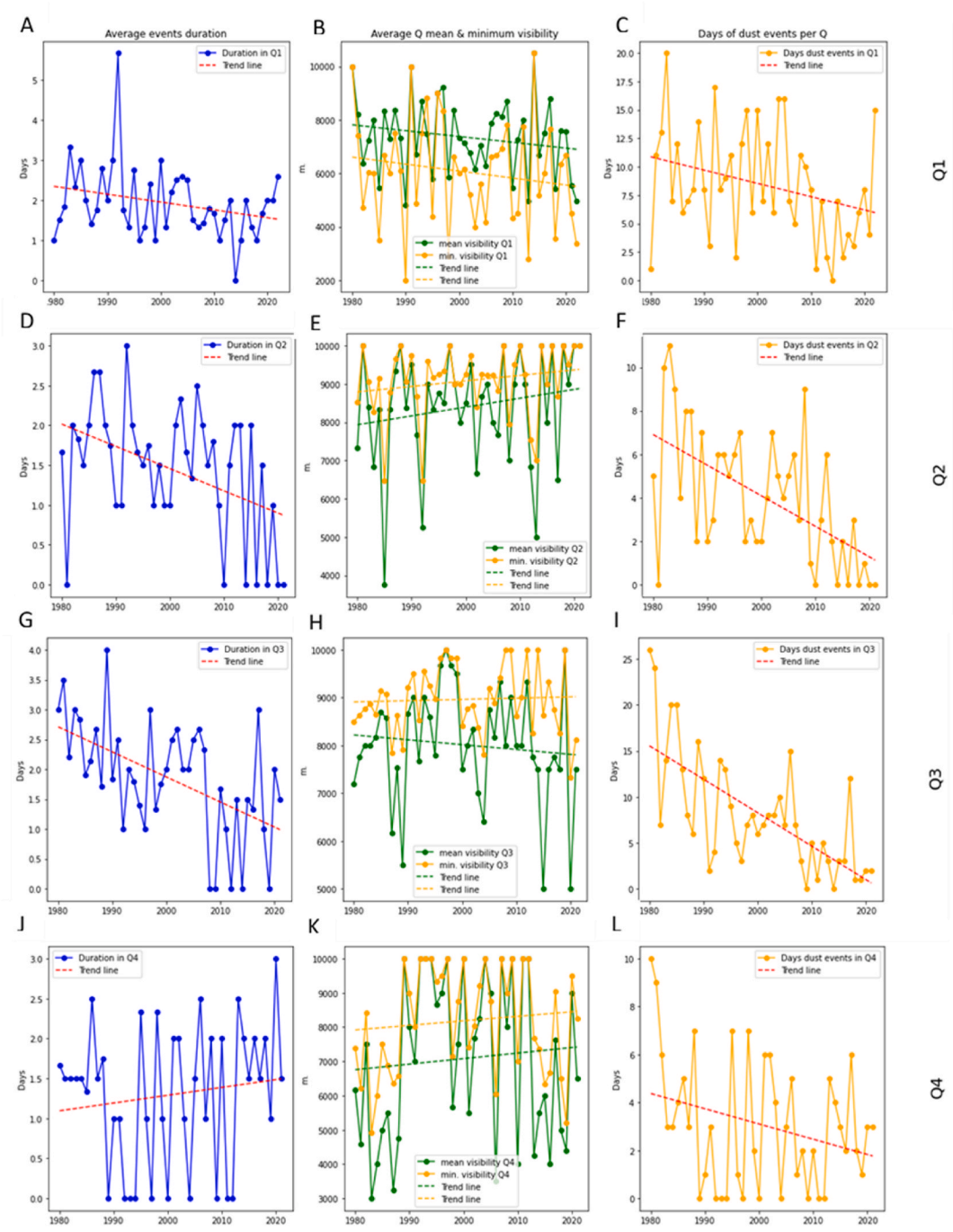

Fig. 5. Quarters evolution of the variables: Average duration of dust events [A, D, G, J]. Average of mean and minimum visibility [B, E, H, K]. Number of days of dust events [C, F, I, L]. Each row corresponds to the quarter indicated on the right (Q1, Q2, Q3, Q4).

During the third quarter (Fig. 8), the geopotential anomalies at the different levels are, in general, less marked than in the other quarters. At the 500 hPa level, it is observed that approximately 65 % of instances are characterized by a dominant positive geopotential anomaly positioned to the north-northwest of the Iberian Peninsula. Within cluster 4 (approximately 19 %), negative geopotential anomalies manifest over the African continent and the southwestern vicinity of the Azores.

The pattern discernible at the 700 hPa level closely resembles that observed at 500 hPa, albeit with the positive geopotential anomalies (Clusters 1 and 4) centered slightly further south. At the 850 hPa level, around 78 % of dust events display inconspicuous geopotential anomalies. Notably, about 22 % (cluster 2) of occurrences in this quarter exhibit dust events transpiring in the presence of a robust anticyclonic system located within the subtropical Atlantic. A parallel circumstance is mirrored at the 925 hPa level, wherein

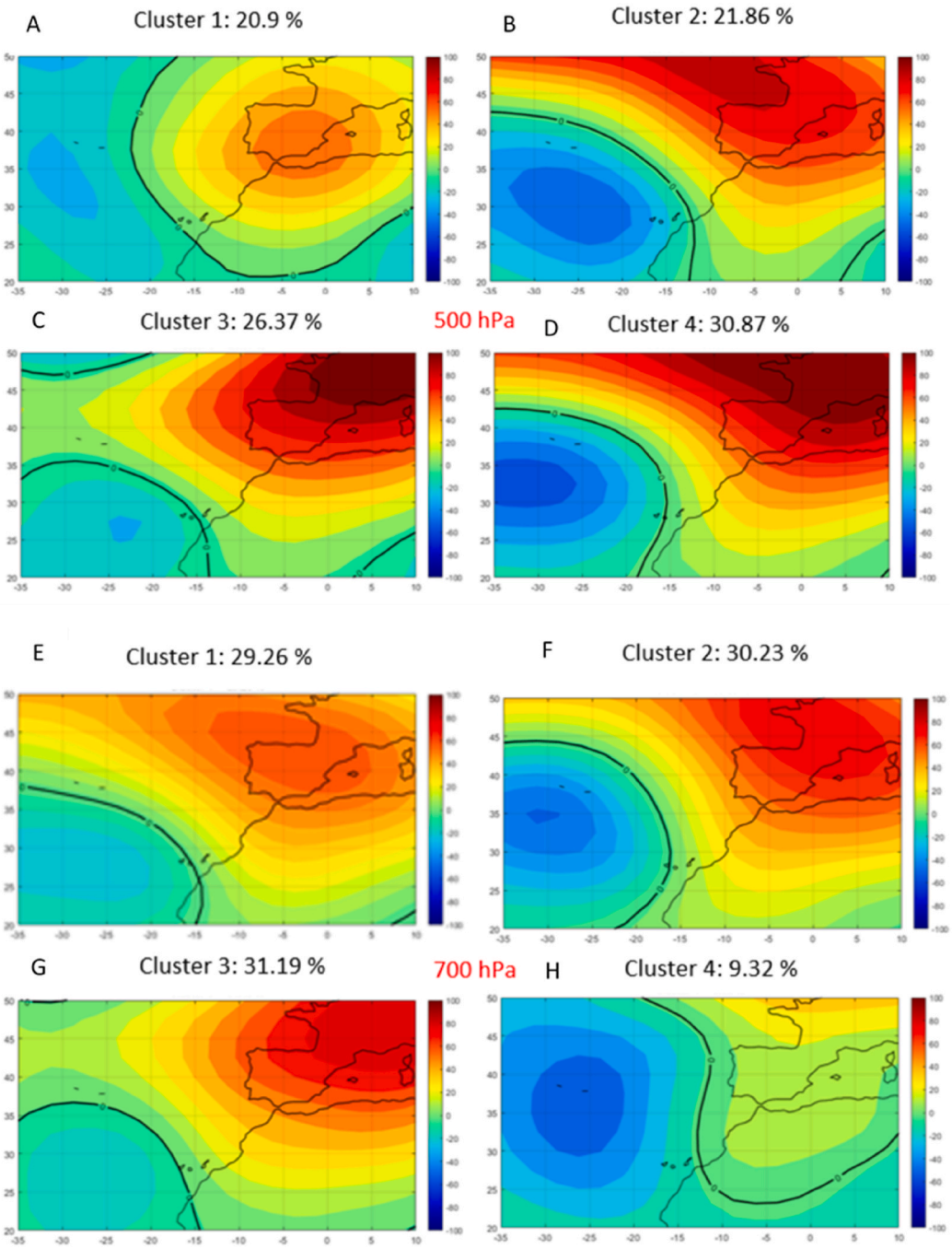

Fig. 6. Clusters of main patterns of geopotential height anomalies for different atmospheric levels and for Q1. [A-D] Panels corresponding to the 500 hPa. [E-H] Panels corresponding to the 700 hPa. [I-L] Panels corresponding to the 850 hPa. [M – P] Panels corresponding to the 925 hPa.

negligible geopotential anomalies are observed throughout this quarter.

During the fourth quarter (Fig. 9), the geopotential anomalies are more noticeable and the high-low dipole structure can be seen in a large part of the middle and lower troposphere (similar to Q1). At 500 hPa, positive anomalies centered north of the Iberian Peninsula are observed in most of the dust events, except for ≈9 % (cluster 4) that appear centered north of the Azores. At this level, the negative geopotential anomalies are centered to the west of the Canary Islands. The low-high dipole interaction produces an intense south-easterly flow that favors aerosol advection from the source region to the Canary Islands.

As we descend in levels, it is observed how the negative geopotential anomalies centered to the west of the Canary Islands decrease

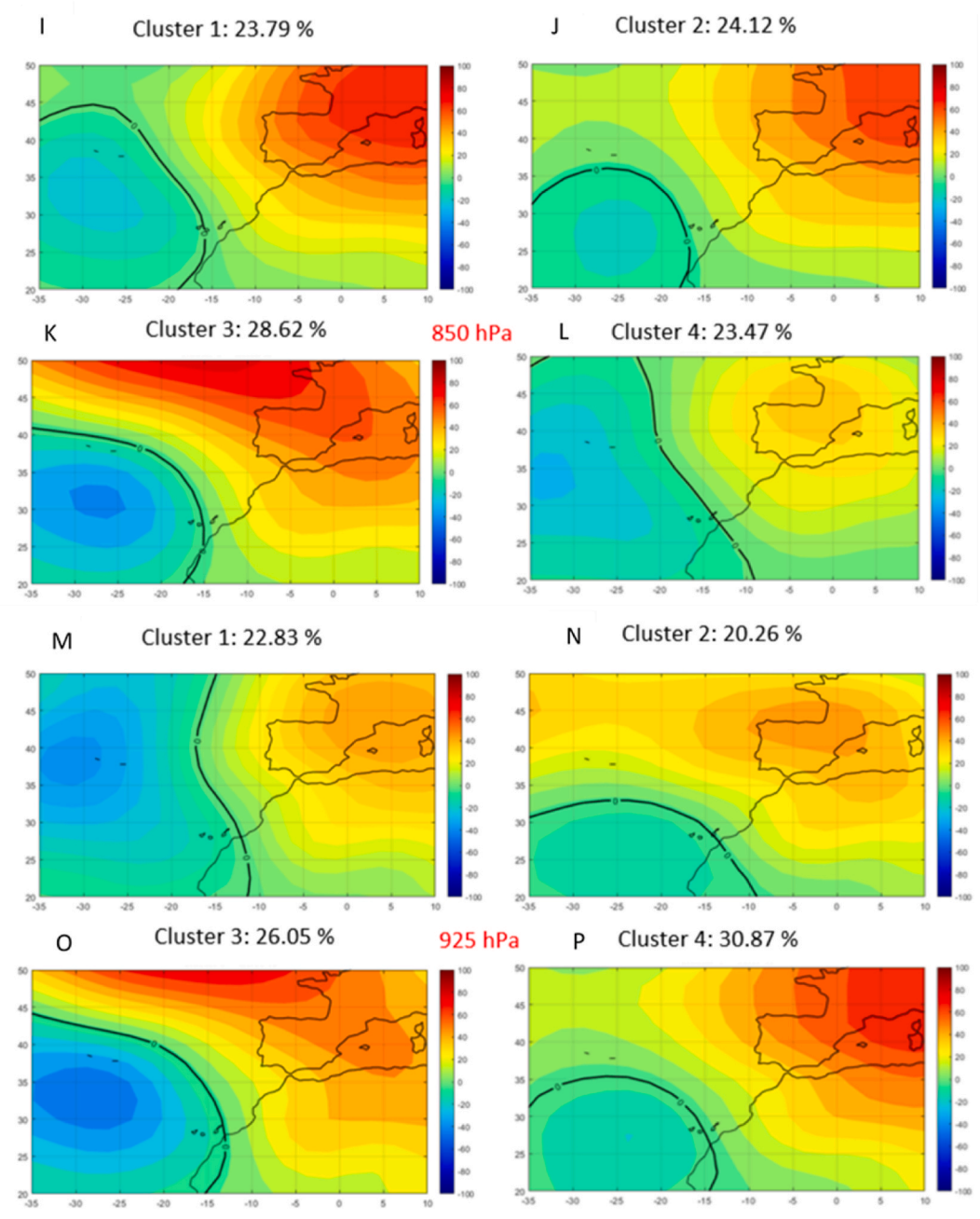

Fig. 6. (*continued*).

in intensity. This is because the systems present during dust events are low cut-off.

Thus, it can be seen that at the 700 hPa level the marked negative geopotential anomalies in the Canary Islands are 50 % (Clusters 3 and 4), 45 % (Clusters 1 and 3) at 850 hPa and 19 % (Cluster 1) at 925 hPa.

3.2. *Dust Adversity Index (DAI)*

Fig. 10 shows the Dust Adversity Index (DAI) values encompassing 483 dust events in the period of interest. The mean value of the DAI stands at 1.27, with the following distribution: 466 occurrences exhibit DAI values of 5 or less, 13 have values between 5 and 10, and only four have values above 10. These four instances are March 1, 1992; December 27, 1988; January 17, 1983; and January 28, 2022 (in descending order of DAI mean value). As the results show, three of the four most intense dust events, based on DAI, have

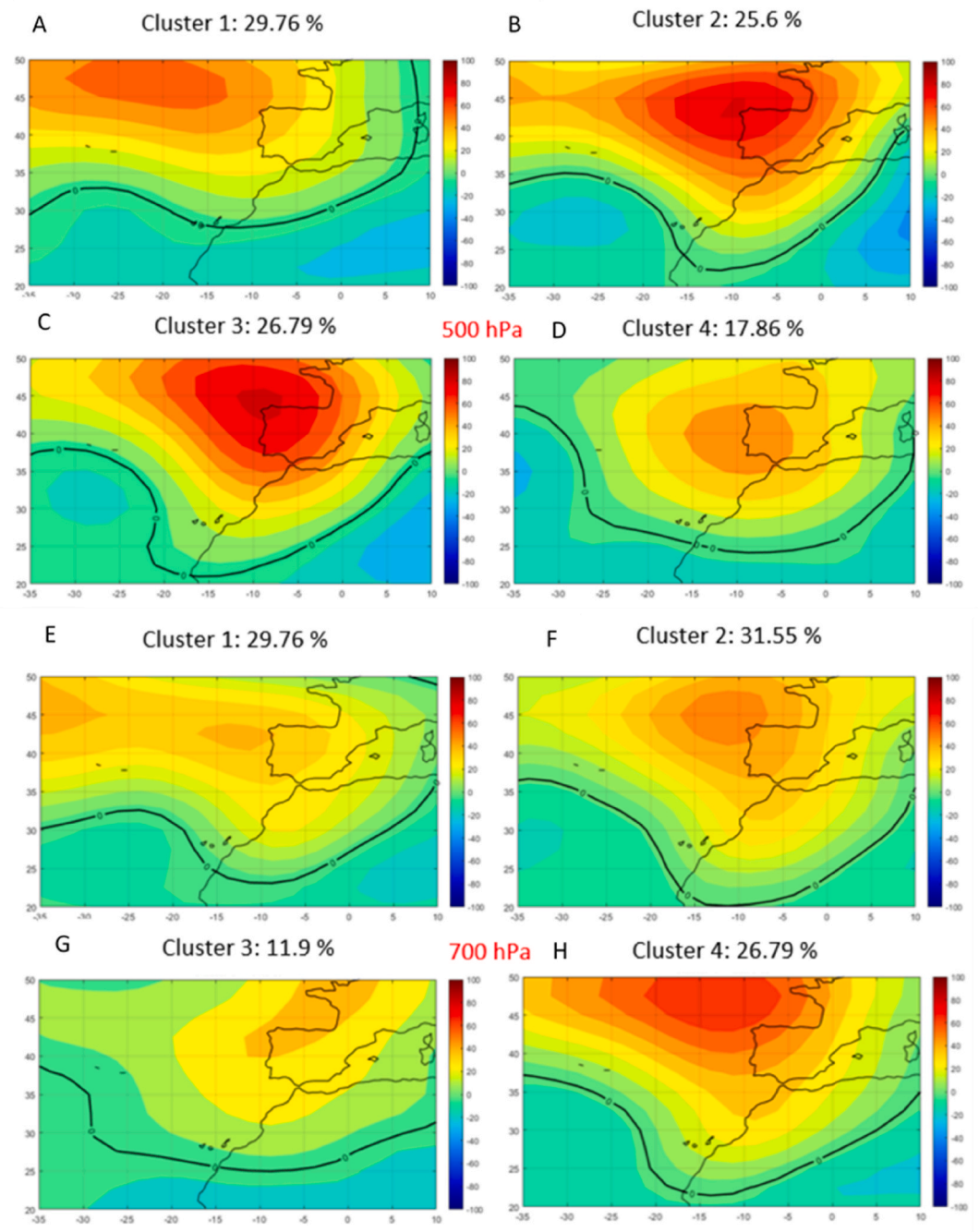

Fig. 7. Clusters of main patterns of geopotential height anomalies for different atmospheric levels and for Q2. [A-D] Panels corresponding to the 500 hPa. [E-H] Panels corresponding to the 700 hPa. [I-L] Panels corresponding to the 850 hPa. [M – P] Panels corresponding to the 925 hPa.

occurred during Q1. This is due to the seasonality of the SAL and the characteristics shown by the desert aerosol intrusions during Q1 in the Canary Islands. In this quarter, the dust intrusions are characterised by the continental air mass replacing the maritime air mass associated with the trade winds due to the eastward displacement of the Azores anticyclone. During these situations, the strong easterly wind in the lower levels of the troposphere causes high concentrations of dust to travel from low levels from the source region to the area of interest, affecting the Canary airports.

Analyzing the annual DAI mean value (shown in Fig. 11), we conclude that most years have values between 0.5 and 2. On the extremes, two years have values below 0.5: 2011 (0.39) and 1996 (0.45), and three years above 2: 1992 (3.02), 1983 (2.47), and 1989 (2.11).

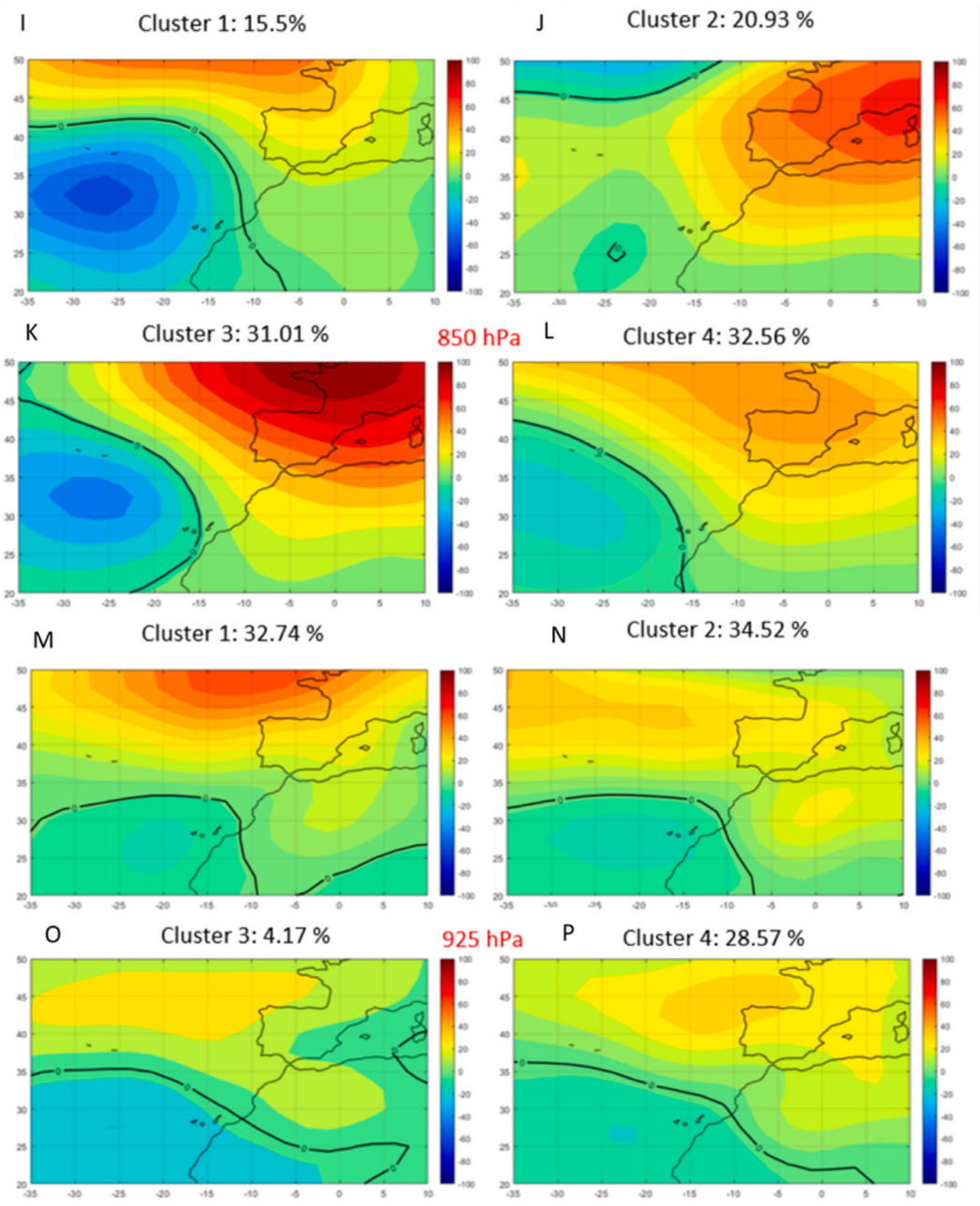

Fig. 7. (*continued*).

Fig. 12 exhibits the monthly mean values of the DAI. The severity of dust events is more pronounced during the winter months, leading to elevated DAI values. This pattern is particularly prominent in January, which boasts the highest monthly mean DAI of 2.42, while the lowest value is observed in May, standing at 0.56.

Fig. 13 offers a depiction of the temporal evolution of DAI from January 1980 to March 2022. The average DAI values for each quarter are 1.79, 0.69, 0.75, and 0.92 for Q1, Q2, Q3, and Q4, respectively and this is consistent with the DAI values obtained in the monthly analysis. The seasonal analysis of DAI shows that throughout the study period, exceeding the DAI threshold of 3 occurred more frequently in Q1 than in the other quarters. Specifically, in the Q1 of the years 1992, 1990, 2022, 1983, 1985, and 2004 (arranged in decreasing order of DAI values), DAI exceeded 3. For Q2, DAI was higher than 3 in 1992, while for Q3 and Q4, it exceeded this threshold in 1989 and 1988, respectively. As the results show, the events that occurred in Q1 are, in general, more intense than in the rest of the year. The above is consistent with other studies carried out in the area of interest [56] and is caused by the seasonal variation in the vertical structure of the Saharan Air Layer (SAL) [57] and in the synotic patterns.

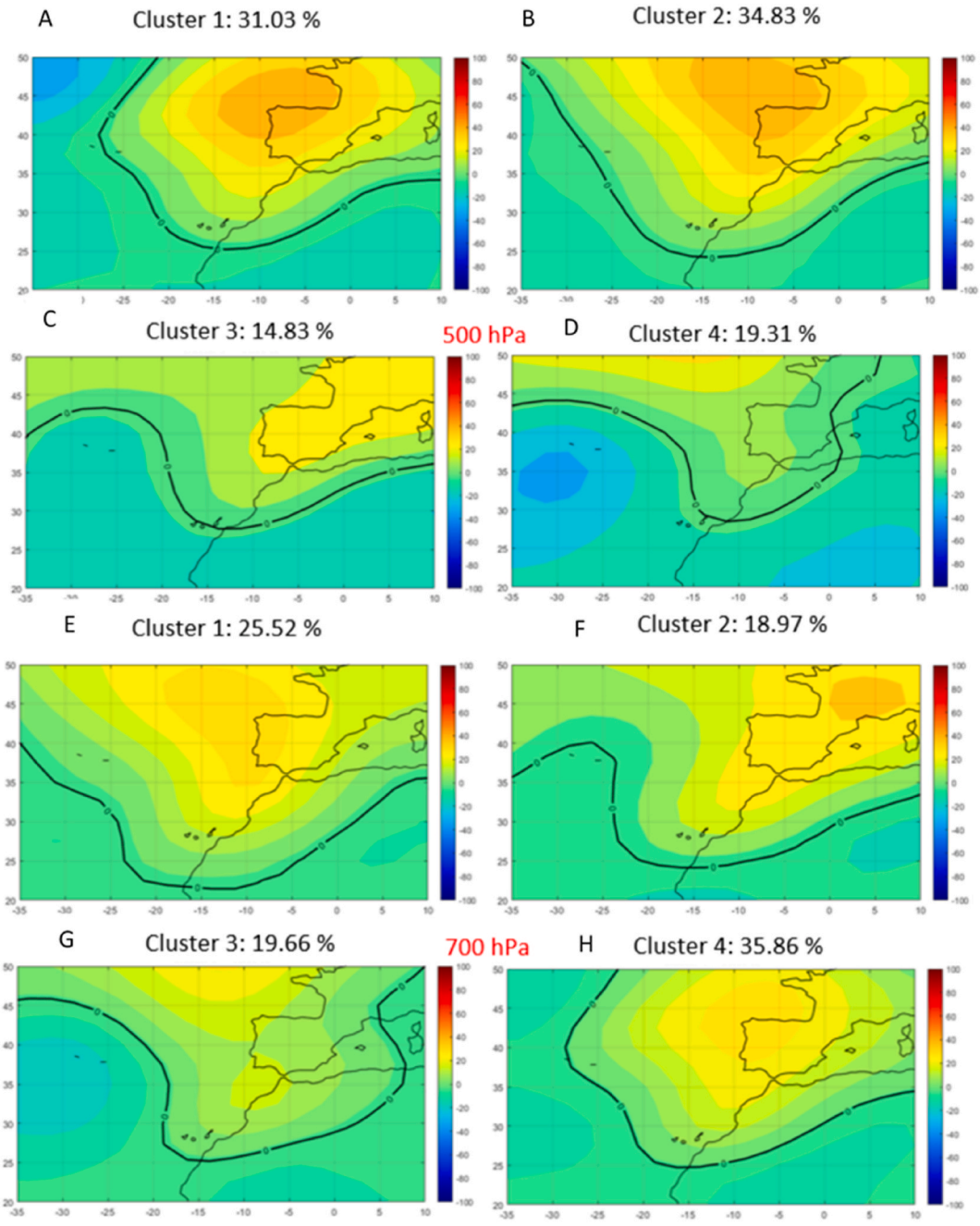

Fig. 8. Clusters of main patterns of geopotential height anomalies for different atmospheric levels and for Q3. [A-D] Panels corresponding to the 500 hPa. [E-H] Panels corresponding to the 700 hPa. [I-L] Panels corresponding to the 850 hPa. [M – P] Panels corresponding to the 925 hPa.

3.3. Case study

To further validate DAI in other regions, DAI was calculated for another study area during an intense dust event. Four stations located in northwest Africa were selected for this purpose: GMML, Laayoune/Hassan Isl (Morocco); GMAD, Agadir Al Massira (Morocco); GMMI, Essaouira - Mogador Intl. Airport (Morocco); and DAOF, Tindouf (Algeria). In this case study, a dust event occurred from 21 to February 25, 2020, lasting for 5 days, which is longer than the 3-day event in the Canary Islands. The average visibility during the event was 6000 m, and the maximum distance between stations was 595.75 km, resulting in an x/x_r value of 1.46.

The DAI value for this case study's dust event is 7.3, while for the Canary Islands event, it is 7.79. Although DAI was applied to areas

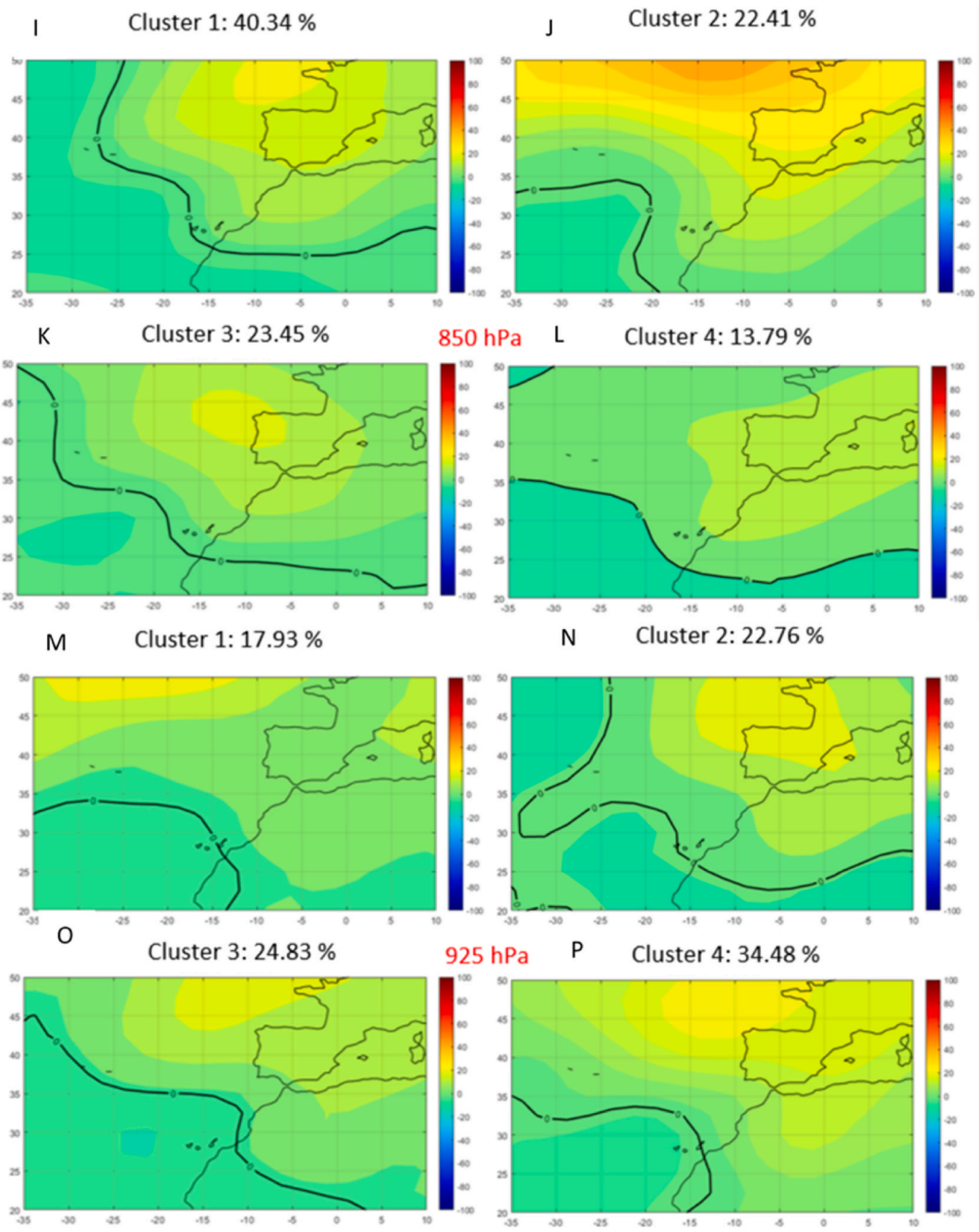

Fig. 8. (*continued*).

of varying characteristics, such as distance between stations and number of stations, the resulting DAI values were similar. This shows the usefulness of DAI in determining the intensity of dust events in different areas and characterising them objectively based on relevance criteria such as visibility, persistence, and affected area. This approach can help us better understand the impact of dust events on different areas and take appropriate measures to mitigate their effects.

4. Conclusions and summary

This article has analyzed the dust events that have affected the Canary Islands during the period between 1980 and 2022. The study encompasses the characterization of dust events across various timeframes and the exploration of trends in key variables of interest,

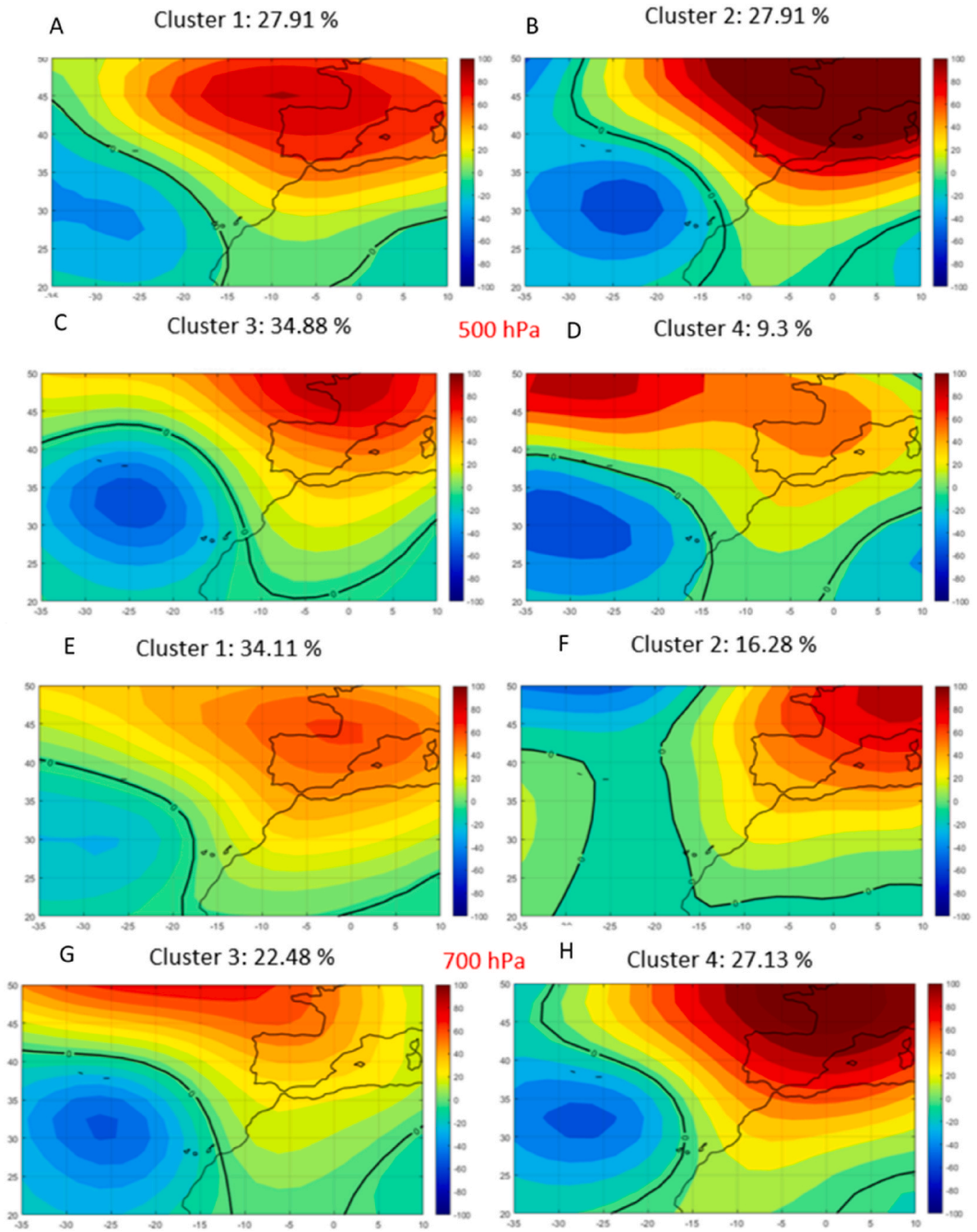

Fig. 9. Clusters of main patterns of geopotential height anomalies for different atmospheric levels and for Q4. [A-D] Panels corresponding to the 500 hPa. [E-H] Panels corresponding to the 700 hPa. [I-L] Panels corresponding to the 850 hPa. [M – P] Panels corresponding to the 925 hPa.

encompassing factors such as event duration, mean visibility, minimum visibility, and event duration.

With the aim of improving the deficiencies found in other severity indices, this article proposes an index (DAI) that objectively allows knowing and comparing the intensity of each dust event In addition, we analyze the prevailing weather patterns that favor desert mineral dust intrusions from source regions and trigger dust events in the Canary Islands.

The main findings of this study are the following.

- A total of 483 dust events have been documented in the Canary Islands between 1980, and 2022. Among these, only 9 events affected all the 6 main airports with an average visibility of less than 5000 m.

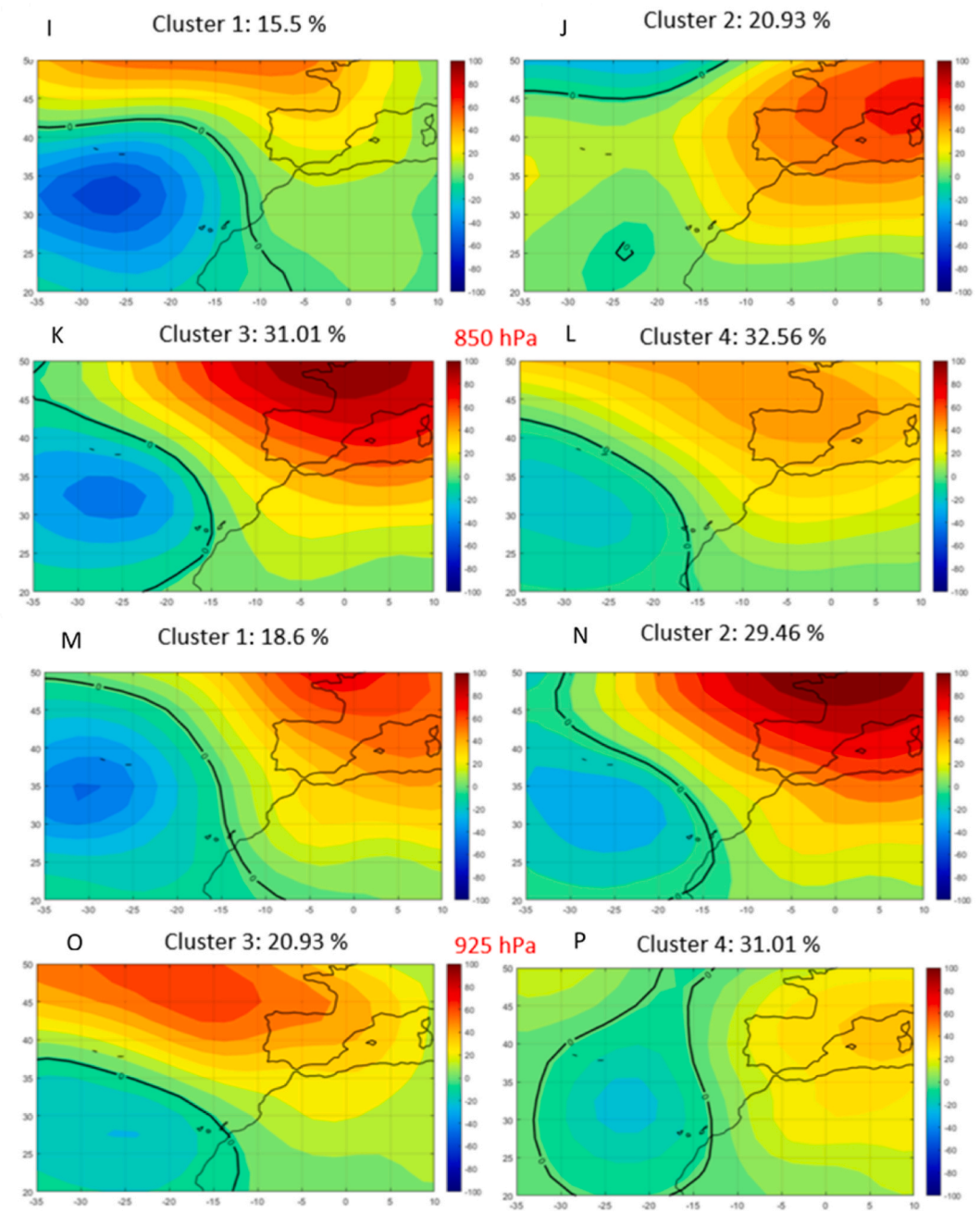

Fig. 9. (*continued*).

- Annual analysis reveals that the variables concerning the number of days and event duration have exhibited a statistically significant decline over the study period. As for visibility-related variables (average and minimum), negative trends indicate heightened event intensity; however, statistical significance is not observed.
- The monthly analysis has revealed that the longest dust events occur in the months of January and February, and that in addition, the events that reduce visibility the most, on average, occur in February. Conversely, the shortest events occur in November and the smallest reductions in visibility occur between April and September.
- The seasonal analysis shows that the longest and most intense events in terms of reduced visibility (medium and minimum) occurred in the Q1 quarter. Trends were analyzed quarterly. This analysis indicates downward and statistically significant trends in the AMJ and JAS quarters for the variables duration and days of dust events. The synoptic patterns prevailing during dust events are investigated via k-means clustering, using geopotential anomalies at distinct tropospheric levels. In the first and fourth quarters, the dust events occur when the dominant synoptic pattern exhibits a prominent high-low dipole structure. Specifically, the high-

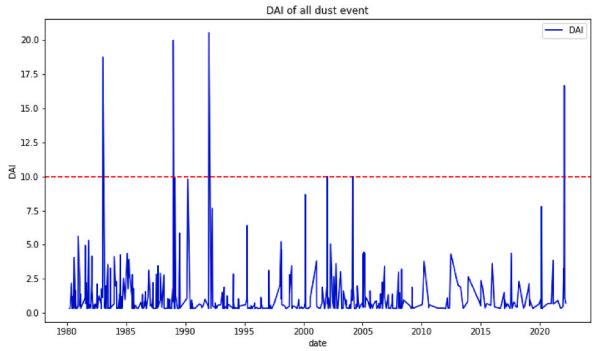

Fig. 10. DAI of all dust events analyzed (483 dust events) in the Canary Islands during the period of interest.

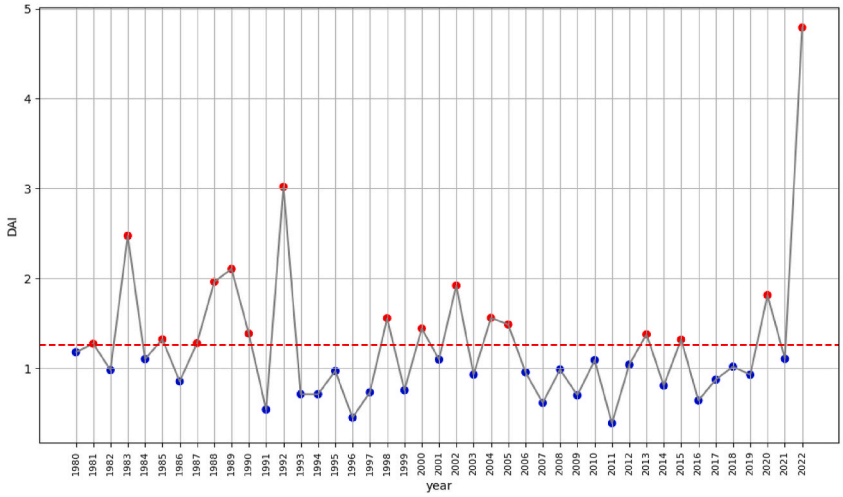

Fig. 11. Annual average of DAI. The red dots indicate years with DAI above the average of the entire series (red dashed line) and the blue ones below. (For interpretation of the references to colour in this figure legend, the reader is referred to the Web version of this article.)

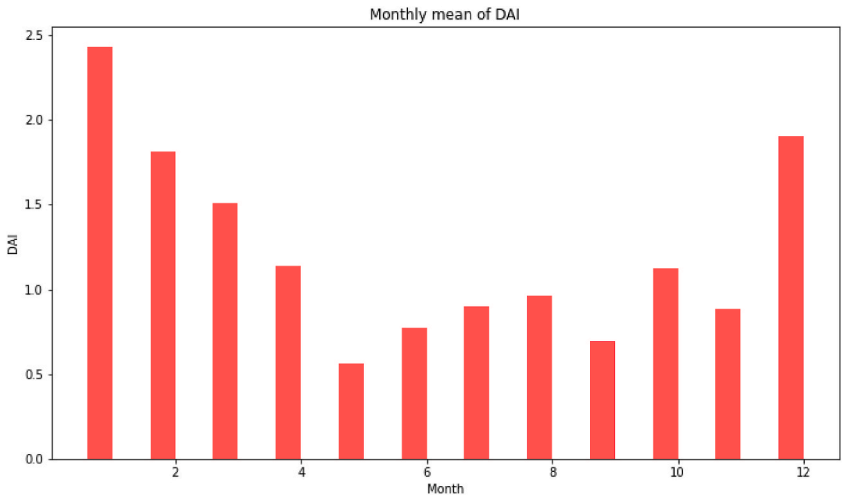

Fig. 12. Monthly average of DAI.

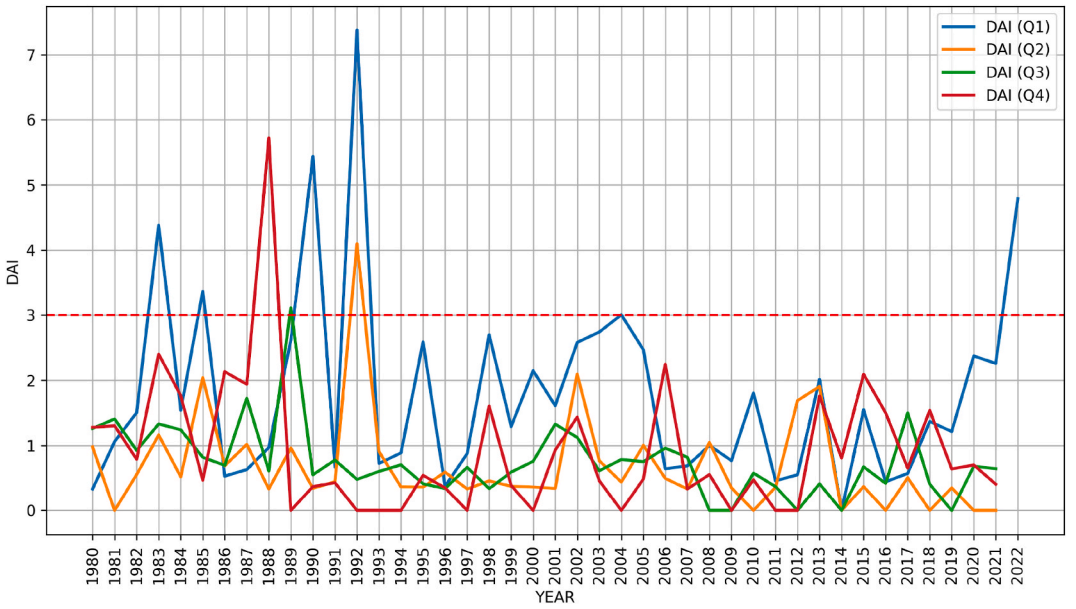

Fig. 13. Seasonal evolution of DAI.

pressure system is located north of the Iberian Peninsula, while the low cut-off is situated to the west of the Canary Islands. In the rest of the year it was observed that the geopotential anomalies were less marked, especially in the Q3 quarter

- In order to know and compare the dust events and determine which have been the most severe, the DAI was calculated. The DAI average throughout the entire period analyzed is 1.27 and only 4 events of the 483 registered show DAI values greater than 10. These most intense dust events based on DAI have been January 03, 1992, December 27, 1988, January 17, 1983 and January 28, 2022. Monthly it is observed that the maximum of DAI occurs in January and the minimum in May. On a quarterly basis, the Q1 quarter posted the highest average DAI values. It is precisely in Q1 when the most exceedances of the DAI = 3 (in the Q1 of 5 years the DAI = 3 has been exceeded) threshold have occurred throughout the study period.

Data availability statement

Data will be made available on request.

CRediT authorship contribution statement

D. Suárez-Molina: Writing – original draft, Visualization, Software, Methodology, Investigation, Formal analysis, Data curation, Conceptualization. **E. Cuevas:** Methodology, Investigation, Conceptualization. **S. Alonso-Pérez:** Writing – review & editing, Visualization, Software. **L. Cana:** Writing – review & editing, Supervision. **G. Montero:** Writing – review & editing, Supervision. **A. Oliver:** Writing – review & editing.

Declaration of competing interest

The authors declare that they have no known competing financial interests or personal relationships that could have appeared to influence the work reported in this paper.

Acknowledgments

The authors would like to thank the staff of the Operational Climatological Applications Area (ACAO) of AEMET for their day-to-day work in maintaining the National Climatic Data Bank. We would also like to thank the Aeronautical Observers at the airports, as without their professionalism this work would not have been possible. We would also like to thank the anonymous reviewers, whose comments have considerably improved the manuscript.

References

[1] S. Kinne, M. Schulz, C. Textor, S. Guibert, Y. Balkanski, S.E. Bauer, T. Berntsen, T.F. Berglen, O. Boucher, M. Chin, W. Collins, F. Dentener, T. Diehl, R. Easter, J. Feichter, D. Fillmore, S. Ghan, P. Ginoux, S. Gong, A. Grini, J. Hendricks, M. Herzog, L. Horowitz, I. Isaksen, T. Iversen, A. Kirkevåg, S. Kloster, D. Koch, J. E. Kristjansson, M. Krol, A. Lauer, J.F. Lamarque, G. Lesins, X. Liu, U. Lohmann, V. Montanaro, G. Myhre, J. Penner, G. Pitari, S. Reddy, O. Seland, P. Stier,

T. Takemura, X. Tie, An AeroCom initial assessment – optical properties in aerosol component modules of global models, Atmos. Chem. Phys. 6 (2006) 1815–1834, https://doi.org/10.5194/acp-6-1815-2006.
[2] N. Huneeus, O. Boucher, F. Chevallier, Atmospheric inversion of SO2 and primary aerosol emissions for the year 2010, Atmos. Chem. Phys. 13 (2013) 6555–6573.
[3] J.F. Kok, D.A. Ridley, Q. Zhou, R.L. Miller, C. Zhao, C.L. Heald, D.S. Ward, S. Albani, K. Haustein, Smaller desert dust cooling effect estimated from analysis of dust size and abundance, Nat. Geosci. 10 (2017) 274–278.
[4] P. Ginoux, J.M. Prospero, T.E. Gill, N.C. Hsu, M. Zhao, Global-scale attribution of anthropogenic and natural dust sources and their emission rates based on MODIS Deep Blue aerosol products, Rev. Geophys. 2012 (2012) 50.
[5] J.F. Kok, A.A. Adebiyi, S. Albani, Y. Balkanski, R. Checa-Garcia, M. Chin, P.R. Colarco, D.S. Hamilton, Y. Huang, A. Ito, M. Klose, L. Li, N.M. Mahowald, R. L. Miller, V. Obiso, C. Pérez García-Pando, A. Rocha-Lima, J.S. Wan, Contribution of the world's main dust source regions to the global cycle of desert dust, Atmos. Chem. Phys. 21 (2021) 8169–8193, https://doi.org/10.5194/acp-21-8169-2021.
[6] J.M. Prospero, P.J. Lamb, African droughts and dust transport to the Caribbean:climate change implications, Science 302 (2003) 1024e1027, https://doi.org/10.1126/science.1089915.
[7] J. Díaz, A. Tobías, C. Linares, Saharan dust and association between particulate matter and case-specific mortality: a case crossover analysis in Madrid (Spain), Environ. Health 11 (2012) 1–6, https://doi.org/10.1186/1476-069X-11-11, 2012.
[8] A. Karanasiou, N. Moreno, T. Moreno, M. Viana, F. de Leeuw, X. Querol, Health effects from Sahara dust episodes in Europe: literature review and research gaps, Environ. Int. 47 (2012) 107e114.
[9] G.R. Foltz, M.J. McPhaden, Impact of Saharan dust on tropical north Atlantic SST, J. Clim. 21 (2008) 5048e5060.
[10] I. Tegen, R. Torres, Global iron connections: desert dust, ocean biogeochemistry and climate, Science 308 (2005) 67e71.
[11] J.M. Prospero, Long-range transport of mineral dust in the global atmosphere: impact of African dust on the environment of the southeastern United States, Proc. Natl. Acad. Sci. USA 96 (7) (1999) 3396e3403, https://doi.org/10.1073/pnas.96.7.3396.
[12] J.M. Prospero, F.-X. Collard, J. Molinié, A. Jeannot, Characterizing the annual cycle of African dust transport to the Caribbean Basin and South America and its impact on the environment and air quality, Glob. Biogeochem. Cycles 29 (2014), https://doi.org/10.1002/2013GB004802.
[13] E. Cuevas, C. Milford, A. Barreto, J.J. Bustos, R.D. García, C.L. Marrero, N. Prats, C. Bayo, R. Ramos, E. Terradellas, D. Suárez, S. Rodríguez, J. de la Rosa, J. Vilches, S. Basart, E. Werner, E. López-Villarrubia, S. Rodríguez-Mireles, M.L. Pita Toledo, O. González, J. Belmonte, R. Puigdemunt, J.A. Lorenzo, P. Oromí, R. del Campo-Hernández, Desert dust Outbreak in the canary islands (February 2020): assessment and impacts, in: E. Cuevas, C. Milford, S. Basart (Eds.), State Meteorological Agency (AEMET), Madrid, Spain and World Meteorological Organization, WMO Global Atmosphere Watch (GAW), Geneva, Switzerland, 2021. Report No. 259, WWRP 2021-1.
[14] M.V. Sivakumar, Impacts of sand storms/dust storms on agriculture, in: Natural Disasters and Extreme Events in Agriculture, Springer, Berlin, Heidelberg, 2005, pp. 159–177.
[15] T.D. Jickells, Z.S. An, K.K. Andersen, A.R. Baker, G. Bergametti, N. Brooks, J.J. Cao, P.W. Boyd, R.A. Duce, K.A. Hunter, H. Kawahata, N. Kubilay, J. laRoche, P. S. Liss, N. Mahowald, J.M. Prospero, A.J. Ridgwell, I. Tegen, R. Torres, Global iron connections between desert dust, ocean biogeochemistry, and climate, Science 308 (5718) (2005) 67–71.
[16] O. Boucher, D. Randall, P. Artaxo, C. Bretherton, G. Feingold, P. Forster, V.-M. Kerminen, Y. Kondo, H. Liao, U. Lohmann, P. Rasch, S.K. Satheesh, S. Sherwood, B. Stevens, X.Y. Zhang, Clouds and aerosols, in: T.F. Stocker, D. Qin, G.-K. Plattner, M. Tignor, S.K. Allen, J. Doschung, A. Nauels, Y. Xia, V. Bex, P.M. Midgley (Eds.), Climate Change 2013: the Physical Science Basis. Contribution of Working Group I to the Fifth Assessment Report of the Intergovernmental Panel on Climate Change, Cambridge University Press, 2013, pp. 571–657. https://www.cambridge.org/core/books/climate-change-2013-the-physical-sciencebasis/clouds-and-aerosols/11F2D995DB0981610675738B72E7AECA.
[17] E. Terradellas, S. Nickovic, X. Zhang, Airborne dust: a hazard to human health, environment and society, World Meteorol. Organ. Bull. 64 (2015).
[18] WMO, in: S. Nickovic, E. Cuevas, J. Baldasano, E. Terradellas, T. Nakazawa, A. Baklanov (Eds.), Sand and Dust Storm Warning Advisory and Assessment System (SDS–WAS): Science and Implementation Plan 2015–2020, World Meteorological Organization, Geneva, 2015, p. 37. WWRP Report 2015 – 5, http://www.wmo.int/pages/prog/arep/wwrp/new/documents/Final_WWRP_2015_5_SDS_IP.pdf.
[19] D. Meloni, A. di Sarra, F. Monteleone, G. Pace, S. Piacentino, D.M. Sferlazzo, Seasonal transport patterns of intense Saharan dust events at the Mediterranean island of Lampedusa, 2008, Atmos. Res. 88 (2) (2008) 134–148, https://doi.org/10.1016/j.atmosres.2007.10.007. ISSN 0169-8095.
[20] H. Cao, C. Fu, W. Zhang, J. Liu, Characterizing sand and dust storms (SDS) intensity in China based on meteorological data, Sustainability 10 (2018) 2372, https://doi.org/10.3390/su10072372.
[21] P. Dorta, Catálogo de riesgos climáticos en Canarias: Amenazas y vulnerabilidad, Geographicalia 51 (2007) 133–160.
[22] S. Feuerstein, K. Schepanski, Identification of dust sources in a saharan dust hot-spot and their implementation in a dust-emission model, Rem. Sens. 11 (1) (2019) 4, https://doi.org/10.3390/rs11010004.
[23] I. Font Tullot, El tiempo atmosférico en las islas Canarias, Servicio Meteorológico Nacional. Serie A 26 (1956) (Instituto Nacional de Meteorología), http://hdl.handle.net/20.500.11765/9616.
[24] J.M. y Prospero, T.N. Carlson, Vertical and real distribution of Saharan dust over the western ecuatorial North Atlantic Ocean, J. Geophys. Res. 77 (1972) 5255–5265.
[25] G. Bergametti, L. Gomes, G. Coudé-Gaussen, P.Y. Rognon, M.N.L. Coustumer, African dust observed over Canary Islands: source regions identification and transport pattern for some summer situation, J. Geophys. Res. 94 (1989) 14855–14864.
[26] I. Chiapello, G. Bergametti, L. y Gomes, B. Chatenet, An additional low layer transport of Sahelian and Saharan dust over the North-Eastern Tropical Atlantic, Geophys. Res. Lett. 22 (23) (1995) 3191–3194.
[27] E. Cuevas, Estudio del comportamiento del ozono troposférico en el observatorio de Izaña y su relación con la dinámica atmosférica. Tesis Doctoral. Facultad de Ciencias Físicas, Universidad Complutense de Madrid, 1995.
[28] J.J. Bustos, E. Cuevas, C. Marrero, S. y Alonso, Caracterización de las masas de aire en la troposfera libre y en la capa de mezcla en Canarias. Proceedings de la IX Asamblea de Geodesia y Geofísica, 1998, pp. 9–13. Aguadulce (Almería).
[29] S. Rodríguez, Comparación de las variaciones de ozono superficial asociadas a procesos de transporte sobre y bajo la inversión de temperatura subtropical en Tenerife, Tesis de Licenciatura, Universidad de La Laguna (1999).
[30] S. Rodríguez, J.C. Gerra, Monitoring of ozone in a marine environment in Tenerife (canary islands), Atmos. Environ. 135 (2001) 18291841.
[31] C.J. Torres, E. Cuevas, J.C. Guerra, V. y Carreño, Caracterización de las Masas de Aire en la Región Subtropical. Proceedings del V Simposio Nacional de Predicción, Instituto Nacional de Meteorología, Madrid, 2001, pp. 20–23. Noviembre, 2001.
[32] M. Viana, Niveles, composición y origen del material particulado atmosférico en los sectores Norte y Este de la Península Ibérica y Canarias. Tesis Doctoral. Consejo Superior de Investigaciones Científicas, Universitat de Barcelona, 2003.
[33] P. Dorta, M.D. Gelado, J.J. Hernández, P. Cardona, C. Collado, S. Mendoza, M.J. Rodríguez, V. Siruela, M.E. Torres, Frecuencia, estacionalidad y tendencias de las advecciones de aire sahariano en Canarias (1976-2003), Invest. Geográficas nº38 (2005) (2005) 23–45. Instituto Universitario de Geografía. Universidad de Alicante.
[34] S. Alonso-Pérez, E. Cuevas, X. Querol, Objective identification of synoptic meteorological patterns favouring African dust intrusions into the marine boundary layer of the subtropical eastern north Atlantic region, Meteorol. Atmos. Phys. 113 (2011) 109–124.
[35] M. Viana, X. Querol, A. Alastuey, E. y Cuevas, S. Rodríguez, Influence of African dust on the levels of atmospheric particulates in the Canary Islands air quality network, Atmos. Environ. 36 (2002) 5861–5875.
[36] Markus Kottek, Jürgen Grieser, Christoph Beck, Bruno Rudolf, Franz Rubel, World Map of the Köppen-Geiger climate classification updated, Meteorol. Z. 15 (3) (2006) 259–263, https://doi.org/10.1127/0941-2948/2006/0130. Bibcode:2006MetZe.15.259K.
[37] AEMET, Atlas climático de los archipiélagos de Canarias, Madeira y Azores, vol. 2012, Ministerio de Agricultura, Alimentación y Medio Ambiente, 2012, https://doi.org/10.31978/281-12-006-X. NIPO: 281-12-006-X.

[38] I. Font Tullot, Climatología de España y Portugal, Instituto Nacional de Meteorología, 1983. ISBN: 978-84-5009-467-4.
[39] WMO-No. 488. Guide to the Global Observing System. Part III, 3.2.2.2.4 Visibility.
[40] WMO-No. 731. Guide to Meteorological Observing and Information Distribution Systems for Aviation Weather Services.
[41] E. Kalnay, M. Kanamitsu, R. Kistler, W. Collins, D. Deaven, L. Gandin, M. Iredell, 1 S. Saha, G. White, J. Woollen, Y. Zhu, A. Leetmaa, R. Reynolds, M. Chelliah, W. Ebisuzaki, W. Higgins, J. Janowiak, K.C. Mo, C. Ropelewski, J. Wang, R. Jenne, D. Joseph, 3 the NCEP/NCAR 40-year reanalysis project, B. Am. Meteorol. Soc. 77 (1996) 437–471.
[42] ICAO, Manual of Aeronautical Meteorological Practice (Doc 8896), International Civil Aviation Organization, 2021. Thirteenth Edition, 2021.
[43] H.B. Mann, Nonparametric tests against trend, Econometrica 13 (1945) 245–259.
[44] M.G. Kendall, Rank Correlation Methods, fourth ed., Charles Griffin, London, 1975.
[45] R.O. Gilbert, Statistical Methods for Environmental Pollution Monitoring, Wiley, NY, 1987.
[46] K.W. Hipel, A.I. McLeod, Time series modelling of water resources and environmental systems. Electronic reprint of our book orginally published in 1994. http://www.stats.uwo.ca/faculty/aim/1994Book/, 2005.
[47] M.C. Baddock, C.L. Strong, J.F. Leys, S.K. Heidenreich, E.K. Tews, G.H. McTainsh, A visibility and total suspended dust relationship, Atmos. Environ., Volume 89, 14, Pages 329-336, ISSN 1352-2310.https://doi.org/10.1016/j.atmosenv.2014.02.038.
[48] A.D. Boloorani, Contingency Planning Process for Catalysing Investments and Actions to Enhance Resilience against Sand and Dust Storms in Agriculture in the Islamic Republic of Iran, FAO, Rome, 2023, https://doi.org/10.4060/cc8401en.
[49] Waleed Hamza, Mohamed Rizk Enan, Huda Al-Hassini, Jan-Berend Stuut, Dirk de-Beer, Dust storms over the Arabian Gulf: a possible indicator of climate changes consequences, Aquat. Ecosys. Health Manag. 14 (3) (2011) 260–268, https://doi.org/10.1080/14634988.2011.601274.
[50] O'LoingsighT., McTainsh G.H., Tews E.K., Strong C.L., Leys J.F., Shinkfield P., Tapper N.J.,The Dust Storm Index (DSI): A method for monitoring broadscale wind erosion using meteorological records,Aeolian Research,Volume 12,2014,Pages 29-40,ISSN 1875-9637,https://doi.org/10.1016/j.aeolia.2013.10.004.
[51] J.B. MacQueen, Some methods for classification and analysis of multivariate observations, in: Proceedings of 5th Berkeley Symposium on Mathematical Statistics and Probability, vol. 1, University of California Press, 1967, pp. 281–297. MR 0214227. Zbl 0214.46201.
[52] N.M. Mahowald, J.A. Ballantine, J. Feddema, N. Ramankutty, Global trends in visibility: implications for dust sources, Atmos. Chem. Phys. 7 (12) (2007) 3309–3339.
[53] Xin Xi, Revisiting the recent dust trends and climate drivers using horizontal visibility and present weather observations, J. Geophys. Res. Atmos. 126 (2021), https://doi.org/10.1029/2021JD034687.
[54] I. Chiapello, C. Moulin, J.M. Prospero, Understanding the long-term variability of African dust transport across the Atlantic as recorded in both Barbados surface concentrations and large-scale Total Ozone Mapping Spectrometer (TOMS) optical thickness, J. Geophys. Res. Atmos. 110 (D18) (2005).
[55] A.T. Evan, C. Flamant, M. Gaetani, F. Guichard, The past, present and future of African dust, Nature 531 (7595) (2016) 493–495.
[56] D. Suárez Molina, C. Marrero, E. Cuevas Agulló, E. Werner, N. Prats Porta, S. Basart, Caracterización de las Intrusiones de Polvo en Canarias, Agencia Estatal de Meteorología, Madrid, Spain, 2021.
[57] Á. Barreto, E. Cuevas, R.D. García, J. Carrillo, J.M. Prospero, L. Ilić, M. Yela, Long-term characterisation of the vertical structure of the Saharan Air Layer over the Canary Islands using lidar and radiosonde profiles: implications for radiative and cloud processes over the subtropical Atlantic Ocean, Atmos. Chem. Phys. 22 (2) (2022) 739–763.

3. Conclusiones finales

La presente tesis, estructurada en un compendio de artículos, aborda una temática de vital importancia para la región de Canarias: los fenómenos meteorológicos adversos, la modelización numérica y los sistemas de alerta temprana. A través de una investigación meticulosa y multidisciplinar, se han logrado avances significativos en la comprensión y manejo de estos fenómenos, y se han proporcionado herramientas y conocimientos valiosos para la mitigación de sus impactos.

3.1. Primera publicación

El primer artículo de la tesis se centró en el análisis de parámetros derivados de sondeos meteorológicos con el objetivo de evaluar episodios de fenómenos meteorológicos adversos en Canarias. Este estudio permitió identificar patrones y características atmosféricas asociadas a eventos extremos, como tormentas y precipitaciones intensas. Los resultados mostraron que ciertos índices de inestabilidad y parámetros termodinámicos pueden servir como indicadores anticipados de estos fenómenos, y proporcionan una base científica sólida para mejorar los sistemas de alerta temprana en la región. A continuación, se enumeran las conclusiones alcanzadas en este artículo:

- Los valores de CAPE estuvieron por debajo de 1000 J/kg en más del 75 por ciento de los casos en las Islas Canarias.

- En el área de interés, los eventos de lluvia con intensidades superiores a muy fuerte (lluvia >30 mm/h) se caracterizan por la mayor mediana de MUCAPE y SBCAPE, una disminución de la tasa de cambio de temperatura ambiental con la altura y un alto contenido total de agua precipitable (TPW). Sin embargo, las categorías 2 y 3 mostraron valores medianos de SBCAPE cercanos a 0. Además, el análisis de los valores de CAPE puede utilizarse para discriminar la categoría 1 (sin tormenta) del resto.

- En las Islas Canarias, los eventos de granizo o ráfagas de viento superiores a 120 km/h se caracterizan por una alta magnitud de "Bulk Shear" entre 0-6 km (HS) y un bajo CAPE (LC), además de un bajo TPW.

- El ciclo estacional de CAPE en las Islas Canarias mostró diferencias con la distribución global de CAPE. Estas diferencias se deben a la fuerza de la inversión de subsidencia en verano en las Islas Canarias, que actúa como una tapa inhibiendo la convección.

- Los valores de las medianas más elevadas de TPW se encuentran durante los meses de agosto, septiembre y octubre, cuando se alcanzan las temperaturas más altas de la superficie del mar en las Islas Canarias y, en consecuencia, el aire en contacto con la superficie del mar tiene más capacidad para almacenar vapor de agua.

- En este estudio, se ha evidenciado que la combinación de parámetros derivados de sondeos puede ayudar al predictor operativo a evaluar el riesgo de fenómenos meteorológicos adversos. Para ilustrar la aplicación del uso combinado de diferentes parámetros, se analizaron dos estudios de caso. Ambos casos mostraron un comportamiento similar a los resultados obtenidos

con el conjunto completo de datos, lo que respalda la importancia de la caracterización y el conocimiento de las condiciones ambientales para las tormentas severas en la región de interés.

- El análisis de datos de sondeos puede ser útil para comprender qué tipos de condiciones atmosféricas se observan típicamente durante un evento de tormenta severa. Ayudan a los predictores a saber cuándo ocurren condiciones inusuales. En la previsión meteorológica, es extremadamente importante que el predictor reconozca las condiciones inusuales cuando se presentan. Los estudios locales de la frecuencia de ocurrencia de condiciones inusuales pueden ser de gran ayuda.

- En este estudio, los sondeos de previsión de modelos de alta resolución mostraron una buena capacidad para reproducir las condiciones observadas. Por lo tanto, se recomienda el uso de sondeos de previsión para anticipar el riesgo de un evento meteorológico severo.

3.2. Segunda publicación

El segundo artículo se dedicó al análisis de sensibilidad del modelo numérico Weather Research and Forecasting (WRF) aplicado a Canarias. Se realizaron múltiples simulaciones para evaluar la respuesta del modelo a diferentes configuraciones y condiciones iniciales. Los hallazgos destacaron la importancia de la elección de parámetros específicos para mejorar la precisión de las predicciones meteorológicas en un entorno complejo como el de Canarias. Este trabajo subraya la necesidad de una calibración cuidadosa del WRF para optimizar su rendimiento y fiabilidad en la previsión de fenómenos adversos. A continuación, se presentan las conclusiones obtenidas en este segundo artículo:

- Esta investigación permitió descartar configuraciones inapropiadas del modelo WRF. Las configuraciones descartadas fueron las combinaciones de los esquemas PBL YSU y MYNN2 con los esquemas MP Kessler, Goddard y Morrison 2 Moment.

- En cuanto a la acumulación de lluvia en 3 horas en las Islas Canarias, el esquema PBL seleccionado tuvo un mayor impacto que el esquema MP utilizado. El esquema PBL MYJ alcanzó el mejor rendimiento para la precipitación. La capacidad de las configuraciones del modelo para pronosticar la precipitación estuvo influenciada por la hora del día.

- La combinación BouLac-Thompson presentó los mejores resultados para T2m.

- La combinación MYJ-WSM6 mostró los mejores resultados para la ráfaga máxima de viento en 1 hora. Todas las configuraciones del modelo siguieron las tendencias de la evolución diaria de las ráfagas de viento promedio. Sin embargo, ninguna fue capaz de pronosticar el jet nocturno de niveles bajos. Aunque el esquema PBL MYJ presentó resultados más estables para las ráfagas de viento con el tiempo, el esquema PBL Boulac exhibió mejores resultados durante la noche y temprano en la mañana.

- Todos los campos presentaron mejores resultados entre los tiempos de pronóstico de 18 y 33 horas.

- Se demostró la influencia de la ubicación. Los peores resultados se obtuvieron en áreas de terreno complejo. Los peores resultados de T2m surgieron en las zonas de transición tierra-mar en las costas orientales de las islas. Además, para la acumulación de lluvia en 3 horas y la ráfaga máxima de viento en 1 hora, el error de pronóstico aumentó con la altitud.

3.3. Tercera publicación

El tercer artículo abordó la caracterización de las intrusiones de polvo en Canarias, un fenómeno que tiene implicaciones significativas tanto para la salud pública como para el medio ambiente. Mediante el análisis de datos meteorológicos, se logró una comprensión detallada de las condiciones que favorecen estas intrusiones y su impacto. Los resultados obtenidos contribuyen a mejorar las estrategias de monitoreo y respuesta ante episodios de polvo, y se integran eficazmente en los sistemas de alerta temprana regionales. A continuación, se detallan las conclusiones derivadas de esta investigación:

- Se han documentado un total de 483 eventos de polvo en las Islas Canarias entre 1980 y 2022. De estos, solo 9 eventos afectaron a los 6 principales aeropuertos con una visibilidad promedio de menos de 5000 m.

- El análisis anual revela que las variables relacionadas con el número de días de eventos de polvo a lo largo de los años y la duración de estos eventos han mostrado una tendencia decreciente que es estadísticamente significativa durante el período de estudio. En cuanto a las variables relacionadas con la visibilidad (promedio y mínima), las tendencias negativas indican una intensidad de evento más alta; sin embargo, no se observa significancia estadística.

- El análisis mensual ha revelado que los eventos de polvo más largos ocurren en los meses de enero y febrero, y que, además, los eventos que reducen más la visibilidad, en promedio, ocurren en febrero. Por el contrario, los eventos más cortos ocurren en noviembre y las reducciones más pequeñas en la visibilidad ocurren entre abril y septiembre.

- El análisis estacional muestra que los eventos más largos y más intensos en términos de reducción de visibilidad (media y mínima) ocurrieron en el primer trimestre (Q1). Se analizaron las tendencias trimestralmente. Este análisis indica tendencias descendentes y estadísticamente significativas en los trimestres AMJ (abril-mayo-junio) y JAS (julio-agosto-septiembre) para las variables duración y días de eventos de polvo. Los patrones sinópticos predominantes durante los eventos de polvo se investigan mediante la agrupación k-means, utilizando anomalías geopotenciales en distintos niveles troposféricos. En el primer y cuarto trimestre, los eventos de polvo ocurren cuando el patrón sinóptico dominante exhibe una estructura prominente de alta-baja. Específicamente, el sistema de alta presión se encuentra al norte de la Península Ibérica, mientras que la baja está situada al oeste de las Islas Canarias. En el resto del año se observó que las anomalías geopotenciales eran menos marcadas, especialmente en el tercer trimestre (Q3).

- Para conocer y comparar los eventos de polvo y determinar cuáles han sido los más severos, se calculó el Índice de Severidad de Polvo (DAI, por sus siglas en inglés). El DAI promedio durante todo el período analizado es de 1.27 y solo 4 eventos de los 483 registrados muestran valores de DAI superiores a 10. Estos eventos de polvo más intensos basados en el DAI han sido el 03 de enero de 1992, el 27 de diciembre de 1988, el 17 de enero de 1983 y el 28 de enero de 2022. Mensualmente se observa que el máximo de DAI ocurre en enero y el mínimo en mayo. Trimestralmente, el primer trimestre (Q1) registró los valores de DAI promedio más altos. Precisamente en el primer trimestre es cuando se han producido la mayoría de las superaciones del umbral de DAI = 3 (en el Q1 de 5 años se ha superado el DAI = 3) durante todo el período de estudio.

3.4. Conclusiones finales y trabajo futuro

Los estudios realizados en esta tesis no solo han ampliado el conocimiento sobre los fenómenos meteorológicos adversos en Canarias, sino que también han proporcionado herramientas prácticas para su manejo. Las conclusiones extraídas de los análisis de sondeos meteorológicos, la optimización del WRF y la caracterización de intrusiones de polvo, ofrecen una base sólida para mejorar los sistemas de alerta temprana, lo que contribuye a una mayor resiliencia de la sociedad canaria frente a eventos extremos.

Como trabajo futuro se recomienda la implementación continua y la actualización de modelos numéricos y sistemas de monitoreo basados en los hallazgos de esta tesis, máxime en un marco como el actual de calentamiento global y del impacto del cambio climático en los fenómenos meteorológicos adversos. Además, es crucial fomentar la colaboración entre investigadores, autoridades y la población para asegurar una respuesta eficaz y coordinada ante futuros eventos meteorológicos adversos.

En resumen, esta tesis ha demostrado que, a través de un enfoque integrador y multidisciplinar, es posible avanzar significativamente en la comprensión y gestión de fenómenos meteorológicos adversos en Canarias, ofreciendo soluciones concretas y aplicables para proteger a la población y el entorno.